Nuclear Safety
NEA/CSNI/R(2020)10
October 2022
www.oecd-nea.org

Reactivity Initiated Accident Benchmark Phase III Report

OECD
BETTER POLICIES FOR BETTER LIVES

NEA
NUCLEAR ENERGY AGENCY

Nuclear Energy Agency

NEA/CSNI/R(2020)10

Unclassified English text only

14 October 2022

NUCLEAR ENERGY AGENCY
COMMITTEE ON THE SAFETY OF NUCLEAR INSTALLATIONS

Reactivity Initiated Accident Benchmark Phase III Report

This document is available in PDF format only.

JT03505043

ORGANISATION FOR ECONOMIC CO-OPERATION AND DEVELOPMENT

The OECD is a unique forum where the governments of 38 democracies work together to address the economic, social and environmental challenges of globalisation. The OECD is also at the forefront of efforts to understand and to help governments respond to new developments and concerns, such as corporate governance, the information economy and the challenges of an ageing population. The Organisation provides a setting where governments can compare policy experiences, seek answers to common problems, identify good practice and work to co-ordinate domestic and international policies.

The OECD member countries are: Australia, Austria, Belgium, Canada, Chile, Columbia, Costa Rica, the Czech Republic, Denmark, Estonia, Finland, France, Germany, Greece, Hungary, Iceland, Ireland, Israel, Italy, Japan, Korea, Latvia, Lithuania, Luxembourg, Mexico, Netherlands, New Zealand, Norway, Poland, Portugal, Slovak Republic, Slovenia, Spain, Sweden, Switzerland, Türkiye, the United Kingdom and the United States. The European Commission takes part in the work of the OECD.

OECD Publishing disseminates widely the results of the Organisation's statistics gathering and research on economic, social and environmental issues, as well as the conventions, guidelines and standards agreed by its members.

NUCLEAR ENERGY AGENCY

The OECD Nuclear Energy Agency (NEA) was established on 1 February 1958. Current NEA membership consists of 34 countries: Argentina, Australia, Austria, Belgium, Bulgaria, Canada, the Czech Republic, Denmark, Finland, France, Germany, Greece, Hungary, Iceland, Ireland, Italy, Japan, Korea, Luxembourg, Mexico, the Netherlands, Norway, Poland, Portugal, Romania, Russia (suspended), the Slovak Republic, Slovenia, Spain, Sweden, Switzerland, Türkiye, the United Kingdom and the United States. The European Commission and the International Atomic Energy Agency also take part in the work of the Agency.

The mission of the NEA is:

- to assist its member countries in maintaining and further developing, through international co-operation, the scientific, technological and legal bases required for a safe, environmentally sound and economical use of nuclear energy for peaceful purposes;
- to provide authoritative assessments and to forge common understandings on key issues as input to government decisions on nuclear energy policy and to broader OECD analyses in areas such as energy and the sustainable development of low-carbon economies.

Specific areas of competence of the NEA include the safety and regulation of nuclear activities, radioactive waste management and decommissioning, radiological protection, nuclear science, economic and technical analyses of the nuclear fuel cycle, nuclear law and liability, and public information. The NEA Data Bank provides nuclear data and computer program services for participating countries.

COMMITTEE ON THE SAFETY OF NUCLEAR INSTALLATIONS

The Committee on the Safety of Nuclear Installations (CSNI) addresses Nuclear Energy Agency (NEA) programmes and activities that support maintaining and advancing the scientific and technical knowledge base of the safety of nuclear installations.

The Committee constitutes a forum for the exchange of technical information and for collaboration between organisations, which can contribute, from their respective backgrounds in research, development and engineering, to its activities. It has regard to the exchange of information between member countries and safety R&D programmes of various sizes in order to keep all member countries involved in and abreast of developments in technical safety matters.

The Committee reviews the state of knowledge on important topics of nuclear safety science and techniques and of safety assessments, and ensures that operating experience is appropriately accounted for in its activities. It initiates and conducts programmes identified by these reviews and assessments in order to confirm safety, overcome discrepancies, develop improvements and reach consensus on technical issues of common interest. It promotes the co-ordination of work in different member countries that serve to maintain and enhance competence in nuclear safety matters, including the establishment of joint undertakings (e.g. joint research and data projects), and assists in the feedback of the results to participating organisations. The Committee ensures that valuable end-products of the technical reviews and analyses are provided to members in a timely manner, and made publicly available when appropriate, to support broader nuclear safety.

The Committee focuses primarily on the safety aspects of existing power reactors, other nuclear installations and new power reactors; it also considers the safety implications of scientific and technical developments of future reactor technologies and designs. Further, the scope for the Committee includes human and organisational research activities and technical developments that affect nuclear safety.

Acknowledgements

This report was prepared by the reactivity-initiated accident (RIA) Benchmark Phase III Task Group of the Working Group on Fuel Safety (WGFS).

Special gratitude is expressed to Jean Baccou, Vincent Georgenthum and Nicolas Tregoures (IRSN, France) for drafting the report, as well as to Asko Arkoma (VTT, Finland), Rolando Calabrese (ENEA, Italy), Charles Folsom (INL, United States), Isabelle Guénot-Delahaie (CEA, France), Lars Olof Jernkvist (Quantum Technologies, Sweden) and Jinzhao Zhang (TRACTEBEL, Belgium) for reviewing the report.

The following WGFS members and experts performed calculations and provided valuable input to various chapters of the report:

Asko Arkoma	VTT, Finland
Jean Baccou	IRSN, France
Felix Boldt	GRS, Germany
Rolando Calabrese	ENEA, Italy
Marco Cherubini	NINE, Italy
Martin Dostal	ÚJV, Czech Republic
Thomas Drieu	TRACTEBEL, Belgium
Charles Folsom	INL, United States
Vincent Georgenthum	IRSN, France
Isabelle Guénot-Delahaie	CEA, France
Hyedong Jeong	KINS, Korea
Lars Olof Jernkvist	Quantum Technologies, Sweden
Jan Klouzal	ÚJV, Czech Republic
Raoul Ngayan-Happy	PSI, Switzerland
Ian Porter	NRC, United States
Heinz Günther Sonnenburg	GRS, Germany
Yutaka Udagawa	JAEA, Japan
Jinzhao Zhang	TRACTEBEL, Belgium

Table of contents

List of figures

List of tables

Executive summary

Following the recommendations from the technical workshop on "Nuclear Fuel Behaviour during Reactivity-Initiated Accidents" organised by the Nuclear Energy Agency (NEA) in September 2009, a first benchmark of the RIA fuel codes was organised between 2010 and 2013. A second phase of the benchmark was launched in 2014, and the reports resulting from these activities were approved by the Committee on the Safety of Nuclear Installations in 2015 and 2016. The main conclusions of the two phases were:

- Regarding fast transient thermal-hydraulic post-DNB (departure from nucleate boiling) behaviour, there are major differences between the modelling approaches, resulting in significant deviations between simulations. Unfortunately, there are currently no simple and representative experimental results that allow the different approaches to be validated.
- The models of fuel and clad thermo-mechanical behaviour and the associated materials properties should be improved and validated for RIA conditions.
- The different influential input parameters were identified for fresh fuel. For instance, injected energy, fuel enthalpy, parameters related to the rod geometry (fuel and clad roughness, cladding inside diameter), fuel thermal-expansion model and full width at half maximum of the power pulse come out as influential regarding the maximum value of each output parameter of interest. However, the most influential parameters in the case of irradiated fuel could be different from those of fresh fuel.
- Uncertainties cannot fully explain the scatter observed during Phase I of this benchmark exercise.

One recommendation from Phase II of the benchmark was to launch a complementary phase focused on uncertainty and sensitivity analyses on an irradiated case in order to identify the corresponding influential input parameters. In particular, the impact of the initial state and key models on the results of the transient needed to be investigated and a sensitivity study needed to be performed in order to identify or confirm the most influential input uncertainties.

RIA benchmark Phase III specifications

Considering the results obtained during the first two phases, mainly the large discrepancy regarding RIA thermal-hydraulics modelling, it was decided to limit the exercise to the pellet-cladding mechanical interaction (PCMI) phase, for which data are available from in-pile tests. It was proposed to use the CIP0-1 test for this exercise performed in the CABRI reactor in the sodium loop (for which it would be easier to reach a consensus between the codes in relation to cladding-coolant heat transfer).

The CIP0-1 rodlet was refabricated from an ENUSA fuel rod with UO_2 high burn-up fuel (75 GWd/tU) and ZIRLO™ cladding irradiated in the pressurised water reactor Vandellos 2 in Spain. The clad oxidation was significant, varying between 50 µm and 110 µm over the length of the sample. The test was performed in 2002, at 280°C and low pressure (~3 bar). The injected energy in the test rod at peak power node was 99 cal/g and the power

pulse width at half maximum 32 ms. No boiling crisis nor failure of the fuel rod occurred during the test.

The assessment of the uncertainty associated with the test prediction is affected by the simulation of the base irradiation to predict the rodlet pre-test conditions. In order to focus this activity on the RIA codes, the state of the rod at the end of the base irradiation, before the transient, was evaluated with the FRAPCON code, whose input data and results were distributed to every participant.

Twelve uncertain input parameters with their reference values and their probability density functions were defined. The probabilistic input uncertainty propagation method was selected and the sample size was set to 200 code runs. The statistical study included not only input parameters already identified for fresh fuel, but also extra "irradiation parameters" such as zirconia thickness, power profile and initial fuel-clad gap.

For the uncertainty analysis, participants provided the lower and upper bounds of an uncertainty interval for the 19 specified output parameters; for the sensitivity analysis, they provided the partial rank correlation coefficients associated with each uncertain input for each specified output parameter at each specified time, including the one for their maximum values.

Participants and codes used

Ten organisations representing nine countries participated in the RIA benchmark Phase III. The range of computer codes used was large, as analyses were performed with ALCYONE, FALCON, FRAPTRAN, RANNS, SCANAIR, TESPA-ROD and TRANSURANUS.

Some participants fully initialised their CIP0-1 analyses with the output from the FRAPCON results. For the other data not provided by FRAPCON and needed for RIA calculations, hypotheses were made.

Those participants who could not fully initialise their CIP0-1 input data with FRAPCON output used their own means of calculating the non-initialisable parameters, and tried to match as much as possible the FRAPCON results, notably for fission gas distribution.

Results and summary

The uncertainty analysis has led to the following main conclusions:

- The experimental results (time/height trend and scalar values) were well captured by most of the participants, except for the fission gas release.
- The strongest agreement with the experimental measurements is associated with the evaluation of clad hoop strain and clad elongation, then sodium temperatures.
- The maximum (relative) uncertainty band width depends on the type of outputs. As in Phase II, the narrowest intervals are obtained for fuel thermal outputs. The uncertainty interval width increases slightly for clad thermal outputs, then more significantly for fuel and clad mechanical ones. Finally, a large uncertainty has been observed for the new outputs (that were not considered in Phase II): gap size, fuel-to-clad heat exchange, fission gas release and clad failure prediction.
- The same magnitude was observed for the relative uncertainty width and for reference calculation dispersion for numerous outputs.

- When comparing participants' uncertainty results for outputs considered in Phase II, the coherence ranking is the same, i.e. the highest coherence is obtained for fuel thermal outputs and fuel and clad mechanical outputs.

The sensitivity analysis has led to the following conclusions:

- The injected energy is the most influential input parameter during the whole transient and on almost all output data.
- Input data related to rod state after base irradiation (initial fuel-clad gap, zirconia thickness, radial power profile, roughness) are also very influential. Initial fuel-clad gap is the most influential one in terms of clad failure prediction.
- Fuel physical properties (fuel thermal-expansion and thermal conductivity models) have a significant impact on behaviour.
- Regarding the fission gas release, except injected energy, participants did not identify any common influential input parameters.
- The clad failure prediction is challenging because it is sensitive to many input data (nine influential input parameters out of the 12 studied here).
- The clad physical properties (thermal-expansion and yield stress) have an impact on few, but major, outputs (clad stress and clad failure prediction).

Conclusions and recommendations

The specifications of the RIA benchmark Phase III decoupled steady-state and transient simulations. Some codes have been developed to perform both base irradiation and transient calculations, which makes it possible to ensure continuity between the two phases, but makes it more difficult to perform the decoupling. Their users thus had difficulties matching the pre-transient state defined in the specifications.

Phase III confirmed the conclusions of Phase II concerning the strong dependence of the uncertainty results on the type of behaviour (in terms of uncertainty band width and coherence between participants). Moreover, it expanded the list of influential input parameters, with some input parameters related to the irradiation period.

Based on the main outcomes of the analysis, recommendations for future work are:

- Safety analysis studies can require uncertainty analysis on parameters associated with the state of the rod at the end of irradiation. However, for some RIA codes, pulse irradiation and base irradiation are not considered separately. It could be interesting to develop strategies to allow the propagation of uncertainties on input parameters associated to irradiation behaviour.
- Further developments are required with a view to validate fission gas release and clad failure prediction models. It first involves gathering more high-quality data.
- Mechanical models need to be improved, including cladding failure criteria and cladding stress behaviour.

A first task to carry out before uncertainty and sensitivity analyses is the quantification of input uncertainties, which was partly performed in this benchmark using expert judgement. The recent SAPIUM guidance could be used for a transparent and rigorous model for input uncertainty quantification in order to minimise the user effect.

List of abbreviations and acronyms

BFC	Bottom of fissile column
CABRI	Test reactor in France
CDF	Cumulative distribution function
CEA	Alternative Energies and Atomic Energy Commission (Commissariat à l'Énergie atomique et aux énergies alternatives, France)
CFP	Clad failure prediction
CSED	Critical strain energy density
CSNI	Committee on the Safety of Nuclear Installations (NEA)
DHR	Variation of radial average enthalpy
DNB	Departure from nucleate boiling
ECT	Clad total axial elongation
ECTH	Clad total (thermal + elastic + plastic) hoop strain
EFT	Fuel column total axial elongation
ENEA	National Agency for New Technologies, Energy and Sustainable Economic Development (Agenzia nazionale per le nuove tecnologie, l'energia e lo sviluppo economico sostenibile, Italy)
EPRI	Electric Power Research Institute
ETZ	Clad residual hoop strain
FGR	Fission gas release
GRS	Gesellschaft für anlagen- und ReaktorSicherheit (Germany)
HBS	High burn-up structure
HFC	Fuel-to-clad heat exchange coefficient
INL	Idaho National Laboratory (United States)
IRSN	Institute for Radiological Protection and Nuclear Safety (Institut de Radioprotection et de Sûreté Nucléaire, France)
J	Rice integral
JAEA	Japan Atomic Energy Agency
KINS	Korean Institute of Nuclear Safety
LUB/UUB	Lower/upper uncertainty bound
LUB_{min}/UUB_{max}	Minimum/maximum of the LUBs/UUBs provided by all participants
MO_X	Mixed oxide fuel (U and Pu)

NEA	Nuclear Energy Agency
NINE	Nuclear and Industrial Engineering (Italy)
NRC	Nuclear Regulatory Commission (United States)
NSRR	Nuclear Safety Research Reactor (Japan)
OECD	Organisation for Economic Co-operation and Development
PCMI	Pellet-cladding mechanical interaction
PNNL	Pacific Northwest National Laboratory (United States)
PPN	Peak power node
PRCC	Partial rank correlation coefficient
PSI	Paul Scherrer Institute
PWR	Pressurised water reactor
q0	Uncertainty interval width
q1	Indicator of the position of the reference calculation within the uncertainty interval
QT	Quantum Technologies AB (Sweden)
RCC	Rank (Spearman's) Correlation Coefficient
REF	Reference calculation
REF_{min}/REF_{max}	Minimum/maximum of the reference calculations provided by all participants
RFO	Fuel outer radius
RIA	Reactivity-initiated accident
SCC	Simple (Pearson's) Correlation Coefficient
SCH	Clad hoop stress at outer part of the clad
SNL	Sandia National Laboratories
SSM	Swedish Radiation Safety Authority (Strålsäkerhetsmyndigheten)
SUNSET	Sensitivity and Uncertainty Statistical Evaluation Tool
TC	Thermocouple
TCI	Temperature of clad inner surface
TCO	Temperature of clad outer surface
TFC	Temperature of fuel centreline
TFM	Maximum fuel temperature
TFO	Temperature of fuel outer surface
ÚJV	Nuclear Research Institute (ÚJV Řež, Czech Republic)
UUB	Upper uncertainty bounds

VTT	VTT Technical Research Centre of Finland Ltd (Teknologian Tutkimuskeskus VTT Oy)
WGFS	Working Group on Fuel Safety (NEA/CSNI)

1. Background and introduction

Following the recommendations from the technical workshop on "Nuclear Fuel Behaviour during Reactivity-Initiated Accidents" organised by the Nuclear Energy Agency (NEA) in September 2009, a first benchmark of the reactivity-initiated accident (RIA) fuel codes was organised within the activities of the Working Group on Fuel Safety. The final report of the first benchmark (NEA, 2013) was approved by the Committee on the Safety of Nuclear Installations (CSNI) in 2013. A second phase of the benchmark was launched in 2014, and those reports were approved by the CSNI in 2015 (NEA, 2016) and 2016 (NEA, 2017). The main conclusions of those two phases were:

- Regarding fast transient thermal-hydraulic post-DNB (departure from nucleate boiling) behaviour, there are major differences between the modelling approaches, resulting in significant deviations between simulations. Unfortunately, there are currently no simple and representative experimental results that allow the different approaches to be validated.
- The models of fuel and clad thermo-mechanical behaviour and the associated materials properties should be improved and validated for RIA conditions.
- The different influential input parameters are identified for fresh fuel. For instance, injected energy, fuel enthalpy, parameters related to the rod geometry (fuel and clad roughness, cladding inside diameter), fuel thermal-expansion model and full width at half maximum of the power pulse come out as influential regarding the maximum value of each output parameter of interest. However, the most influential parameters in the case of irradiated fuel could be different than with fresh fuel.
- Uncertainties cannot fully explain the scatter observed during Phase I of this benchmark exercise.

One recommendation from Phase II of the benchmark was to launch a complementary phase focused on uncertainty and sensitivity analyses on an irradiated case in order to identify the corresponding influential input parameters. In particular, uncertainties regarding fission products distribution, fuel microstructure, clad corrosion state and gap conductance should be investigated.

Considering the results obtained during the first two phases, mainly the large discrepancy regarding RIA thermal-hydraulics modelling, it was decided to limit the exercise to the "PCMI phase", for which data are available from in-pile tests. Therefore, it was proposed to use the CIP0-1 test for this exercise. This test was performed in the CABRI reactor in the sodium loop (for which it would be easier to reach a consensus between the codes in relation to cladding-coolant heat transfer) on an irradiated ZIRLO™-clad UO_2 fuel.

This phase was focused on the assessment of the uncertainty of the results. In particular, the impact of the initial state and key models on the results of the transient were investigated. In addition, a sensitivity study was performed to identify or confirm the most influential input uncertainties.

The assessment of the uncertainty associated with the test prediction is affected by the simulation of the base irradiation to predict the rodlet pre-test conditions. In order to focus this activity on the RIA codes, the state of the rod at the end of the base irradiation, before

the transient, was evaluated with the FRAPCON code, whose input data and results were distributed to every participant.

This report is organised as follows:

- Chapter 2 briefly describes the specifications of the RIA benchmark Phase III;
- Chapter 3 presents the participants and their adopted codes;
- Chapter 4 discusses the main findings of this benchmark, which are illustrated by selected plots comparing the solutions provided by the participants;
- Chapter 5 gives the conclusions of this phase of the RIA benchmark and provides some recommendations for follow-up activities.

References

NEA (2017), "Reactivity-Initiated Accident (RIA) Fuel-Codes Benchmark Phase II: Uncertainty and Sensitivity Analyses, NEA/CSNI/R(2017)1, OECD Publishing, Paris, https://www.oecd-nea.org/jcms/pl_19762.

NEA (2016), "Reactivity Initiated Accident (RIA) Fuel Codes Benchmark Phase II: Volume 1: Simplified Cases Results – Summary and Analysis", NEA/CSNI/R(2016)6/VOL1, OECD Publishing, Paris, https://www.oecd-nea.org/jcms/pl_19710.

NEA (2013), "RIA Fuel Codes Benchmark - Volume 1", NEA/CSNI/R(2013)7, OECD Publishing, Paris, https://www.oecd-nea.org/jcms/pl_19332.

2. Summary of the RIA benchmark Phase III specifications

2.1. Description of the CIP0-1 case

The CIP0-1 experiment was performed in 2002 with UO_2 high burn-up fuel (75 GWd/tU) with ZIRLO™ cladding in the CABRI sodium loop facility, at 280°C and low pressure (~3 bar). No boiling crisis nor failure of the fuel rod occurred during the test.

2.1.1. Characteristics of the CIP0-1 rodlet before the test

The CIP0-1 rodlet was refabricated from an ENUSA fuel rod irradiated in the pressurised water reactor Vandellos 2 in Spain in the frame of a joint Japanese-Spanish R&D programme aimed at studying the behaviour of UO_2 fuel at high burn-up (Watanabe et al., 2005). The UO_2 rod, with an initial uranium 235 enrichment of 4.5% and a ZIRLO™ cladding, had been irradiated for five cycles, from June 1994 to September 2000, until a rod average burn-up of 68 GWd/tU. The burn-up distribution measured along the rod is represented in Figure 2.1.

The detailed characteristics of the rod and the irradiation history in the Vandellos reactor are given in NEA (2013) and Watanabe et al. (2005).

Figure 2.1. CIP0-1 mother rod: Axial burn-up profile

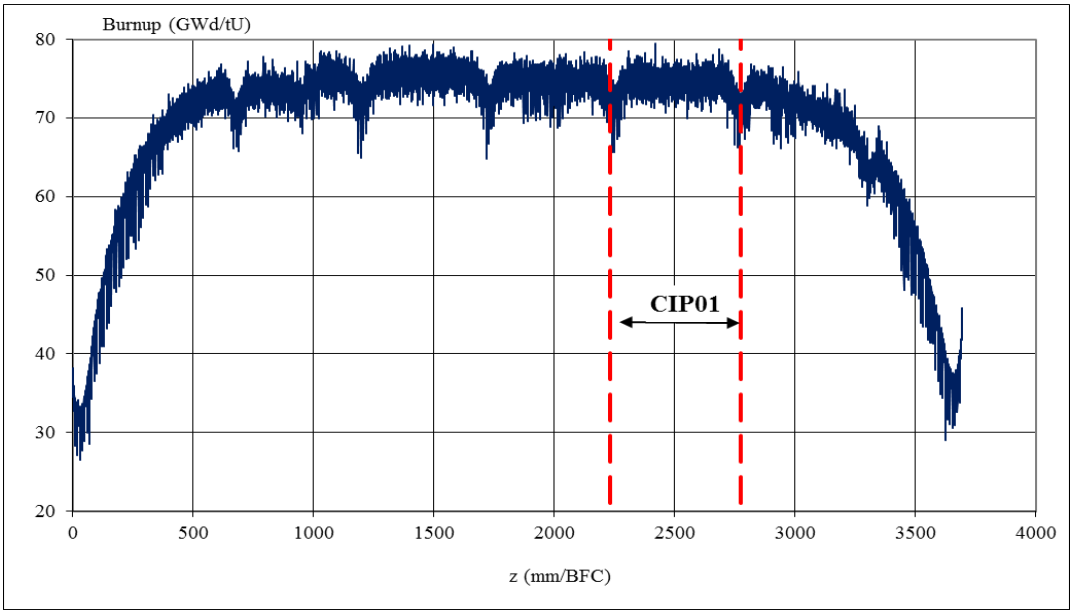

Source: IRSN, 2019.

The examinations performed in the Swedish Studsvik laboratory on the mother rod after irradiation have shown the following results (Petit et al., 2007; Georgenthum et al., 2017):

- rod axial elongation of about 0.8%;
- fissile column axial elongation of 0.93%;

- fission gas release in the free volume: 7.4% of the total fission gas created during the irradiation;
- free volume: 12.26 cm^3;
- plenum pressure: 5.85 MPa at 0°C.

The CIP0-1 rodlet was refabricated from the fifth span of the rod. The rod refabrication and some non-destructive examinations on the rodlet were performed in the Studsvik laboratory. The length of the CIP0-1 test rod was 541 mm. Figure 2.2 represents the measurements of diameter and zirconia thickness on the outer part of the clad. The clad oxidation was significant: the mean zirconia thickness was 80 µm, varying between 50 µm and 110 µm over the length of the sample.

Figure 2.2. CIP0-1 clad zirconia thickness and diameter before the test

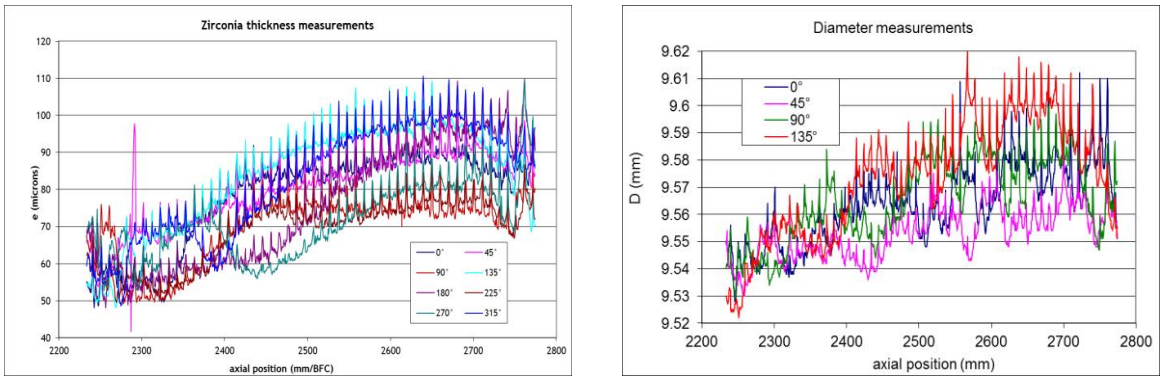

Source: IRSN, 2019.

The cladding was highly hydrided with a mean hydride concentration of about 1 000 ppm. The hydrides were long and oriented in the circumferential direction. No hydride blisters were found, but hydride rims with a thickness of 50 µm were present. On fuel examinations, one can estimate the visible high burn-up structure width to be about 120 ± 30 µm (probably corresponding to a fully restructured high burn-up structure). It is also worth noting the very tight bonding between the fuel and the inner zirconia layer. The inner zirconia thickness is estimated to be roughly equal to 10 µm.

2.1.2. CIP0-1 test characteristics and results

The CABRI CIP0-1 test was performed in 2002 in the sodium loop of the CABRI facility in Cadarache, France. The main characteristics of the power transient were (Petit et al., 2007; Georenthum et al., 2017) (see Figure 2.3):

- maximum core power: P_{max} = 3 692 ± 222 MW;
- core energy deposition: E_{core} = 189.6 ± 11.4 MJ (1.2 s after the beginning of the energy deposition);
- power pulse width at half maximum: 32.4 ± 0.5 ms;
- injected energy in the test rod at peak power node (PPN): 99 ± 6 cal/g (1.2 s after the beginning of the energy deposition.

Figure 2.3. Axial power profile (left), core power and injected energy during the CIP0-1 test (right)

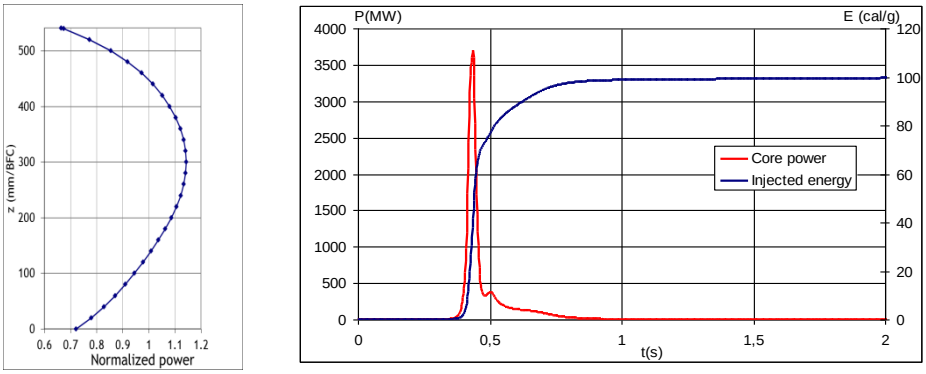

Source: Georgenthum et al., 2017.

According to the measurements performed during and after the test, the rod underwent the power transient without clad failure.

Visual examinations confirmed the non-failure of the rod and showed the high oxide spallation of the rod along all angular orientations with many spalled areas (see Figure 2.4, left panel, white area) of large dimensions (several mm wide and often several cm long). The oxide spalling phenomenon is also noticeable on the clad diameter and zirconia thickness measurements that were performed along four and eight azimuths, respectively (see Figure 2.4, middle and right panels).

Direct comparison between raw clad diameter measurements before and after the test does not allow the clad residual hoop strain to be estimated. The clad diameter measurements have been corrected based on the zirconia thickness measurements before and after the test (see Figure 2.5) in order to calculate the sound clad diameter before and after the test and thus the clad residual hoop strain. The clad residual hoop strain ranges from 0% at both extremities of the rod to 0.5 ± 0.1% at the PPN location. According to the rod puncturing, the fission gas release was estimated to be 13-16% of the creation and the final free volume pressure at 20°C was 29 ± 22.6 bar.

Figure 2.4. Visual examination of the rod after the test (left), zirconia thickness (middle) and clad diameter measurements (right)

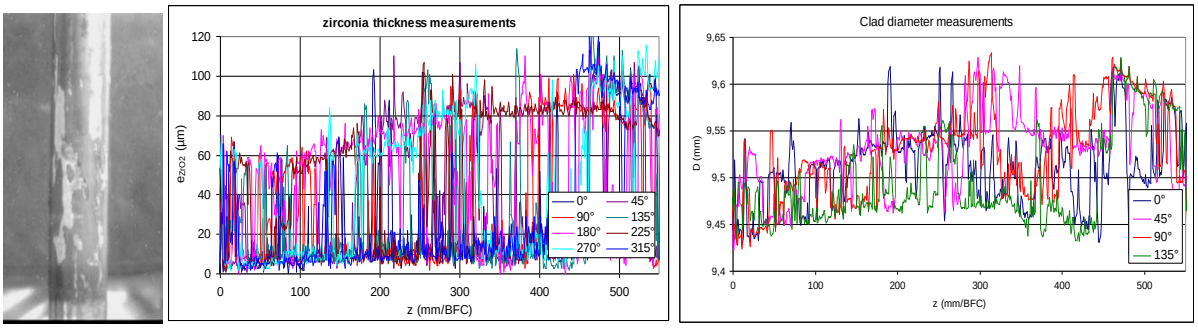

Source: Georgenthum et al., 2017.

Figure 2.5. Zirconia thickness measurements before and after the test (left), raw clad diameter measurements before and after the test (middle) and corrected diameter (i.e. sound clad diameter) measurements before and after the test (right)

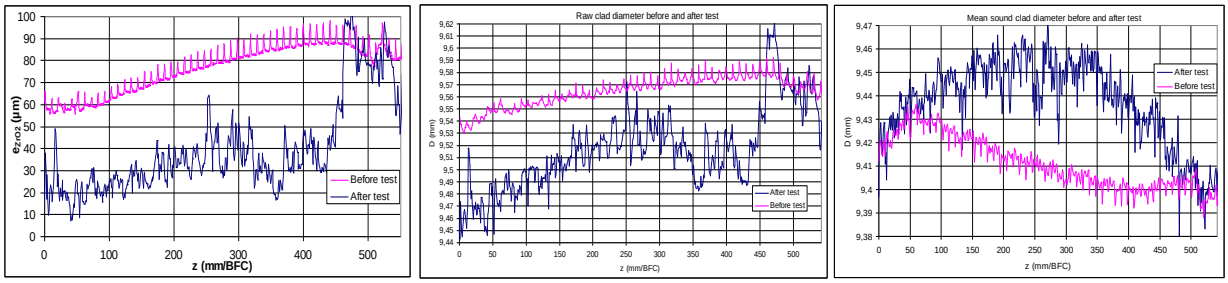

Source: Georgenthum et al., 2017.

2.2. CIP0-1 initial state evaluation

As stated in the introduction, the initial state of the rod, after base irradiation, was evaluated with the FRAPCON V4.0 P1 code.

FRAPCON calculations were done considering 18 axial meshes, 16 radial meshes in the fuel for the thermo-mechanical calculations, 45 radial meshes and a FRAPFGR model for the gas calculations. Some end-of-base irradiation data mandatory for the reactivity-initiated accident (RIA) test calculation were extracted from the axial meshes 12, 13 and 14, corresponding to the span five of the rod.

The corresponding FRAPCON input and output data files were given to the participants.

The following extracted data were also given to the participants (some examples are illustrated in Figure 2.6):

- Rod geometry after cooling down (at 20°C): fuel outer, clad inner and outer radii in each axial mesh.
- In the fuel, as a function of radial and axial meshes or nodes:
  - plutonium content at the nodes (%);
  - local burn-up at the nodes (at% or GWd/tU);
  - end-of-life temperature (before cooling phase) at the nodes;
  - radial power profile at the nodes;
  - fuel density in each mesh (cm^3/g);
  - porosity at the nodes;
  - stoichiometry in each mesh;
  - grain radius: in each mesh (µm);
  - total gas retained in the meshes (cm^3STP/g) (STP: standard temperature and pressure, 0°C and one bar);
  - intragranular gas in the meshes (cm^3STP/g).

Figure 2.6. Examples of FRAPCON radial profile output at peak power node location

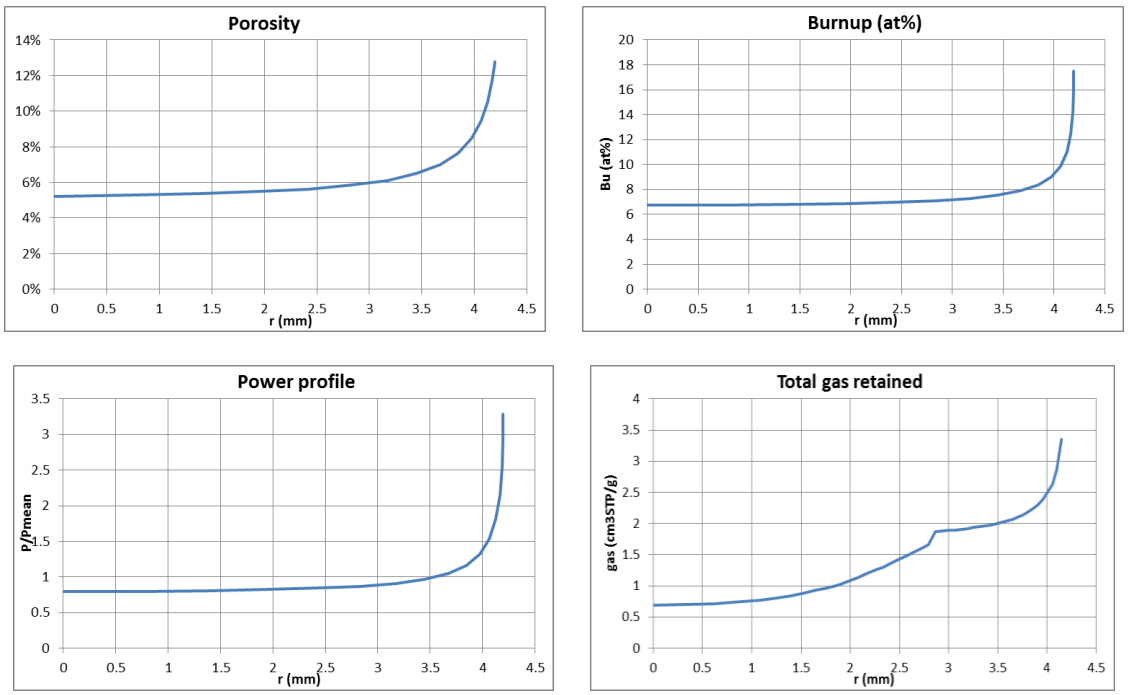

Source: IRSN, 2019.

2.3. Methodology

2.3.1. Uncertainty analysis methodology

Among all the available uncertainty analysis methods, the probabilistic input uncertainty propagation method is so far the most widely used in nuclear safety analysis (Glaeser, 2008). With this method, the fuel codes are treated as "black boxes" and the input uncertainties are propagated to the simulation model output uncertainties via the code calculations, with sampled data from known or assumed distributions for key input parameters (Zhang, Segurado and Schneidesch, 2011). The input parameters of interest may also include uncertain material properties, model parameters, etc.

The method consists of the following steps:

- Specification of the problem: all relevant code outputs and corresponding uncertain parameters for the codes, plant modelling schemes, and plant operating conditions are identified.
- Uncertainty modelling: the uncertainty of each uncertain parameter is quantified by a probability density function based on engineering judgement and experience feedback from code applications to separate tests, integral tests and to full plant simulation. If dependencies between uncertain parameters are known and judged to be potentially important, they can be quantified by correlation coefficients.
- Uncertainty propagation through the computer code: the propagation is represented by Monte-Carlo simulations (Gentle, 1985). In Monte-Carlo simulations, the

computer code is run repeatedly, each time using different values for each of the uncertain parameters. These values are drawn from the probability distributions and dependencies chosen in the previous step. In this way, one value for each uncertain parameter is sampled simultaneously in each repetition of the simulation. The results of a Monte-Carlo simulation lead to a sample of the same size for each output quantity.

- Statistical analysis of the results: the output sample is used to get any typical statistics of the code response, such as mean or variance, and to determine the cumulative distribution function (CDF). The CDF makes it possible to derive the percentiles of the distribution.

A simple way to get information on percentiles is to use order statistics (Conover, 1999), which is a well-established and shared methodology in the nuclear community, and hence recommended for this activity.

The principle of order statistics is to derive results from the ranked values of a sample. If $(X^1,\ldots,X^N)$ denotes a sample of any random variable, X, and $(X^{(1)},\ldots,X^{(N)})$ the corresponding ranked one, order statistics first provide an estimation of the percentile of interest since the α-percentile can be estimated by $X^{(\alpha N)}$. Moreover, it turns out that the CDF of $X^{(k)}$, $F_X(X^{(k)})$, follows the beta law $\beta(k,N-k+1)$, which does not depend on the distribution of X. This key result allows quantifying the probability that any ranked value is smaller than any percentile by the following formula:

$$P(X^{(k)} \leq X_\alpha) = F_{\beta(k,N-k+1)}(\alpha)$$

where $F_{\beta(k,N-k+1)}$ denotes the CDF of the beta law $\beta(k,N-k+1)$.

This equation can then be used to derive:

1. Lower and upper bounds of a percentile of interest, given the sample size N and the confidence level γ that controls the probability that $X^{(k)} \leq X_\alpha$. For this purpose, it is necessary to solve the equation $F_{\beta(k,N-k+1)}(\alpha)= \gamma$.
2. The minimal sample size (and therefore the minimal number of code runs) to perform in order to obtain a lower or upper bound of a given percentile with a given confidence level. It leads to the so-called Wilks' formula (Wilks, 1941):

$$N = \ln(1-\gamma)/\ln(\alpha)$$

and Guba's estimate in case of multiple output parameters in Guba, Makai and Pal (2003).

Order statistics are widely used since no information is needed on the distribution of the random variable. Moreover, this method is very simple to implement, which makes it extremely interesting for licensing applications to nuclear safety analyses.

The probabilistic input uncertainty propagation method was selected due to its simplicity, robustness and transparency. The highly recommended sample size is set to 200 (i.e. 200 code runs must be performed). Strong justifications should be given if a lower number of code runs is performed. The sample is constructed according to the selected probability density functions coming from the uncertainty modelling step and assuming independence between input parameters following a simple random sampling.

We focus on the estimation of a lower (or upper) bound of the 5% (or respectively 95%), percentiles (α) at confidence level (γ) higher than 95%.

For N = 200 and α= 0.05 or 0.95, the previous equations lead to:

$$P(X^{(5)} \leq X_{5\%}) = 0.97$$

$$P(X^{(196)} > X_{95\%}) = 0.97$$

the lower (or upper) bound is defined in this benchmark by $X^{(5)}$ (or respectively $X^{(196)}$). They are denoted LUB and UUB respectively in this document. Note that a one-sided approach is used here, i.e. we focus on percentiles and not on interval and that the bounds are estimated separately.

2.3.2. Sensitivity analysis methodology

In addition to the uncertainty analysis, a complementary study was performed to gain qualitative insight on the most influential input parameters.

This work was done based on a sensitivity analysis using the 200 code runs previously obtained. More precisely, if Y denotes the response of interest and $\{X_i\}_{i=1,\ldots,p}$ the set of p uncertain input parameters (also called regressors), it is recommended to compute Spearman-type correlation coefficients.

The Spearman's rank correlation coefficient (RCC) is similar to the classical linear simple correlation coefficient (i.e. $\rho_i = \frac{Cov(Y, X_i)}{\sigma_X \sigma_Y}$), but replaces input and output values by their respective ranks. Working with ranks allows one to extend the previous underlying linear regression model to a monotonic non-linear one. In the presence of non-linear but monotonic relationships between the response and each of the p regressors, use of the rank transform can substantially improve the resolution of sensitivity analysis results (McKay, 1988).

The partial rank correlation coefficient (PRCC) provides an improved measure of the monotonic relation between the response and one of the p regressors by removing trends associated with other variables.

Based on this information (RCC or PRCC), the most influential uncertain input parameters can be identified.

2.4. Specification of uncertain input parameters

In the RIA benchmark Phase II, the influence of 19 uncertain input parameters was studied on the results of a fresh fuel RIA test in pressurised water reactor conditions. The input parameters were classified into four categories:

- parameters associated with the fuel rod design, bounded by allowable manufacturing tolerances;
- thermal-hydraulics boundary conditions;
- core power boundary conditions;
- physical properties/key models.

End-of-life fuel state parameters were added in the present study; on the other hand, parameters associated with the fuel rod design and the thermal-hydraulic boundary conditions were not considered.

Table 2.1 provides the specified input parameters as well as the information related to their uncertainty. In most cases, a normal distribution has been assigned to input parameters for simplicity's sake. Their standard deviation has been taken as half of the maximum of the absolute value of the difference between their nominal value and their upper or lower bound. In order to avoid unphysical numerical values, the sampling is performed (i.e. truncated) between the upper and lower bounds.

Note that some uncertainties on input parameters displayed by Table 2.1 have been fixed by expert judgement. The question of the influence of the uncertainty modelling and more generally of the quantification process to derive input uncertainties is beyond the scope of this benchmark. This topic could be studied in further work.

Finally, although the dependency between the pulse width and the injected energy was well known, it was not considered.

Depending on the code used, it might be difficult to modify some recommended input parameters. In this case, the parameters could be discarded, but this information had to be clearly mentioned in the participants' contributions.

Table 2.1. List of time/height-dependent output parameters to be provided

Input parameter uncertainty	Distribution				
	Reference/ mean value	Standard deviation	Type	Lower bound	Upper bound
1. End-of-life fuel state					
Fuel-clad radial gap (at 20°C) (µm)	10.		Uniform	0.1	20
Cladding roughness (µm)	0.1		Uniform	10^{-6}	2.
Fuel roughness (µm)	0.1		Uniform	10^{-6}	2.
Zirconia thickness (multiplying coefficient C)	Half of the upper value (C =1/2)		Uniform	Total spalling (C=0)	Before test measurement (C=1)
2. Core power boundary conditions					
Injected energy in the rod at peak power node location (cal/g)	99	3	Normal	93	105
Radial power profile ("peaking factor")	FRAPCON results (i.e. 0)	0.125	Normal	-0.25	0.25
Pulse width (ms)	Measurement 32	0.75	Normal	30.5	33.5
3. Physical properties/key models					
Fuel thermal conductivity model (multiplying coefficient)	1.00	5%	Normal	0.90	1.10
Fuel thermal-expansion model (multiplying coefficient)	1.00	5%	Normal	0.90	1.10
Fuel enthalpy/heat capacity (multiplying coefficient)	1.00	1.5%	Normal	0.97	1.03
Clad thermal-expansion model (multiplying coefficient)	1.00	5%	Normal	0.90	1.10
Clad yield stress (multiplying coefficient)	0.9	5%	Normal	0.81	0.99

2.5. Output specification

After input uncertainty propagation, each participant gave lower and upper bounds associated with all time/height trended output parameters listed in Table 2.2.

In addition, the results of the calculation with the nominal value of the input parameters, also called reference calculation, were provided.

Among the outputs of interest, the clad failure prediction parameter (CFP) had to be defined by each participant as a function of time. This parameter should be a continuous function such that: if CFP < 1 no failure is predicted, if CFP ≥1 a failure is predicted (example: J/Jc, SED/CSED, ECTH/ECTHc, with respectively Jc, CSED and ECTHc the critical values of J, SED and ECTH).

Moreover, the reference, lower and upper bound values for the maximum of each output parameter in Table 2.2 had to be given.

Table 2.2. List of time/height-dependent output parameters to be provided

Parameter	Unit	Description (function of time/height parameter)
EINJ	cal/g	Injected energy (radial averaged) as a function of time (at z= peak power node)
DHR	cal/g	Variation of radial average enthalpy with respect to initial conditions of the transient in the rodlet as a function of time (at z=peak power node) (please note that DHR(t=0)=0)
TFC	°C	Temperature of fuel centreline as a function of time (at z= peak power node)
TFM	°C	Maximum fuel temperature as function time (at z= peak power node)
TFO	°C	Temperature of fuel outer surface as a function of time (at z= peak power node)
TCI	°C	Temperature of clad inner surface as a function of time (at z= peak power node)
TCO	°C	Temperature of clad outer surface as a function of time (at z= peak power node)
TNa1	°C	Temperature of Na coolant as a function of time (at z=25 cm/BFC)
TNa2	°C	Temperature of Na coolant as a function of time (at z=47 cm/BFC)
ECTH	%	Clad total (thermal + elastic + plastic) hoop strain at the outer part of the sound clad as a function of time (at z= peak power node)
ECT	mm	Clad total axial elongation as a function of time
EFT	mm	Fuel column total axial elongation as a function of time
SCH	MPa	Clad hoop stress at outer part of the clad as a function of time (at z= peak power node)
RFO	mm	Fuel outer radius as a function of time (at z= peak power node)
GAP	µm	Fuel-clad gap width as a function of time (at z= peak power node)
HFC	W/m²/K	Fuel-to-clad heat exchange coefficient as a function of time (at z= peak power node)
ETZ	%	Clad permanent hoop strain at the end of transient at the metal/oxide interface at end of the transient as a function of height
FGR	mm^3	Fission gas volume release as a function of time, at one bar and 0°C
CFP	()	Clad failure prediction as a function of time

Finally, regarding the sensitivity analysis, participants evaluated the partial rank correlation coefficients (or Spearman's if the PRCC was not available) associated to each uncertain input parameter and for each output of interest, at the times defined in Table 2.3. It was also requested to perform the same analysis for the maximum (with respect to time or height) of each output parameter.

Table 2.3. List of different times for sensitivity analysis scalar output

Time parameters	t_1	t_2	t_3	t_4
Definition	Beginning of power pulse	Time of pulse maximum power	End of power pulse	End of calculation
Value	0.0s	0.437s	1.2s	50s

References

Conover, W. (1999), *Practical Non-parametric Statistics*, Wiley, New York, NY.

Gentle, E. (1985), "Monte-Carlo methods", *Encyclopaedia of Statistics*, Vol. 5, pp. 612-617, John Wiley and Sons, New York, NY.

Georgenthum, V., C. Folsom, A. Moal, O. Marchand, R. Williamson, H. Ban and D. Wachs (2017), "SCANAIR-BISON Benchmark on CIP0-1 RIA Test", 2017 Water Reactor Fuel Performance Meeting, 10-14 September 2017, Jeju Island, Korea, www.osti.gov/biblio/1409689.

Glaeser, H. (2008), "GRS method for uncertainty and sensitivity evaluation of code results and applications", *Science and Technology of Nuclear Installations*, Vol. 2008, http://dx.doi.org/10.1155/2008/798901.

Guba, A., M. Makai and L. Pal (2003), "Statistical aspects of best-estimate method-I", *Reliability Engineering & System Safety*, Vol. 80/3, pp. 217-232, https://doi.org/10.1016/S0951-8320(03)00022-X.

McKay, M.D. (1988), "Sensitivity and uncertainty analysis using a statistical sample of input values", Chapter 4 in: Ronen, Y. (ed.), *Uncertainty Analysis*, CRC Press, FL.

NEA (2013), "RIA Fuel Codes Benchmark - Volume 1", NEA/CSNI/R(2013)7, OECD Publishing, Paris, https://www.oecd-nea.org/jcms/pl_19332.

Petit, M., V. Georgenthum, J. Desquines, T. Sugiyama and M. Quecedo (2007), "A comparative analysis of CABRI CIP0-1 and NSRR VA-2 reactivity initiated accident", EUROSAFE 2007: Towards convergence of technical nuclear safety practices in Europe, Berlin, Germany, 5-6 November 2007.

Watanabe, S., S. Abeta, J. Serna, J. Alonso, T. Sendo and P. Gonzalez (2005), "Post-irradiation examinations on 67-75 GWd/t rods for confirmation of the integrity and appropriate performance of the claddings for future", *Proceedings of the 2005 Water Reactor Fuel Performance Meeting*, Kyoto, Japan, 2-6 October 2005.

Wilks, S.S. (1941), "Determination of sample sizes for setting tolerance limits", *The Annals of Mathematical Statistics*, Vol. 12/1, pp. 91-96, https://www.jstor.org/stable/2235627.

Zhang, J., J. Segurado and C. Schneidesch (2011), "Towards an industrial application of statistical uncertainty analysis methods to multi-physical modelling and safety analyses", Proceedings of the OECD/CSNI Workshop on Best-Estimate Methods and Uncertainty Evaluations, Barcelona, Spain, 16-18 November 2011.

3. Participants and codes used

The participants of the RIA benchmark Phase III, which represented nine countries, were:

- TRACTEBEL (ENGIE) from Belgium;
- ÚJV Řež (ÚJV) from the Czech Republic;
- Institute for Radiological Protection and Nuclear Safety (IRSN) and Alternative Energies and Atomic Energy Commission (CEA) from France;
- VTT Technical Research Centre of Finland Ltd (VTT) from Finland;
- Gesellschaft für Anlagen- und Reaktorsicherheit (GRS) GmbH from Germany;
- Italian National Agency for New Technologies, Energy and Sustainable Economic Development (ENEA) from Italy;
- Japan Atomic Energy Agency (JAEA) from Japan;
- Swedish Radiation Safety Authority (SSM) represented by Quantum Technologies from Sweden (QT);
- Paul Scherrer Institut (PSI) from Switzerland.

As can be seen, research institutions, utilities, technical safety organisations and safety authorities were all well represented. Ten participants contributed to the study. They are listed in Table 3.1 along with the codes they used for base irradiation, transient simulation and sensitivity/uncertainty analyses.

In terms of computer fuel rod codes used, the spectrum was also large for base irradiation and transient simulations. Brief descriptions of the computer codes are given in Annexes A and B.

Table 3.1. Benchmark collected contributions (code combinations used for Phase III)

Organisation	Codes		
	Base irradiation	Transient simulation	Statistical analysis
CEA	ALCYONE V1.4	ALCYONE V1.4	URANIE V4.1
ENEA	TRANSURANUS	TRANSURANUS, Version 2018	TRANSURANUS (TuStat)
GRS	Given FRAPCON results	TESPA-ROD_20.3.1	SUSA 4.1
IRSN	FRAPCON 4.0 P1	SCANAIR V_7_8	SUNSET V2.1
JAEA	FEMAXI-8	RANNS 8.1.102f	DAKOTA 6.5
PSI	FALCON	FALCON v1.4.1, GRSW-A 3.02	Python internal tool
QT-SSM	Given FRAPCON results	SCANAIR V_7_8	SUNSET V2.1
TRACTEBEL	FRAPCON 4.0P1	FRAPTRAN 2.1	DAKOTA 6.2
ÚJV	TRANSURANUS	TRANSURANUS v1m3j12modCEZ18	ROOT
VTT	Given FRAPCON results	SCANAIR V_7_8	Python internal tool

Source: IRSN, 2019.

Some participants fully initialised their CIP0-1 analyses with the output from the FRAPCON results. For other data needed for the RIA calculations but not provided by FRAPCON, hypotheses were formulated.

Those participants who could not fully initialise their CIP0-1 input data with FRAPCON output used their own means of calculating the non-initialisable parameters, and tried to match the FRAPCON results as much as possible, notably fission gas distribution.

As an illustration, the intragranular and grain boundary gas distributions, as given by the participants, are plotted in Figure 3.1 and compared to the FRAPCON output data. While the grain boundary gas distributions are quite similar for all participants and consistent with FRAPCON output, this is not the case for intragranular gas distributions.

Figure 3.1. Intragranular and grain boundary gas radial distribution for different participants

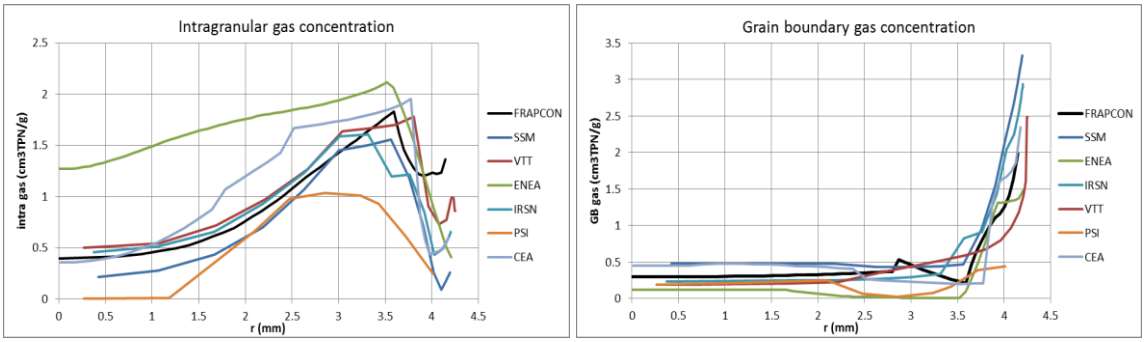

Source: IRSN, 2019.

4. Results summary and analysis

This chapter is devoted to the synthesis of the RIA benchmark Phase III results. The first two sections focus on the available experimental results that are used in the analysis of participants' contributions and on the methodology to perform the analysis. They are followed by a summary of the main points.

4.1. Experimental results

Among the outputs listed in Table 2.2, experimental information is available for the Na coolant temperature (TNa1, TNa2), clad elongation (ECT), clad residual hoop strain (ETZ) and fission gas release (FGR).

Figures 4.1-4.3 display the experimental time trends associated to TNa1, TNa2, ECT and ETZ. They correspond to measurements and associated uncertainty defined according to an internal experimental report. More precisely:

- TNa1, TNa2 (Figures 4.1 and 4.2): the left panel provides the time trends given by three sensors. The right panel includes the average temperature of the three sensors as well as the experimental uncertainty. This last quantity is defined, for each time considered, as the interval [TNa_{min} – 3°C; TNa_{max} + 3°C] where TNa_{min}, (or respectively TNa_{max}), is the minimum (or respectively the maximum), of the temperature measured by the three sensors.
- ECT (Figure 4.3, left panel): the three time trends correspond to the raw measurements (exp) and to the uncertainty defined for each considered time as [exp – 2 mm; exp + 2 mm]. The uncertainty was set to zero before the transient.
- ETZ (Figure 4.3, right panel): the three times trends correspond to a smoothing of the measurements computed by (quadratic) regression and to an uncertainty of 22.

Finally, the experimental value for the FGR is the final value of the experimental time trend. It is equal to 88 298 mm^3 with an uncertainty of 6.3%.

Figure 4.1 Experimental data for TNa1 (z=25cm/BFC)

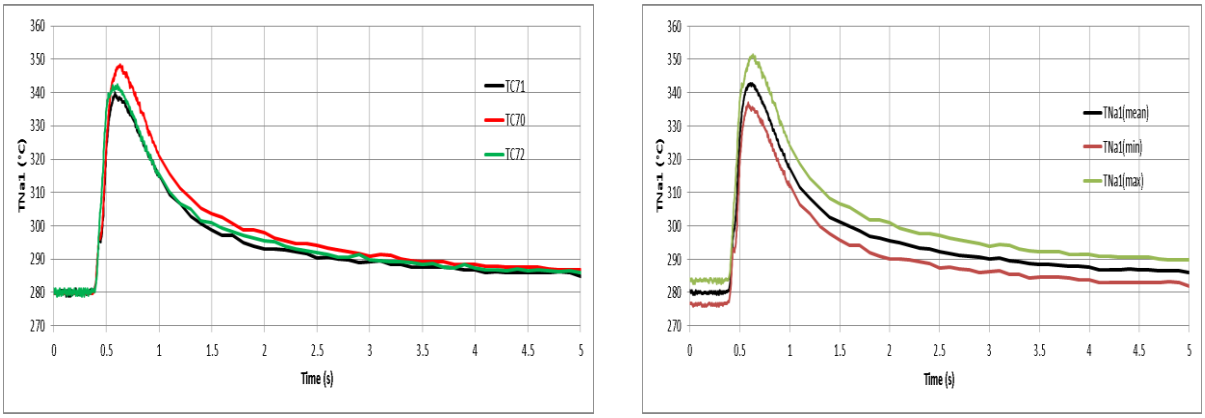

Source: IRSN, 2019.

Figure 4.2. Experimental data for TNa2 (z=47 cm/BFC)

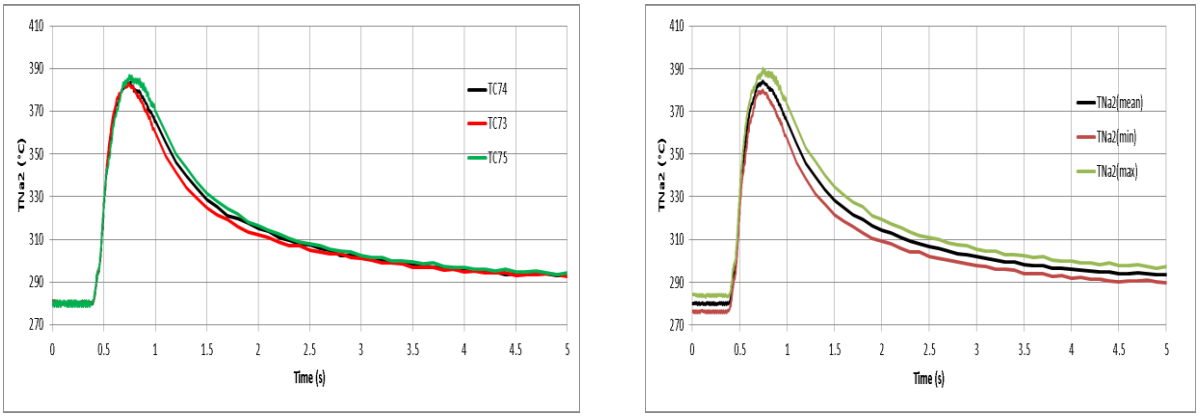

Source: IRSN, 2019.

Figure 4.3. Experimental data for clad total axial elongation and clad residual hoop strain

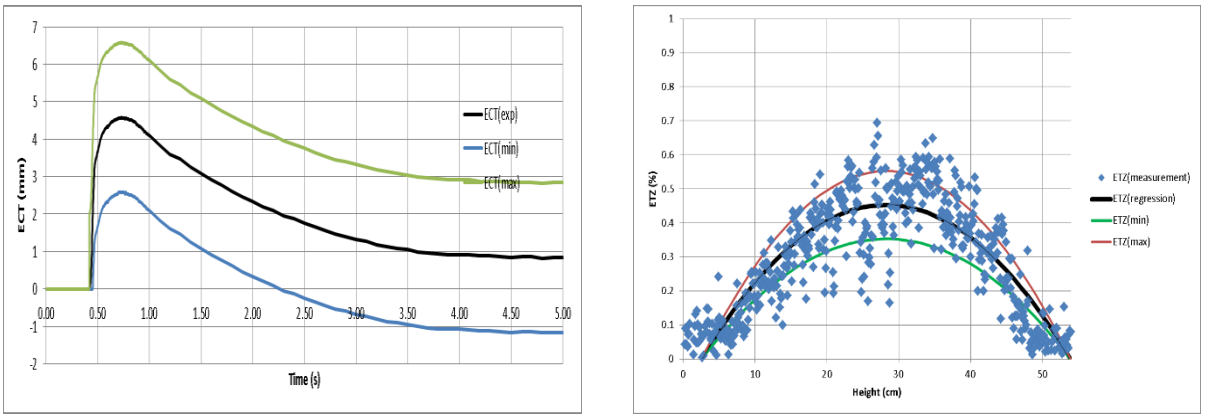

Note: ECT: clad total axial elongation; ETZ: clad residual hoop strain.
Source: IRSN, 2019.

4.2. Methodology

This section provides an overview of the methods and tools that were used to analyse the participants' results.

4.2.1. Uncertainty analysis

A first study is performed on the time/height trend outputs. The focus then moves to the results associated with scalar outputs.

Time/height trend outputs

For each output, the analysis is focused on the uncertainty interval ([LUB, UUB]). More precisely, three kinds of synthesis have been performed.

They are based on the evolution with respect to the time of:

- the union of all participants' intervals, i.e. [LUB_{min}, UUB_{max}] with LUB_{min} (respectively UUB_{max}) defined as the minimum (respectively maximum) of all lower uncertainty bounds (LUBs) and upper uncertainty bounds (UUBs) (Figure 4.4);
- the uncertainty interval (or band) width of each participant:

$$q_0 = UUB - LUB$$

- for sodium temperature, ECT and ETZ, the position of the experimental value within the uncertainty band and computed for each participant as:

$$r_{exp} = \frac{UUB - EXP}{UUB - LUB}$$

By construction, if this last quantity varies between zero and one, the experimental value is inside the uncertainty band. Otherwise, it is outside.

Figure 4.4. Example of union of participants' intervals

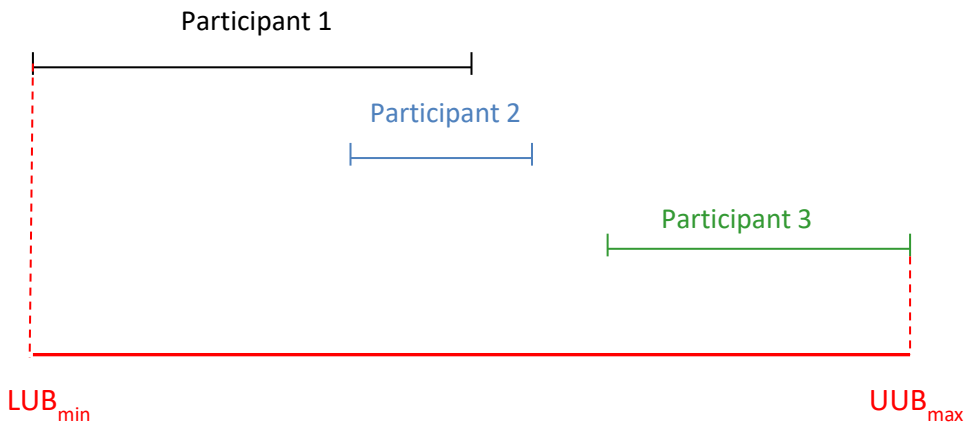

Source: NEA, 2018

Scalar outputs

The maximal values (as a function of time or height) are considered for each output.

A first synthesis relies on the aggregation of all participants' results: it is based on two different treatments. The relative uncertainty interval is first computed. For each scalar output, the interval bounds are defined respectively by LUB_{min} and UUB_{max} divided by the average of all of the reference calculations. The relative uncertainty width is then the difference between these bounds.

Moreover, it is also interesting to analyse each participant's uncertainty result separately and to compare them to reference data when experimental information is available. This can be achieved with the formal approach of information synthesis developed by the IRSN (Baccou and Chojnacki, 2014). This approach was introduced in Destercke and Chojnacki (2008) and already applied during the PREMIUM benchmark (NEA, 2017a). It is composed of three steps, which are fully described in Baccou and Chojnacki (2014).

For the purpose of this study, we only focus on:

- information modelling;
- information evaluation.

The two steps are briefly recalled in the sequel starting from participants' contributions, i.e. uncertainty interval ($[LUB, UUB]$) and reference value (REF) and from LUB_{min} (respectively UUB_{max}) defined as the minimum (respectively maximum) of all LUBs (respectively UUBs).

Information modelling - A triangular model as displayed in Figure 4.5 is associated with each output of interest and each contribution. For a source s (i.e. a contribution) and an output variable *v*, its parameterisation is denoted $\pi_{s,v}(t)$ and defined by:

$$\pi_{s,v}(t) = \begin{cases} \dfrac{1}{REF - LUB}(t - LUB), & if\ t \in [LUB, REF], \\ \dfrac{1}{REF - UUB}(t - UUB), & if\ t \in [REF, UUB] \end{cases} \quad (1)$$

Figure 4.5. Information modelling associated with a source

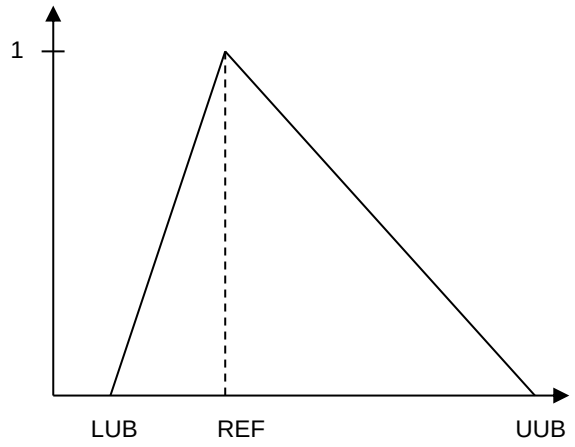

Source: NEA, 2018.

Information evaluation - It is achieved by computing the two following quantities:

- Informativeness: this indicator measures the precision of the information. It does not require any experimental information. It is related to the ratio between the area of the triangle (A(T)) and the area associated to the uniform possibility defined on $[LUB_{min}, UUB_{max}]$ (A(U)) (Figure 4.6, left panel) and that represents the complete ignorance:

$$I_v = 1 - \frac{A(T)}{A(U)} = 1 - \frac{UUB - LUB}{2(UUB_{max} - LUB_{\min})}$$

A value close to one (respectively zero point five) therefore means that the uncertainty range is narrow (respectively large).

Figure 4.6. Computation of the informativeness (left) and calibration (right) indicators associated to a given output.

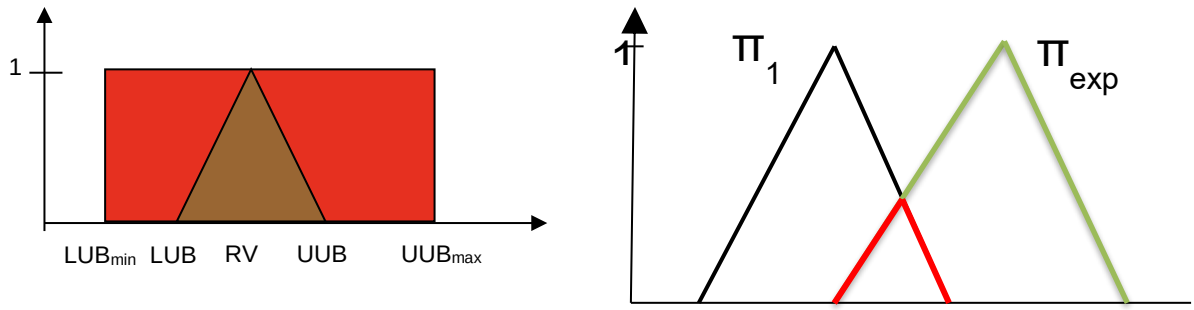

Note:$I_v = 1 - r$ where r is the ratio between the area in brown and the sum of the area in brown and red, C_v is the ratio between the red triangle (intersection between participant and experimental results) and green one (experimental result).

Source: IRSN, 2019.

- **Calibration:** This indicator measures the agreement between information provided by the source and experimental information (experimental value, EXP and experimental uncertainty [LUB_{exp},UUB_{exp}] in our case). Similarly to each participant's contribution, this experimental information can be represented by a triangle function of type (1) (denoted T_{exp}) where REF, LUB and UUB are replaced by EXP, LUB_{exp}, UUB_{exp} respectively. The calibration indicator is then defined by the ratio between the area of the intersection between the source and experimental results and the area of the experimental result (Figure 4.6, right panel):

$$C_v = \frac{A(T \cap T_{exp})}{A(T_{exp})}$$

A value close to one (respectively zero) therefore represents a high (respectively low) coherence with the experimental results.

4.2.2. Sensitivity analysis

Several approaches are available to perform sensitivity analysis (Iooss and Lemaitre, 2015). However, their mathematical treatment follows the same steps as for uncertainty analysis: input sampling, propagation through the evaluation model and analysis of the results leading to qualitative insight on the most influential input parameters.

In this benchmark, the input sample comes from the random sample constructed after uncertainty analysis and the analysis step consists of evaluating correlation coefficients.

As mentioned in the specifications, the sensitivity analyses are based on Spearman rank correlation coefficients (rank [Spearman's] correlation coefficient – RCC; or partial rank correlation coefficient – PRCC). The most influential input parameters have been identified for each participant, based on their calculated correlation coefficients and using a fixed significance threshold (to be exceeded) of 0.25.

The synthesis is achieved by averaging, for each output, the number of participants that consider a given parameter as influential. This short calculation has been repeated for the

four fixed times (see Table 2.3) when the correlation coefficients were evaluated and for maximum values, as required in the specifications. Moreover, in order to draw conclusions, for practical issues, the results have been summarised with respect to groups of outputs corresponding to one type of behaviour (fuel thermal and mechanical behaviour, clad thermal and mechanical behaviour, gap size, fuel-to-clad heat exchange, fission gas release and clad failure), following the rule that if an input parameter is influential for an output associated with a given behaviour, it is considered as influential for the whole group.

4.3. Comparison with experimental results

This analysis is focused on the outputs for which experimental information is available.

4.3.1. Reference case vs. experimental measurements

The coolant temperature calculations and measurements during the transient are represented in Figure 4.7 for the two axial locations (TNa1 and TNa2).

Figure 4.7. Sodium temperature TNa1 (z=25 cm/BFC) and TNa2 (z=47 cm/BFC)

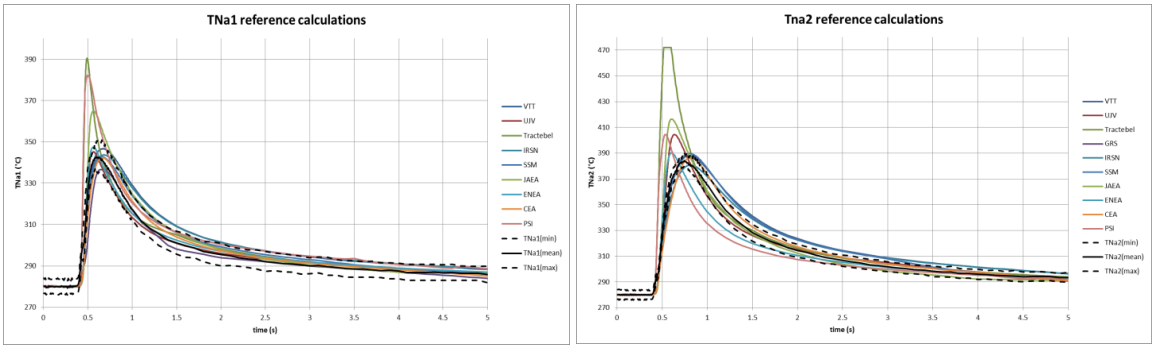

Source: IRSN, 2019.

The experimental measurement general trend was well caught by all of the participants. The coolant temperature increase was nevertheless too quick and too large for a majority of the participants.

The dispersion of reference calculations at the beginning of the transient and on the peak temperature (~90°C) is large, especially for TNa2, which is measured at a higher axial location: the forced convection in sodium coolant is probably not correctly computed for some codes. In the second phase (time >1 s), the dispersion is rather low (< 20°C).

As shown in Figure 4.8, there is some dispersion of the clad permanent hoop strain calculations with a ratio of two between the highest (~0.5%) and the lowest values (~0.25%). Nevertheless, even if participants' calculations slightly underestimated the measurements, the calculations are consistent and close to the lower bound of the measurements.

Figure 4.8. Clad permanent hoop strain at the end of the transient as a function of axial location

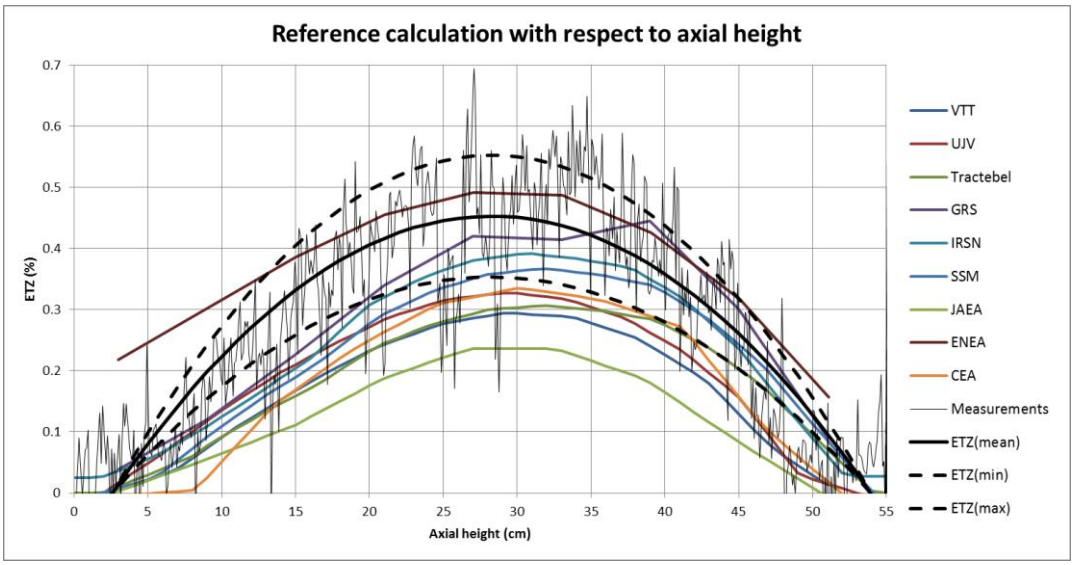

Source: IRSN, 2019.

There is a good agreement between calculations and measurements for the clad elongation (Figure 4.9): the calculations are rather dispersed, but remain in the uncertainty band for all participants almost all along the transient.

Figure 4.9. Clad elongation as a function of time

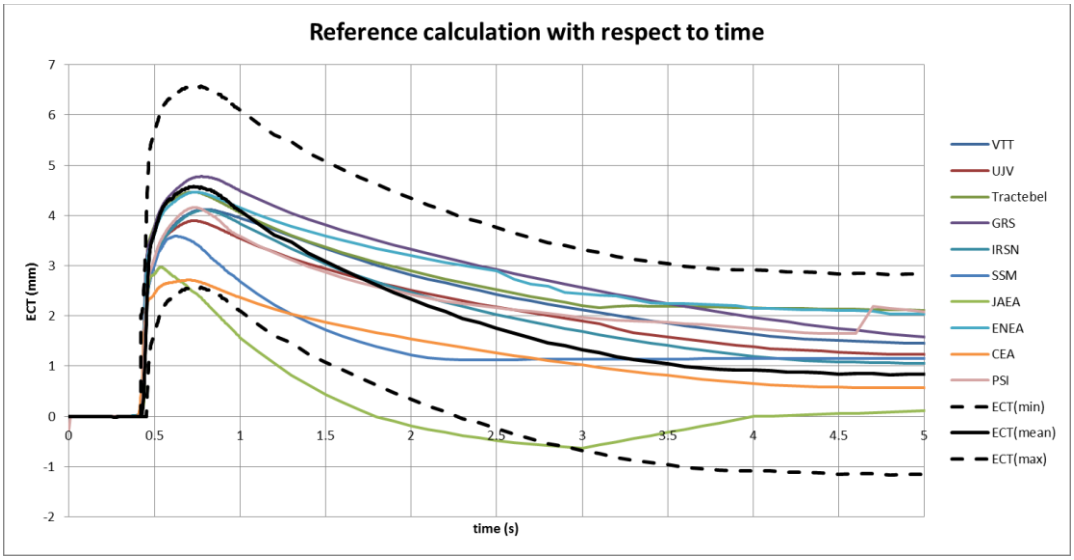

Source: IRSN, 2019.

As already observed in Phase I, the fission gas release calculations are strongly dispersed, with one order of magnitude between the highest and the lowest evaluations (Figure 4.10).

Only one of the participants calculated a final FGR inside the experimental uncertainty band.

Figure 4.10. Fission gas release calculation as a function of time and measurements after the test

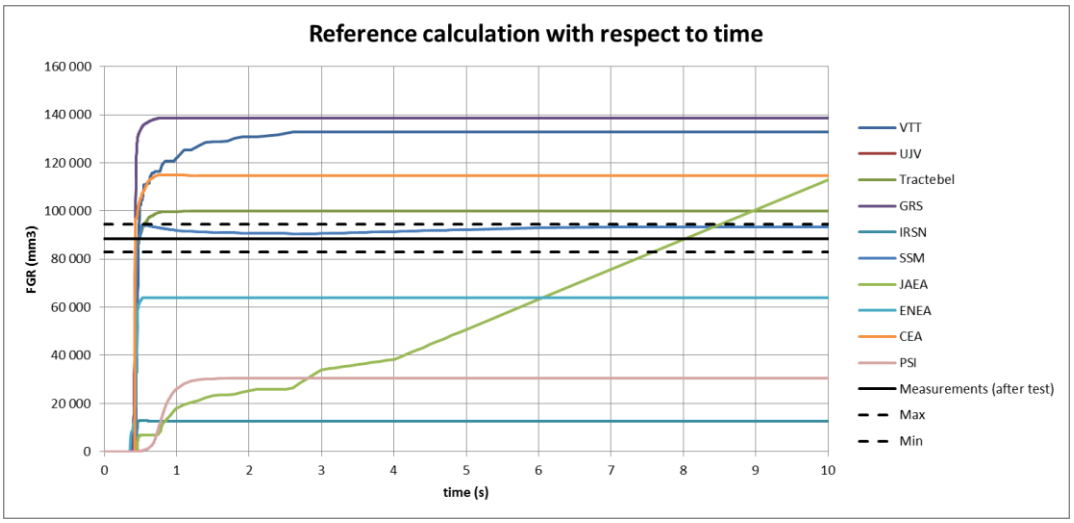

Source: IRSN, 2019.

4.3.1. Uncertainty results vs. experimental measurements

This section is devoted to a comparison of the participants' contributions, taking into account the uncertainties on input data. See above for a description of the synthesis method.

Time/height trend output

The uncertainty interval width calculated by every participant for TNa1 and TNa2 is represented in Figure 4.11.

Except for one participant, the uncertainty interval widths are very similar for all participants and very low after 1.5 s.

Figure 4.11 Uncertainty interval widths for sodium coolant temperatures TNa1 and TNa2

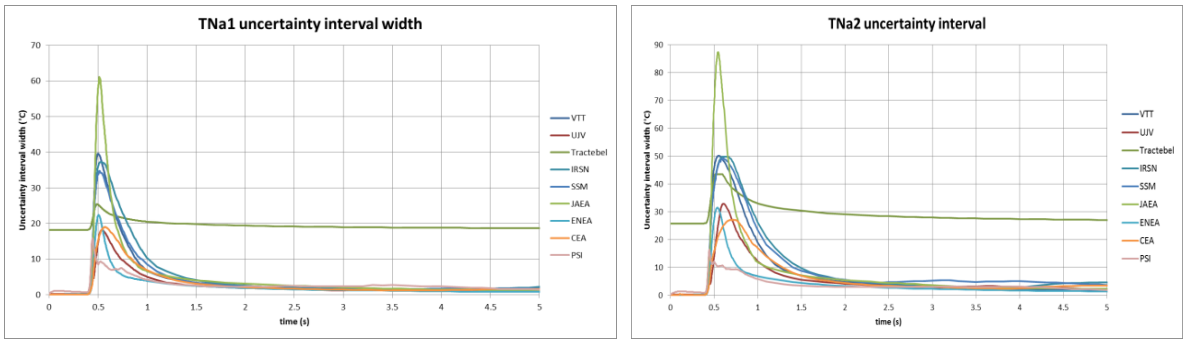

Source: IRSN, 2019.

The position of the average experimental measurement in the uncertainty band (r_{exp}) is presented in Figure 4.12 for sodium temperature at the two axial locations (TNa1 and TNa2) between 0.4 s (beginning of power pulse) and 1.5 s. We recall that the value of r_{exp} is between zero and one when the measurement is inside the uncertainty band. Even with the input data uncertainty propagation, participants had difficulties to catch the very beginning of the sodium heat-up; nevertheless, after 0.5 s, the agreement between calculations and measurements is good (r_{exp} between or very close to [0;1] interval).

Figure 4.12. Position of the experimental value within the uncertainty band (r_{exp}) for TNa1 (left) and TNa2 (right)

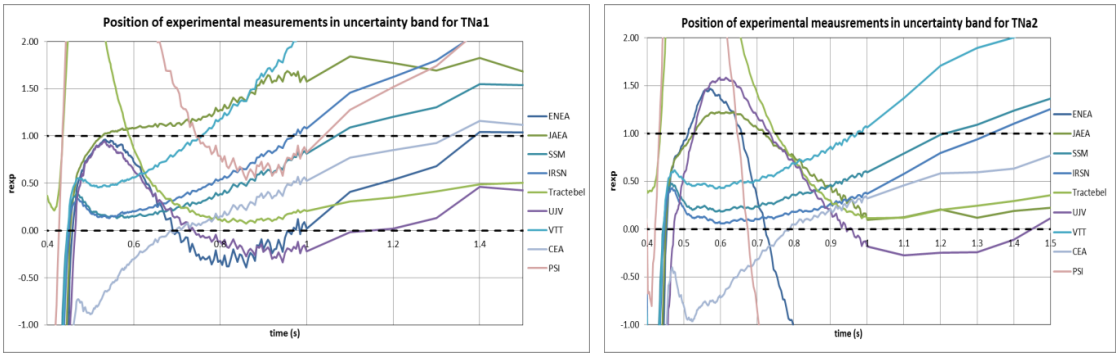

Source: IRSN, 2019.

The impact of input data uncertainty on the clad hoop strain as a function of axial height (ETZ) is illustrated in Figure 4.13.

Figure 4.13. Clad residual hoop strain UUB (left) and LUB (right) for all participants as a function of axial height

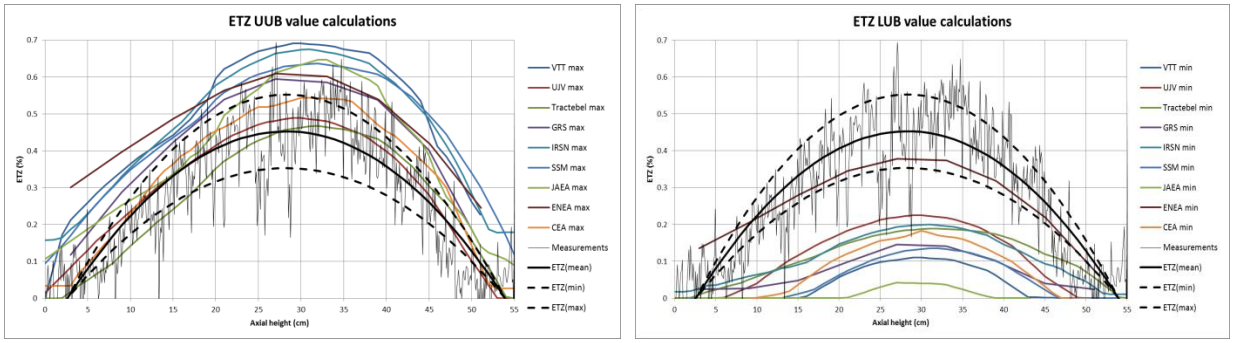

Note: ETZ: clad residual hoop strain; UUB: upper uncertainty bound; LUB: lower uncertainty bound.
Source: IRSN, 2019.

The average measurement is bounded by the LUB and the UUB, i.e. r_{exp} is between [0;1], for almost all participants along the entire axial height, as illustrated in Figure 4.14.

Figure 4.14. r_{exp} value for clad residual hoop strain as a function of axial height

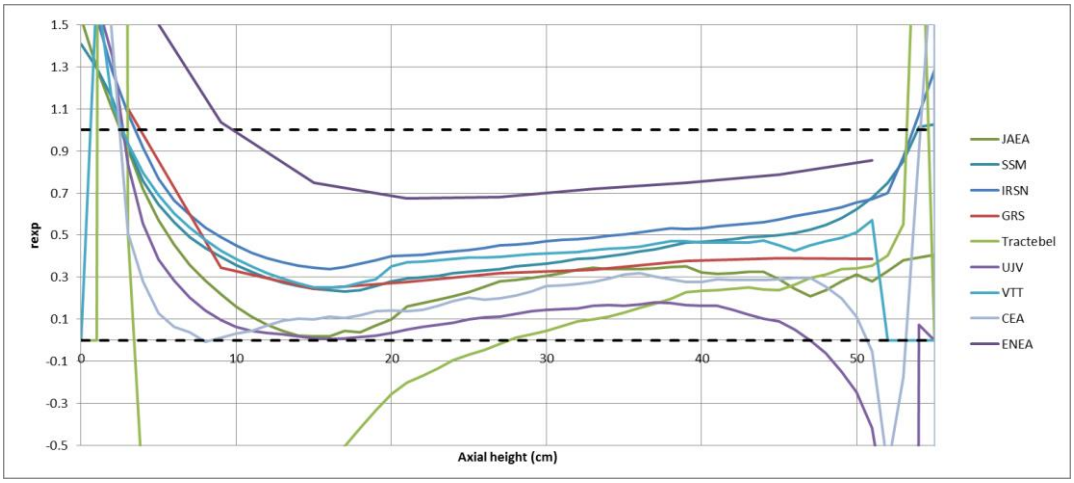

Source: IRSN, 2019.

The effect on uncertainty of input data on clad elongation (ECT) is shown in Figure 4.15.

Figure 4.15. UUB and LUB for all participants (left) and position of the experimental value within the uncertainty band (r_{exp}) (right) for clad total axial elongation

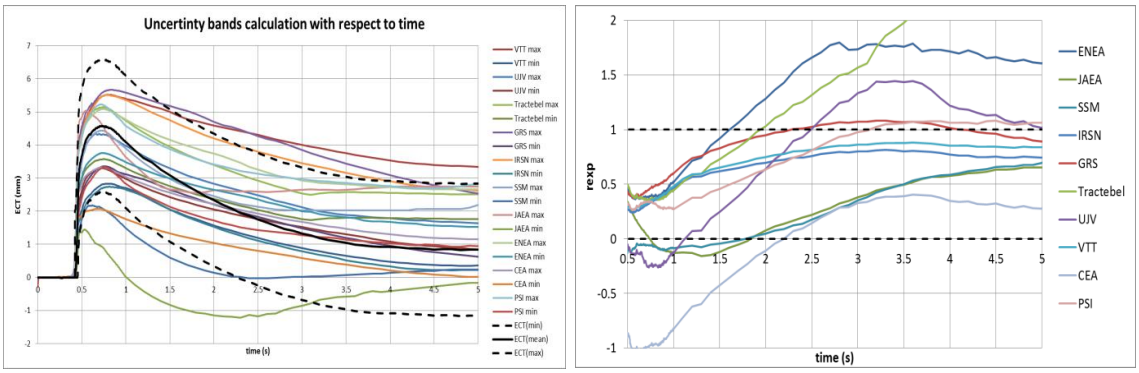

Source: IRSN, 2019.

Globally, considering the uncertainty around input data for the calculations and the experimental measurement uncertainties, there is a good agreement between the calculations and the measurements.

Scalar output

Figure 4.16 displays the average of participants' calibration indicator value for each output (maximal value of TNa1, TNa2, ECT and ETZ). It can first be noticed that this indicator is strictly positive, meaning that, on average, the intersection between simulation and experimental results is not empty. However, the agreement depends on the output. The strongest one is associated to clad hoop strain evaluation, then to the group (TNa1, TNa2, ECT) and finally, the lowest one corresponds to the FGR.

Figure 4.16. Average calibration indicator value for each output

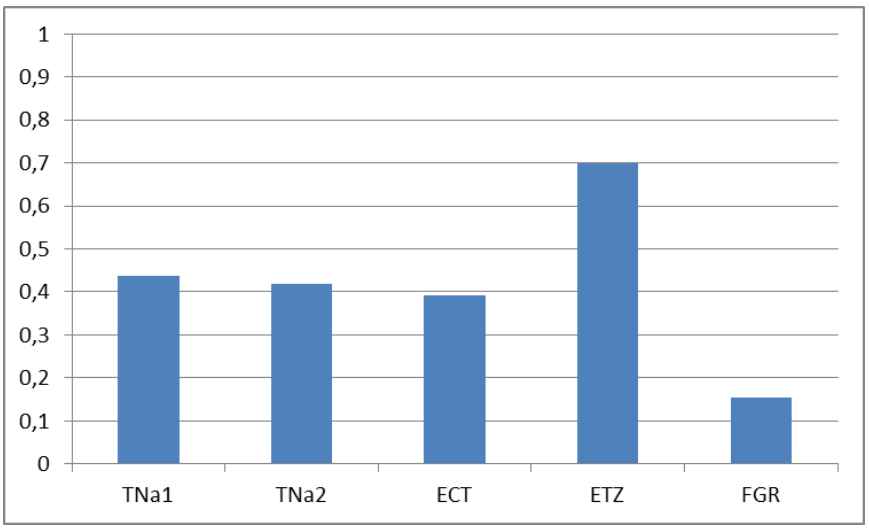

Note: ECT: clad total axial elongation; ETZ: clad residual hoop strain; FGR: fission gas release.
Source: IRSN, 2019.

It is also interesting to analyse each participant's contribution separately. Figure 4.17 provides two types of graphical representation for each scalar output.

Figure 4.17. Comparison of participants' contribution with experimental results based on a qualitative graphical comparison (left) and on the computation of information evaluation indicators (right)

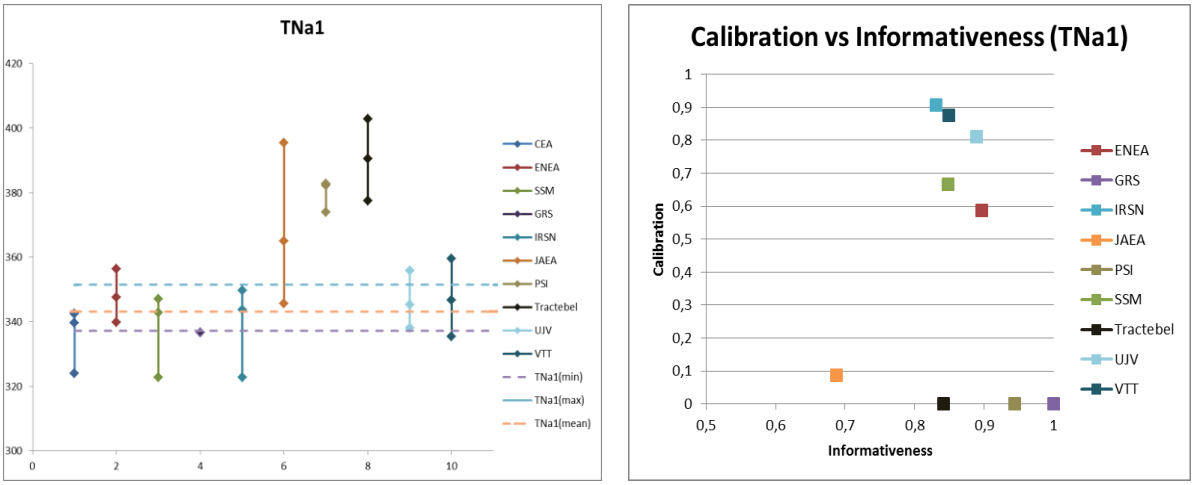

Figure 4.17. Comparison of participants' contribution with experimental results based on a qualitative graphical comparison (left) and on the computation of information evaluation indicators (right) (Continued)

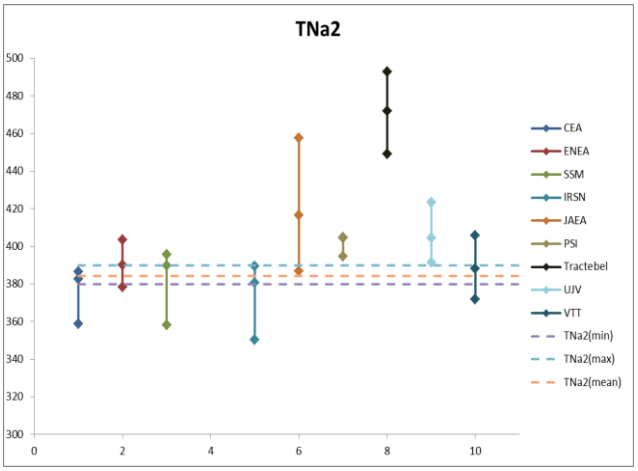

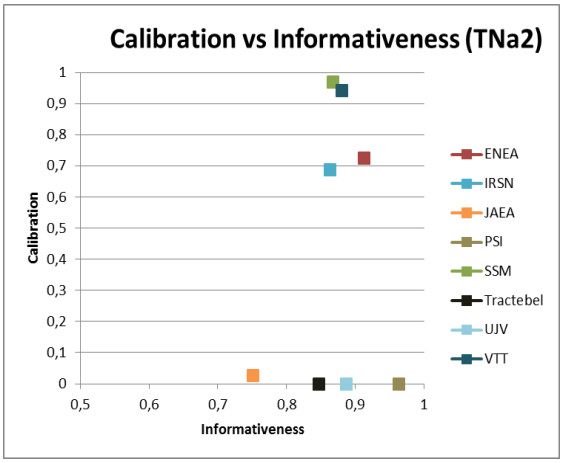

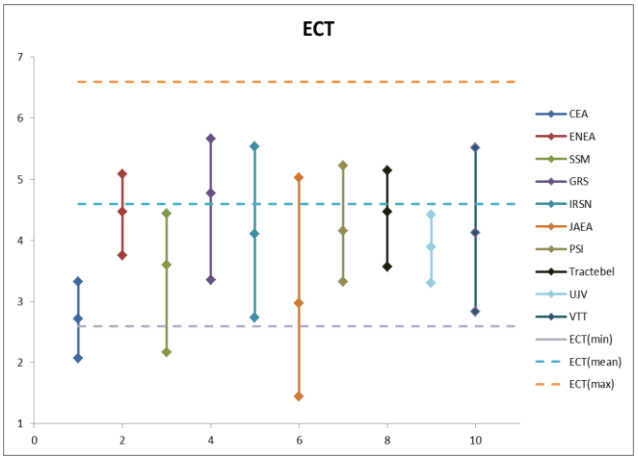

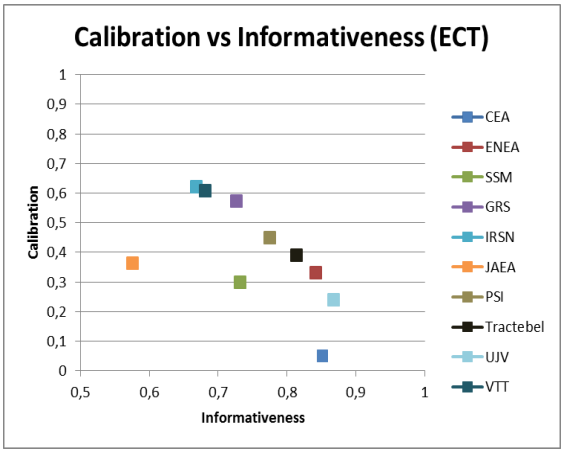

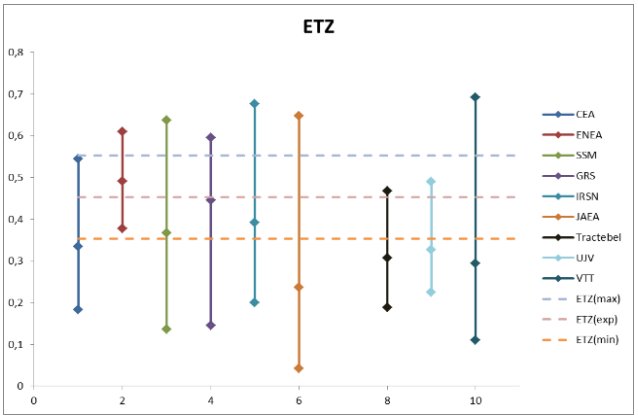

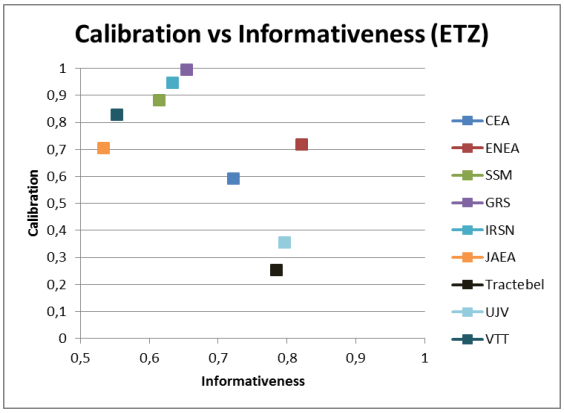

Figure 4.17. Comparison of participants' contribution with experimental results based on a qualitative graphical comparison (left) and on the computation of information evaluation indicators (right) (Continued)

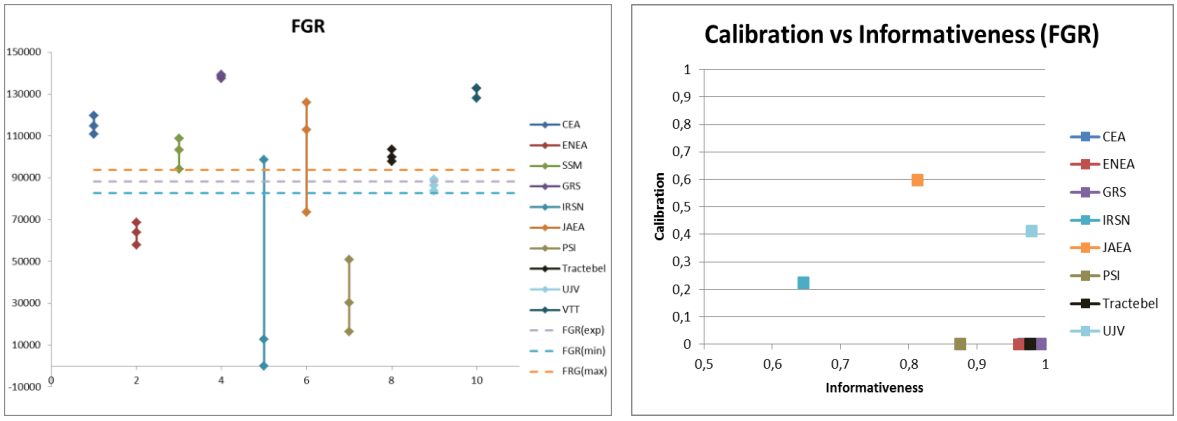

Note: ECT: clad total axial elongation; ETZ: clad residual hoop strain; FGR: fission gas release.
Source: IRSN, 2019.

Concerning sodium temperatures, a dispersion between reference calculations is noticeable (~ 50°C for TNa1 and ~ 90°C for TNa2). As a result, at most half of the participants' reference calculation falls inside the experimental interval for these outputs. Taking into account uncertainty makes it possible to improve the results with a non-empty intersection for a majority of the participants. However, the uncertainty interval widths are also dispersed (from 0.01°C to 50°C for TNa1 and from 10°C to 70°C for TNa2), which leads to the low average calibration indicator value already noticed on Figure 4.16.

When focusing on clad mechanical behaviour, ECT and ETZ, all clad elongation reference calculations are encompassed by the experimental uncertainty interval while less than 50% are for residual hoop strain reference calculations. When adding the uncertainty result, the intersection with the experimental interval is non-empty for both outputs, leading to a higher coherence between participants' contributions compared to sodium temperatures. However, it is important to mention that, contrary to ETZ, the uncertainty interval width for ECT is always smaller than the width of the experimental one. As a result, ETZ results are better calibrated on average than ECT ones.

Figure 4.17 also shows that, for sodium temperatures, the highest calibration is not obtained for the lowest informativeness (i.e. the largest uncertainty bands). It is not the case for ECT and ETZ, where a negative trend between calibration and informativeness is noticeable, indicating that a large uncertainty band (low informativeness) is more likely to encompass the experimental value (high calibration).

Finally, there is a very low coherence for the FGR. This can be explained by the dispersion of reference calculations and narrow uncertainty intervals for a majority of the participants.

4.4. Additional analysis of uncertainty results

This section is devoted to the analysis without taking account of experimental results. It therefore concerns all of the outputs.

4.4.1. Time trend outputs

Some time trend outputs are presented in Figures 4.18-4.24.

As in the RIA benchmark Phase II, the fuel thermal outputs (DHR, temperature of fuel centreline [TFC], maximum fuel temperature as function time [TFM] and temperature of fuel outer surface [TFO]) are consistent for all participants during the transient. As an example, the reference calculations for enthalpy variation (DHR) are represented in Figure 4.18. The dispersion on maximal enthalpy increase is about five cal/g. Except for one participant, there is also a good consistency on the uncertainty interval widths.

Figure 4.18. Enthalpy increase as a function of time: Reference calculations and uncertainty interval widths for all participants

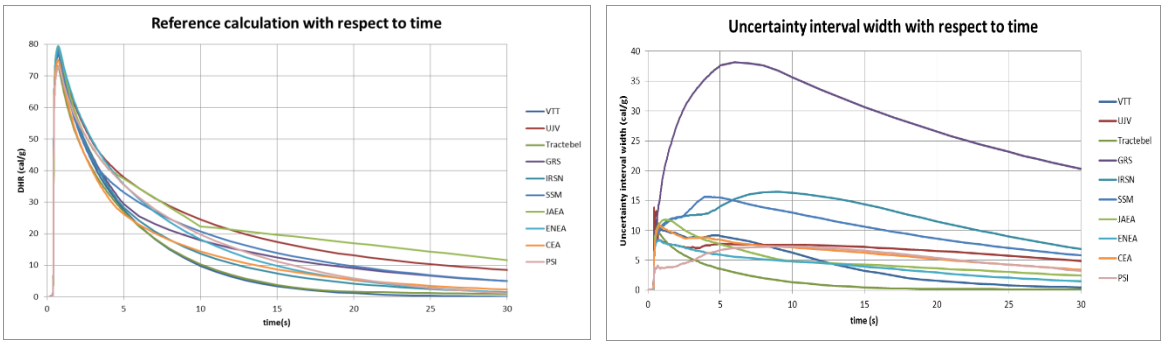

Source: IRSN, 2019.

Regarding the cladding thermal behaviour (Figure 4.19), the clad inner temperature (TCI) is more consistent between participants than the clad outer temperature (TCO). This behaviour is probably explained by clad-to-coolant heat exchange. The modelling of this quantity is different between the codes.

Figure 4.20 gathers the reference calculations, the uncertainty interval widths and the reference calculation dispersion for the fuel elongation (EFT). Contrary to the DHR, there is quite a large dispersion of the reference calculations and uncertainty interval widths for this output. It is worth noting that there is already a discrepancy on the initial fuel elongation before the transient. This difference between the codes is greater than for the fresh fuel case studied during Phase II.

As illustrated in Figure 4.20 (right panel), the reference calculation dispersion is close to the total uncertainty width and larger than any uncertainty band width provided by all participants. The code effect is very significant for this output.

Figure 4.19. Clad inner and outer temperature calculations: Reference cases

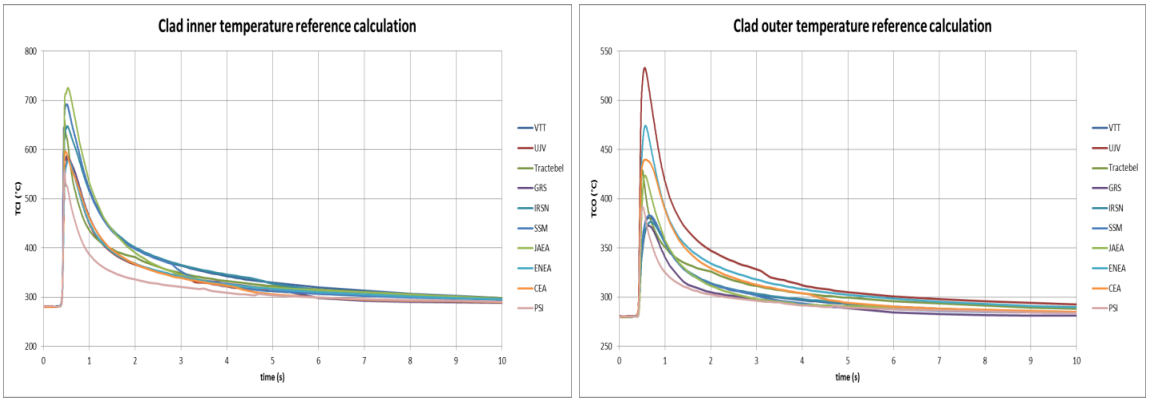

Source: IRSN, 2019.

Figure 4.20. Fuel elongation reference calculations (left) – participants' uncertainty interval widths, global uncertainty width and reference calculation dispersion (right)

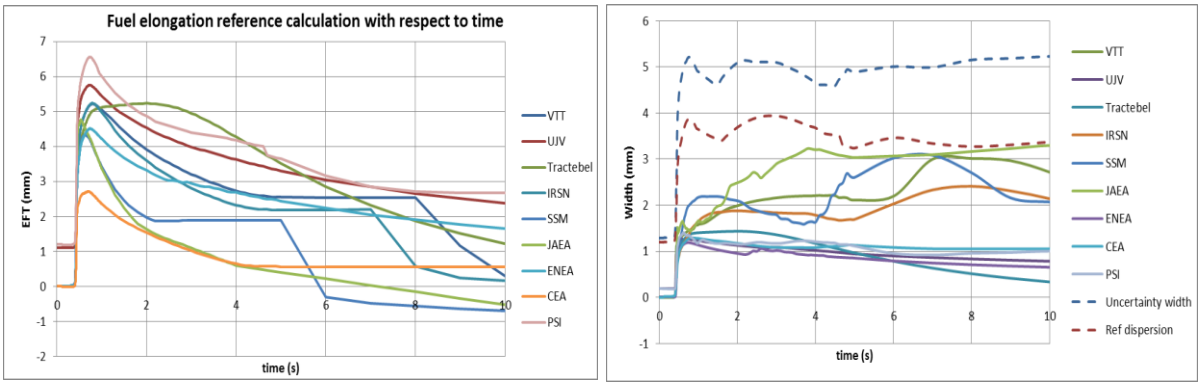

Source: IRSN, 2019.

The clad hoop stress reference calculations and interval widths have the same time trend for all participants, but with significantly different maximal values, in particular for the uncertainty band width (Figure 4.21). This difference on the maximum value has been identified as a result of different yield stress models in the codes.

Figure 4.21. Clad hoop stress reference calculations and uncertainty interval widths

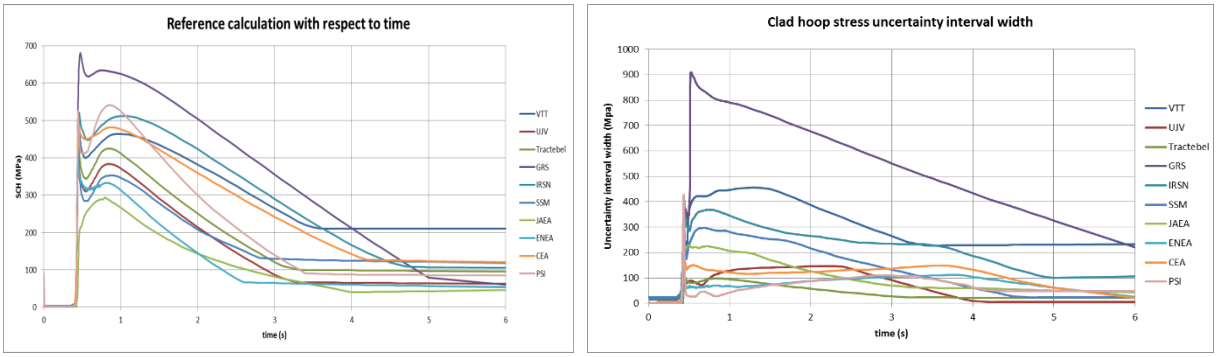

Source: IRSN, 2019.

Regarding the fuel-to-clad heat exchange coefficient, both the reference calculations and the uncertainty band widths are really dispersed with different time trends (Figure 4.22). This result is probably partially linked to the gap width evolutions that are also significantly dispersed between the participants (Figure 4.23).

Figure 4.22. Fuel-to-clad heat exchange coefficient reference calculations and uncertainty interval widths

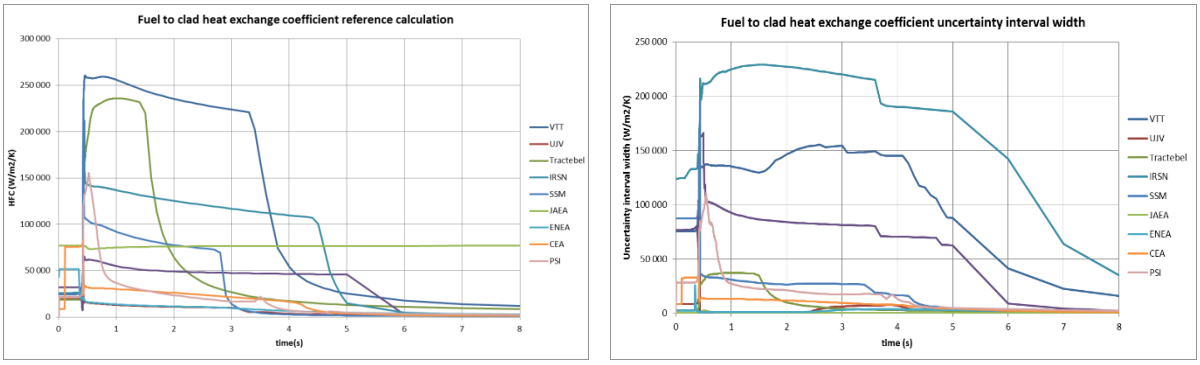

Source: IRSN, 2019.

Figure 4.23. Gap width reference calculations and uncertainty interval widths

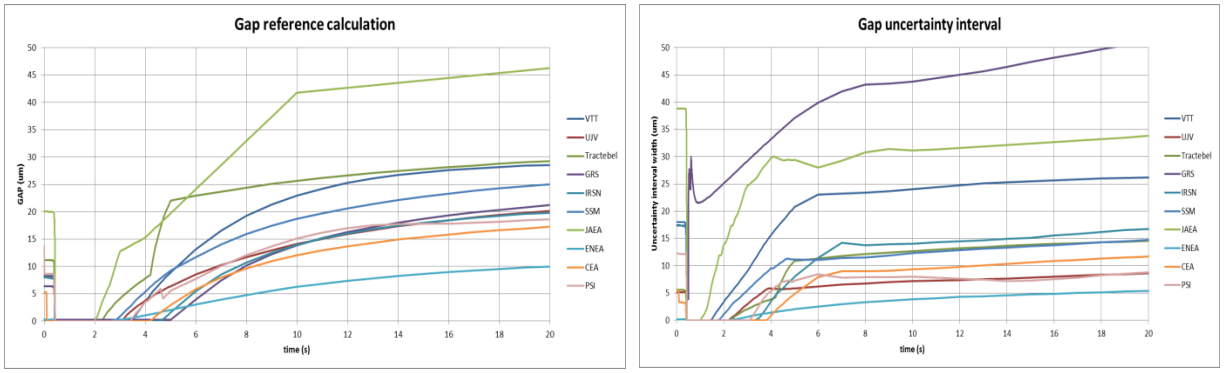

Source: IRSN, 2019.

Only six participants provided a clad failure prediction. As shown in Figure 4.24, the dispersion on reference calculations and on uncertainty interval widths is very large.

Figure 4.24. Clad failure prediction/reference calculations and uncertainty interval widths

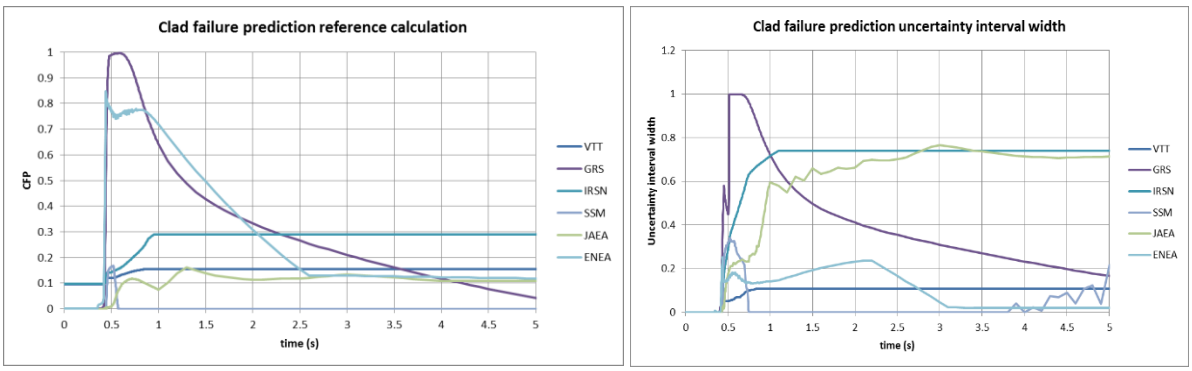

Source: IRSN, 2019.

4.4.1. Scalar output

Figure 4.25 displays the relative uncertainty interval for each output.

Figure 4.25. Relative uncertainty interval for each output

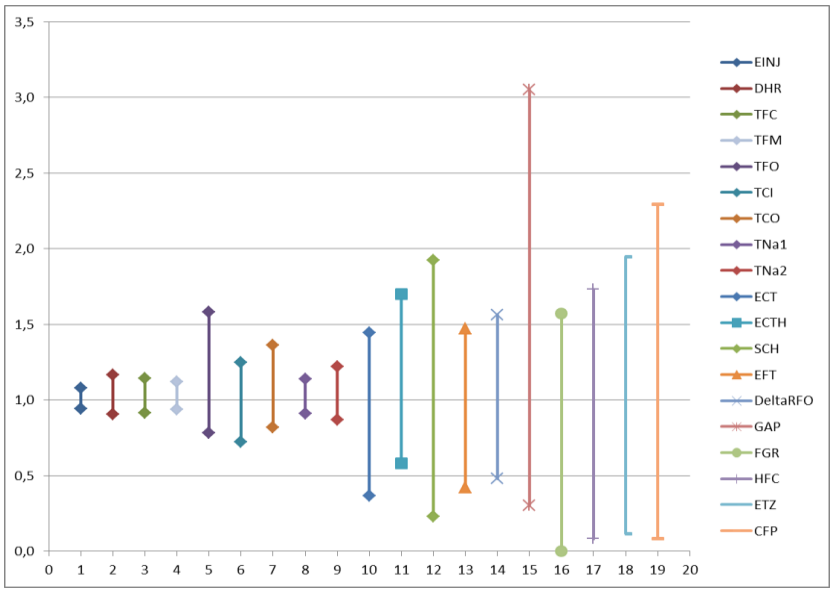

Source: IRSN, 2019.

The results show that the relative uncertainty width depends on the type of parameter observed. More precisely, the narrowest intervals are obtained for fuel and fluid thermal behaviour outputs (DHR, TFC, TFM, TNa1, TNa2 and TFO to a lesser extent). The uncertainty width increases slightly for clad thermal outputs (TCI, TCO), then more significantly for fuel and clad mechanical ones (EFT, fuel outer radius [RFO], ECT, ECTH, clad hoop stress at outer part of the clad [SCH]). Among clad mechanical outputs, a large relative uncertainty width can be observed for the ETZ and a similar conclusion also holds for the fuel-clad gap width (GAP), the FGR, the fuel-to-clad heat exchange coefficient (HFC) and the clad failure prediction (CFP).

The relative uncertainty interval was also studied in Phase II (see Figure 4.26 extracted from the Phase II report). Even if some outputs are different, it appears that, as for fresh fuel, the relative uncertainty width is lower for fuel thermal outputs. Moreover, there are globally larger relative uncertainties for irradiated fuels.

To continue the analysis of the relative uncertainty, Figure 4.27 plots the relative dispersion of reference calculations, which is defined as the difference between the maximum and the minimum of all reference calculations divided by the average of all reference calculations versus the relative uncertainty width (difference between maximal and minimal relative uncertainty bounds). The same magnitude is observed for the relative uncertainty width and for the relative reference calculation dispersion. Moreover, the results are clustered with respect to the type of behaviour considered. The smallest relative uncertainty width and relative dispersion are associated with thermal outputs. They then increase when moving to mechanical outputs.

Figure 4.26. Relative uncertainty interval for each output in Phase II

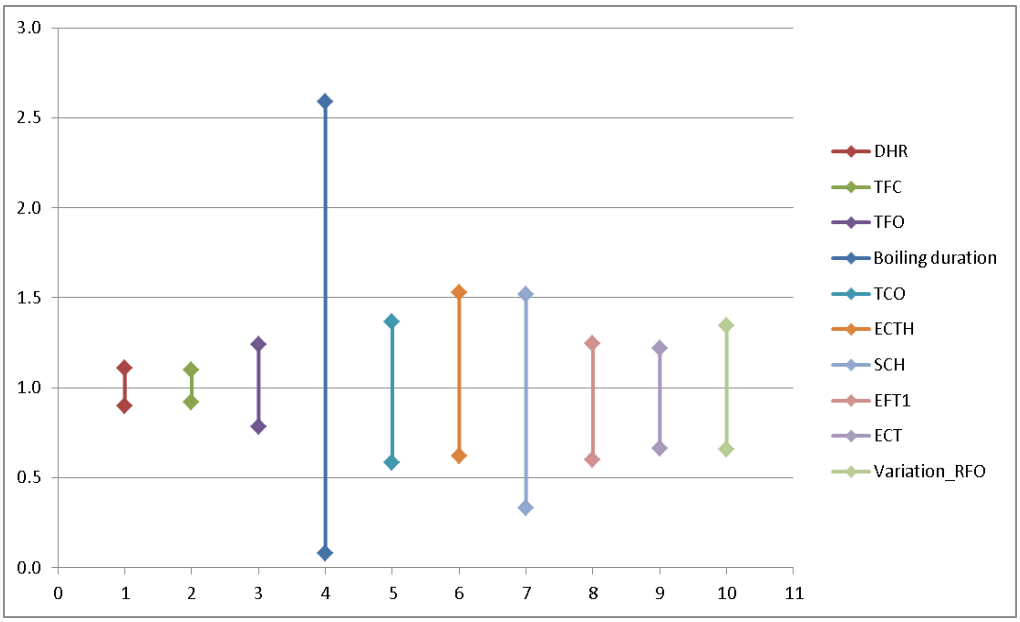

Note: DHR: variation of radial average enthalpy: TFC: temperature of fuel centreline: TFO: temperature of fuel outer surface; TCO: temperature of clad outer surface; ECTH: clad total (thermal + elastic + plastic) hoop strain; SCH: clad hoop stress at outer part of the clad; EFT: fuel column total axial elongation; ECT: clad total axial elongation; RFO: fuel outer radius.

Source: IRSN, 2019.

Figure 4.27. Relative dispersion of reference calculations vs. relative uncertainty width

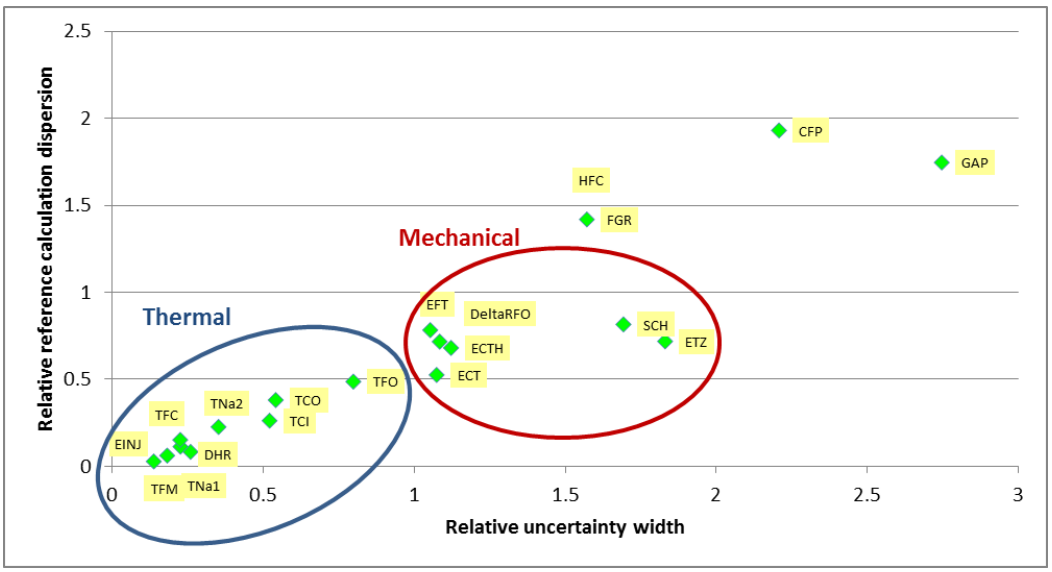

Note: CFP: clad failure prediction; DHR: variation of radial average enthalpy: ECT: clad total axial elongation; ECTH: clad total (thermal + elastic + plastic) hoop strain; EFT: fuel column total axial elongation; EINJ: injected energy (radial averaged); ETZ: clad residual hoop strain; FGR: fission gas release; GAP: fuel-clad gap width; HFC: fuel-to-clad heat exchange coefficient RFO: fuel outer radius; TCI: temperature of clad inner surface; TCO: temperature of clad outer surface; TFC: temperature of fuel centreline; TFM: maximum fuel temperature; TFO: temperature of fuel outer surface; SCH: clad hoop stress at outer part of the clad.

Source: IRSN, 2019.

It is also interesting to analyse the coherence between participants' contributions for each output. Figures 4.28-4.32 provide uncertainty interval and reference calculation values for each participant with respect to the type of outputs.

Figure 4.28. Uncertainty results and reference calculation values for fuel thermal outputs

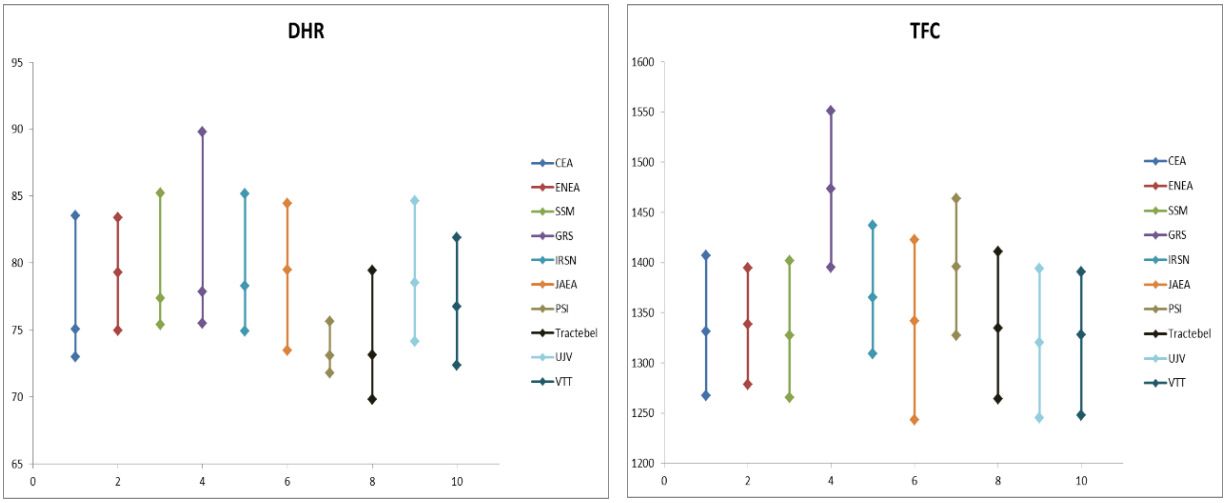

Figure 4.28. Uncertainty results and reference calculation values for fuel thermal outputs (Continued)

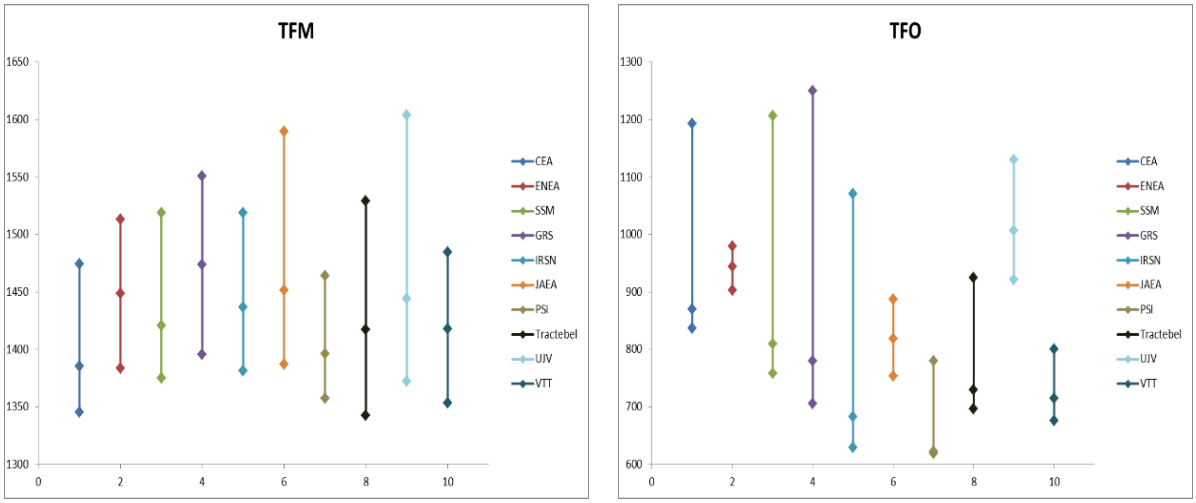

Note: DHR: variation of radial average enthalpy: TFC: temperature of fuel centreline: TFM: maximum fuel temperature; TFO: temperature of fuel outer surface.

Source: IRSN, 2019.

As already observed, there is a quite good consistency between participants both on reference calculation value and uncertainty interval width for the fuel thermal output, except for the fuel outer temperature. This last value is linked to the fuel thermal behaviour, but also to the HFC.

Figure 4.29. Uncertainty results and reference calculation values for the fuel-to-clad heat exchange and the fuel-clad gap

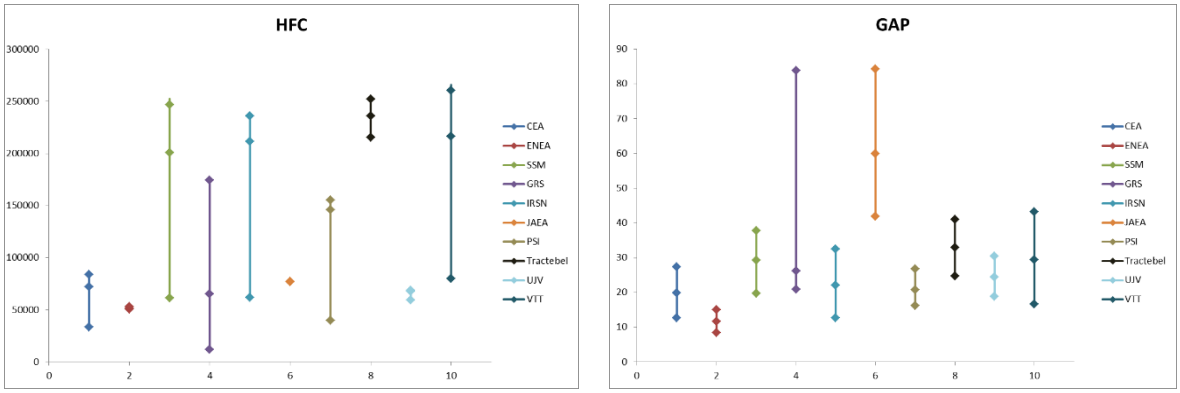

Note: HFC: fuel-to-clad heat exchange coefficient; GAP: fuel-clad gap width.

Source: IRSN, 2019.

Figure 4.30. Uncertainty results and reference calculation values for clad and fluid thermal outputs

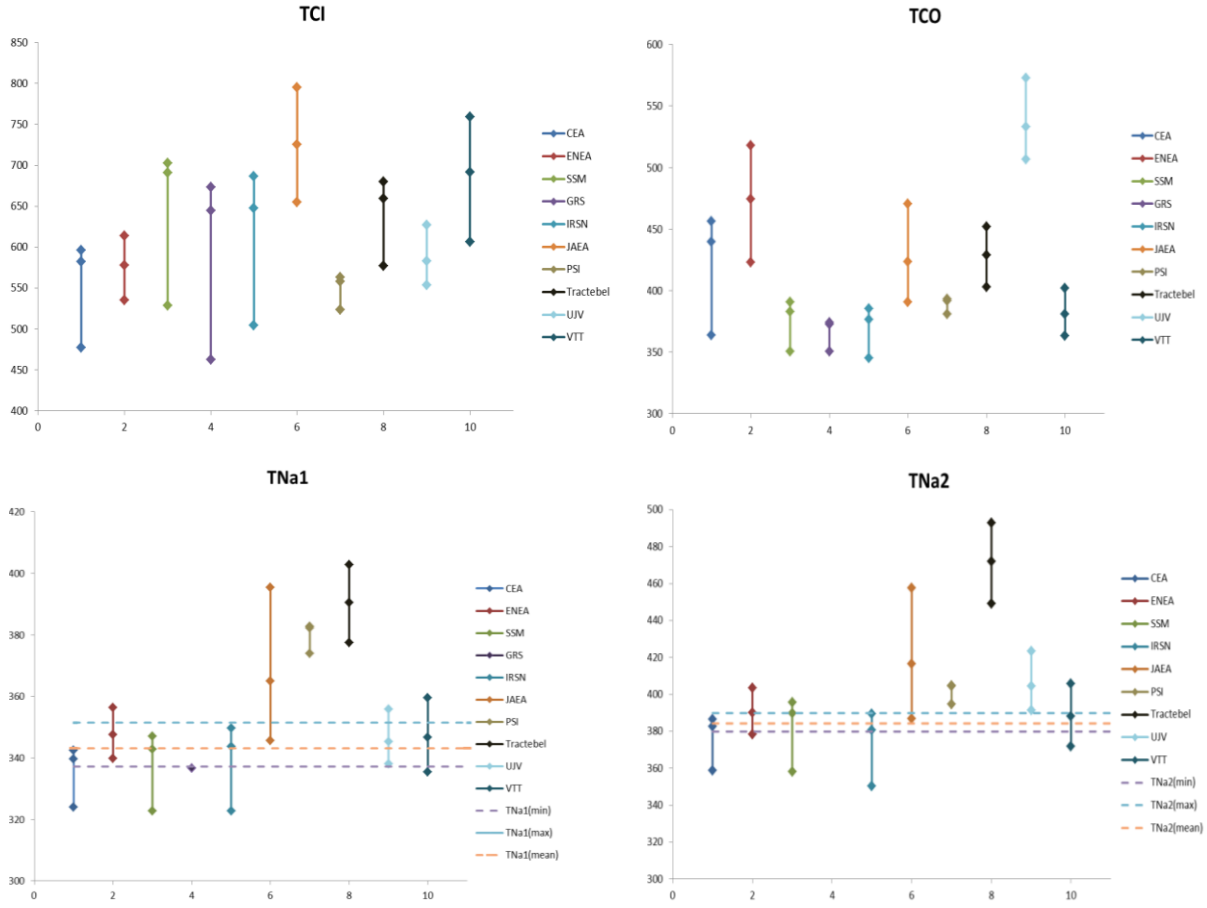

Note: TCI: temperature of clad inner surface; TCO: temperature of clad outer surface.

Source: IRSN, 2019.

Figure 4.31. Uncertainty results and reference calculation values for fuel and clad mechanical outputs

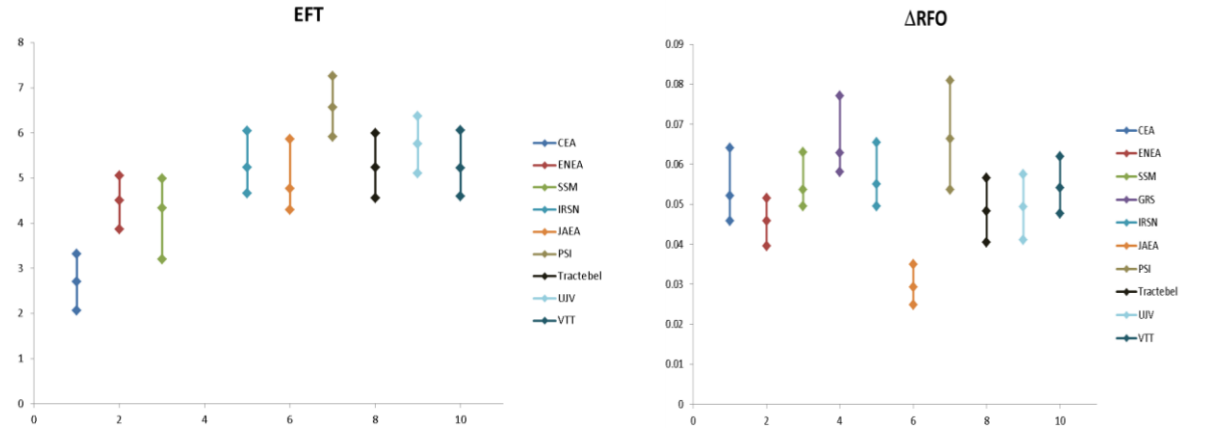

Figure 4.31. Uncertainty results and reference calculation values for fuel and clad mechanical outputs (Continued)

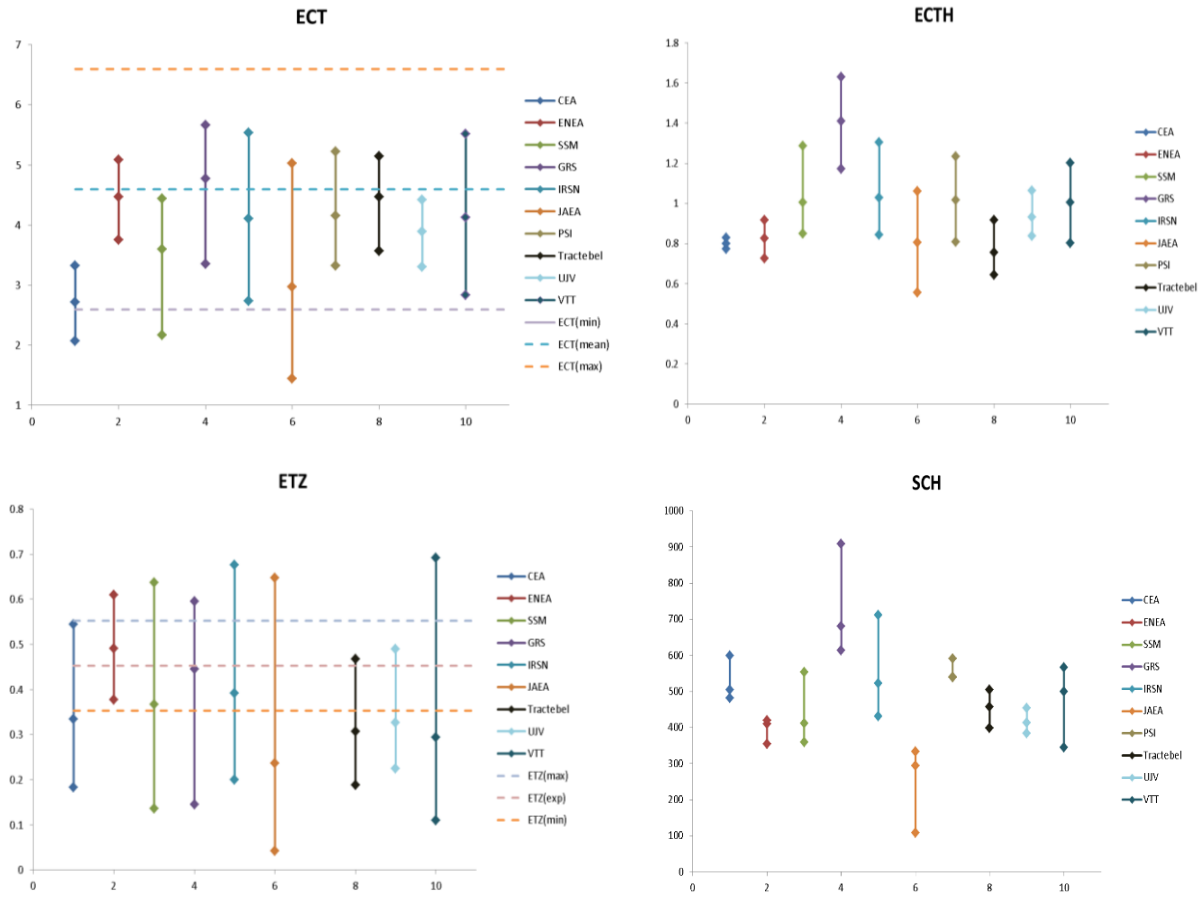

Note: EFT: fuel column total axial elongation; RFO: fuel outer radius; ECT: clad total axial elongation; ECTH: clad total (thermal + elastic + plastic) hoop strain; ETZ: clad residual hoop strain; SCH: clad hoop stress at outer part of the clad.

Source: IRSN, 2019.

Figure 4.32. Uncertainty results and reference calculation values for the fuel-clad gap, fuel-to-clad heat exchange, fission gas release and clad failure prediction

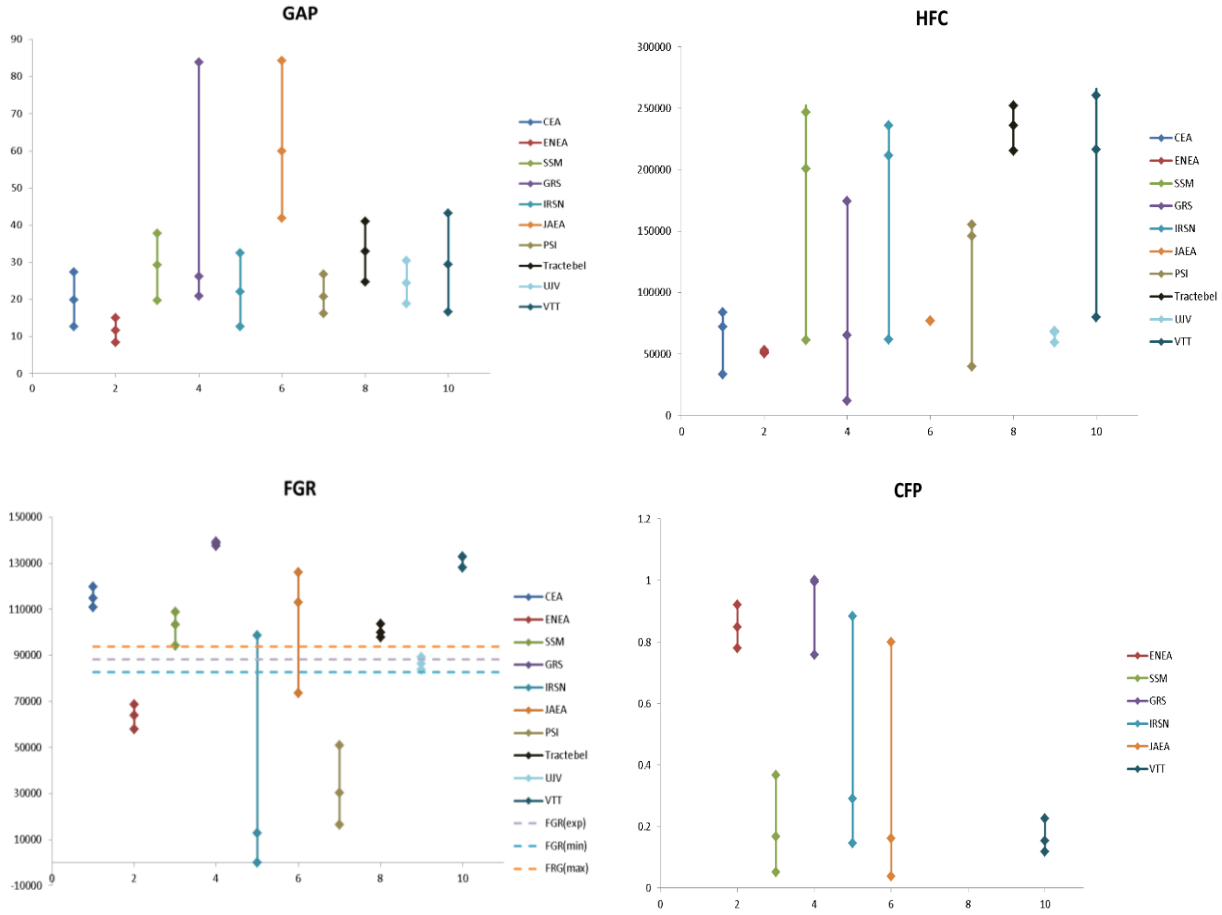

Note: GAP: fuel-clad gap width; HFC: fuel-to-clad heat exchange coefficient; FGR: fission gas release; CFP: clad failure prediction.

Source: IRSN, 2019.

It appears that the results are highly conflicting if all participants' contributions are taken into account (i.e. empty intersection of all uncertainty intervals) except for the DHR, the TFM and the ETZ. However, an empty intersection can be due to a single contribution and further qualitative analysis is required. A closer look at the previous figures reveals that the coherence between participants depends on the type of outputs. This point had already been observed in the RIA benchmark Phase II. More precisely, the uncertainty results exhibit four main levels of coherence:

- High coherence: includes participants' results that are, for a large majority, in agreement as regards to the uncertainty interval width and reference calculation. It corresponds to fuel thermal behaviour outputs, except the TFO.
- Medium coherence: concerns participants' results exhibiting coherent uncertainty interval width for a large majority, but with dispersion in the reference calculations due to a few participants' contributions. This is the case for fuel and clad mechanical behaviour output except for the SCH.

- Low coherence: corresponds to participants' results exhibiting dispersion for both reference calculation and uncertainty interval width. This is the case for the TFO, the SCH, GAP as well as for clad and fluid thermal outputs.
- No coherence: this last level is associated with large dispersion for both reference calculation and uncertainty interval width. It includes the remaining outputs: the HFC, the FGR and the CFP.

Only three levels of coherence were introduced in the Phase II report. In Phase III, four levels are defined in order to take account of the results associated with the extra outputs HFC, FGR and CFP that exhibit strong disagreement. However, for the outputs considered in both phases, the same coherence ranking has been found.

4.5. Sensitivity analysis

The most influential input parameters have been identified for each participant, based on the correlation coefficients they calculated and using a fixed significance threshold of 0.25.

The synthesis methodology was recalled above.

Tables 4.1-4.5 summarise the results in terms of percentage of participants with respect to groups of outputs corresponding to a type of behaviour. We recall the followed rule: if an input parameter is found to be influential for an output associated with a given behaviour, it is considered as influential for the whole group. A dark blue cell in the tables means that more than 50% of the participants identified the corresponding input parameter as influential for the type of behaviour.

- At the beginning of power pulse (t1):

Before the transient, there is a strong agreement on influential parameters (very high or very low percentage). The state of the rod, before the energy injection, depends only on a few input parameters, mainly the initial fuel-to-clad radial gap, the fuel and clad thermal-expansion (Table 4.1).

Table 4.1. Influential input parameters with respect to the type of behaviour when focusing on the beginning of power pulse

	Fuel thermal (DHR, TFC, TFM, TFO)	Clad thermal (TCI, TCO)	Fluid thermal (TNa1, TNa2)	Fuel mechanical (EFT, RFO)	Clad mechanical (ECT, ECTH, SCH)	GAP	HFC	FGR	CFP
Fuel-to-clad radial gap	37.5%	12.5%	14.3%	37.5%	87.5%	87.5%	62.5%	28.6%	60.0%
Cladding roughness	30.0%	10.0%	11.1%	0.0%	10.0%	10.0%	60.0%	0.0%	16.7%
Fuel roughness	0.0%	0.0%	0.0%	0.0%	0.0%	0.0%	50.0%	0.0%	0.0%
Zirconia thickness	25.0%	33.3%	25.0%	0.0%	66.7%	0.0%	0.0%	0.0%	0.0%
Injected energy in the rod	30.0%	20.0%	11.1%	0.0%	0.0%	0.0%	0.0%	0.0%	0.0%
Radial power profile	25.0%	12.5%	14.3%	0.0%	0.0%	0.0%	0.0%	0.0%	0.0%
Power pulse width	66.7%	55.6%	37.5%	37.5%	44.4%	0.0%	0.0%	0.0%	20.0%
Fuel thermal conductivity model	60.0%	10.0%	11.1%	10.0%	10.0%	10.0%	10.0%	0.0%	0.0%
Fuel thermal-expansion model	30.0%	10.0%	0.0%	80.0%	50.0%	90.0%	70.0%	0.0%	33.3%
Fuel enthalpy	11.1%	0.0%	0.0%	0.0%	10.0%	0.0%	10.0%	0.0%	0.0%
Clad thermal-expansion	0.0%	0.0%	0.0%	10.0%	50.0%	60.0%	50.0%	0.0%	33.3%
Clad yield stress	0.0%	0.0%	0.0%	0.0%	0.0%	0.0%	0.0%	0.0%	0.0%

Notes: DHR: variation of radial average enthalpy; TFC: temperature of fuel centreline; TFM: maximum fuel temperature; TFO: temperature of fuel outer surface; TCI: temperature of clad inner surface; TCO: temperature of clad outer surface; EFT: fuel column total axial elongation; RFO: fuel outer radius; ECT: clad total axial elongation; ECTH: clad total (thermal + elastic + plastic) hoop strain; SCH: clad hoop stress at outer part of the clad; GAP: fuel-to-clad gap width; HFC: fuel-to-clad heat exchange coefficient; FGR: fission gas release; CFP: clad failure prediction.
A dark blue cell in the tables means that more than 50% of the participants have identified the corresponding input parameter as influential for the type of behaviour.

- At the time of pulse maximum power (t2):

There is less agreement among participants at the pulse maximum power time than before the pulse. Injected energy and initial gap are identified as influential for most of the outputs. Fuel enthalpy and thermal-expansion models, zirconia thickness, fuel and clad roughness, power profile and pulse width are also influential for several thermal and mechanical outputs. These last outcomes are consistent with what was reported by the RIA benchmark Phase II.

As in Phase II, at time t2, the fuel thermal conductivity has a low impact on fuel thermal behaviour because the fuel behaviour is close to adiabaticity during the power pulse first part.

The GAP output has no influential input parameters because at the time of pulse maximal power the gap is closed, whatever the case. Consequently, the sole influential parameters on the fuel-to-clad heat exchange are the fuel and clad roughness.

Table 4.2 Influential input parameters with respect to the type of behaviour when focusing on the time of pulse maximum power

	Fuel thermal (DHR, TFC, TFM, TFO)	Clad thermal (TCI, TCO)	Fluid thermal (TNa1, TNa2)	Fuel mechanical (EFT, RFO)	Clad mechanical (ECT, ECTH, SCH)	GAP	HFC	FGR	CFP
Fuel-clad radial gap	50.0%	62.5%	57.1%	85.7%	87.5%	28.6%	37.5%	37.5%	100.0%
Cladding roughness	60.0%	60.0%	44.4%	11.1%	20.0%	11.1%	60.0%	20.0%	33.3%
Fuel roughness	50.0%	50.0%	37.5%	12.5%	12.5%	0.0%	50.0%	12.5%	0.0%
Zirconia thickness	11.1%	77.8%	75.0%	0.0%	44.4%	0.0%	11.1%	0.0%	50.0%
Injected energy in the rod	100.0%	80.0%	66.7%	80.0%	80.0%	0.0%	40.0%	50.0%	66.7%
Radial power profile	75.0%	75.0%	85.7%	25.0%	37.5%	0.0%	37.5%	37.5%	0.0%
Power pulse width	66.7%	66.7%	75.0%	50.0%	44.4%	12.5%	22.2%	44.4%	20.0%
Fuel thermal conductivity model	30.0%	40.0%	11.1%	11.1%	10.0%	0.0%	20.0%	0.0%	0.0%
Fuel thermal-expansion model	0.0%	20.0%	22.2%	100.0%	100.0%	11.1%	10.0%	10.0%	83.3%
Fuel enthalpy	90.0%	20.0%	0.0%	66.7%	50.0%	0.0%	0.0%	40.0%	50.0%
Clad thermal-expansion	0.0%	0.0%	0.0%	33.3%	40.0%	11.1%	0.0%	0.0%	33.3%
Clad yield stress	0.0%	0.0%	0.0%	0.0%	0.0%	0.0%	0.0%	0.0%	0.0%

Notes: DHR: variation of radial average enthalpy; TFC: temperature of fuel centreline; TFM: maximum fuel temperature; TFO: temperature of fuel outer surface; TCI: temperature of clad inner surface; TCO: temperature of clad outer surface; EFT: fuel column total axial elongation; RFO: fuel outer radius; ECT: clad total axial elongation; ECTH: clad total (thermal + elastic + plastic) hoop strain; SCH: clad hoop stress at outer part of the clad; GAP: fuel-clad gap width; HFC: fuel-to-clad heat exchange coefficient; FGR: fission gas release; CFP: clad failure prediction.
A dark blue cell in the tables means that more than 50% of the participants have identified the corresponding input parameter as influential for the type of behaviour.

- At the end of power pulse (t3):

At the end of the power pulse, injected energy is still identified as a very influential input. The initial zirconia thickness and radial power profile and the fuel enthalpy are also very influential parameters.

The fuel thermal conductivity model is now identified as influential for fuel and clad outer temperature and clad stress. The fuel-to-clad initial gap has a strong influence on the fuel and clad mechanical behaviour and clad failure prediction.

Table 4.3. Influential input parameters with respect to the type of behaviour when focusing on the end of power pulse

	Fuel thermal (DHR, TFC, TFM, TFO)	Clad thermal (TCI, TCO)	Fluid thermal (TNa1, TNa2)	Fuel mechanical (EFT, RFO)	Clad mechanical (ECT, ECTH, SCH)	GAP	HFC	FGR	CFP
Fuel-clad radial gap	12.5%	25.0%	14.3%	71.4%	87.5%	14.3%	37.5%	37.5%	60.0%
Cladding roughness	60.0%	50.0%	44.4%	30.0%	40.0%	11.1%	60.0%	10.0%	33.3%
Fuel roughness	50.0%	37.5%	37.5%	12.5%	25.0%	0.0%	50.0%	12.5%	0.0%
Zirconia thickness	77.8%	77.8%	37.5%	75.0%	66.7%	0.0%	55.6%	22.2%	83.3%
Injected energy in the rod	100.0%	80.0%	88.9%	100.0%	90.0%	11.1%	30.0%	80.0%	50.0%
Radial power profile	75.0%	62.5%	85.7%	57.1%	62.5%	0.0%	12.5%	25.0%	60.0%
Power pulse width	33.3%	33.3%	50.0%	22.2%	33.3%	0.0%	22.2%	44.4%	0.0%
Fuel thermal conductivity model	80.0%	80.0%	100.0%	50.0%	60.0%	0.0%	30.0%	20.0%	33.3%
Fuel thermal-expansion model	0.0%	0.0%	10.0%	100.0%	100.0%	0.0%	20.0%	50.0%	50.0%
Fuel enthalpy	100.0%	50.0%	60.0%	80.0%	70.0%	0.0%	30.0%	60.0%	66.7%
Clad thermal-expansion	0.0%	0.0%	0.0%	11.1%	20.0%	0.0%	0.0%	0.0%	16.7%
Clad yield stress	11.1%	0.0%	0.0%	55.6%	66.7%	0.0%	22.2%	11.1%	20.0%

Notes: DHR: variation of radial average enthalpy; TFC: temperature of fuel centreline; TFM: maximum fuel temperature; TFO: temperature of fuel outer surface; TCI: temperature of clad inner surface; TCO: temperature of clad outer surface; EFT: fuel column total axial elongation; RFO: fuel outer radius; ECT: clad total axial elongation; ECTH: clad total (thermal + elastic + plastic) hoop strain; SCH: clad hoop stress at outer part of the clad; GAP: fuel-clad gap width; HFC: fuel-to-clad heat exchange coefficient; FGR: fission gas release; CFP: clad failure prediction.
A dark blue cell in the tables means that more than 50% of the participants have identified the corresponding input parameter as influential for the type of behaviour.

- At the end of calculation (t4):

Similar to the time t3, the injected energy is still influential (for a large majority of participants) for every output. It is also important to point out that the fuel properties (enthalpy, conductivity and thermal-expansion model) have some effects on the final state of the rod (clad hoop strain, fuel and clad elongation).

Table 4.4. Influential input parameters with respect to the type of behaviour when focusing on the end of the calculation

	Fuel thermal (DHR, TFC, TFM, TFO)	Clad thermal (TCI, TCO)	Fluid thermal (TNa1, TNa2)	Fuel mechanical (EFT, RFO)	Clad mechanical (ECT, ECTH, SCH)	GAP	HFC	FGR	CFP
Fuel-clad radial gap	25.0%	12.5%	25.0%	62.5%	87.5%	12.5%	25.0%	25.0%	60.0%
Cladding roughness	40.0%	30.0%	30.0%	30.0%	10.0%	10.0%	20.0%	10.0%	33.3%
Fuel roughness	37.5%	25.0%	25.0%	12.5%	12.5%	0.0%	37.5%	12.5%	0.0%
Zirconia thickness	55.6%	66.7%	50.0%	50.0%	55.6%	66.7%	55.6%	22.2%	50.0%
Injected energy in the rod	90.0%	80.0%	77.8%	80.0%	90.0%	100.0%	90.0%	80.0%	83.3%
Radial power profile	37.5%	12.5%	14.3%	50.0%	25.0%	25.0%	37.5%	37.5%	40.0%
Power pulse width	44.4%	33.3%	44.4%	22.2%	44.4%	22.2%	33.3%	44.4%	20.0%
Fuel thermal conductivity model	60.0%	40.0%	55.6%	40.0%	10.0%	0.0%	0.0%	30.0%	33.3%
Fuel thermal-expansion model	70.0%	50.0%	55.6%	90.0%	100.0%	100.0%	80.0%	40.0%	66.7%
Fuel enthalpy	30.0%	20.0%	22.2%	40.0%	70.0%	70.0%	50.0%	40.0%	50.0%
Clad thermal-expansion	10.0%	0.0%	0.0%	11.1%	30.0%	30.0%	10.0%	0.0%	33.3%
Clad yield stress	33.3%	11.1%	11.1%	22.2%	55.6%	44.4%	44.4%	0.0%	0.0%

Notes: DHR: variation of radial average enthalpy; TFC: temperature of fuel centreline; TFM: maximum fuel temperature; TFO: temperature of fuel outer surface; TCI: temperature of clad inner surface; TCO: temperature of clad outer surface; EFT: fuel column total axial elongation; RFO: fuel outer radius; ECT: clad total axial elongation; ECTH: clad total (thermal + elastic + plastic) hoop strain; SCH: clad hoop stress at outer part of the clad; GAP: fuel-clad gap width; HFC: fuel-to-clad heat exchange coefficient; FGR: fission gas release; CFP: clad failure prediction.
A dark blue cell in the tables means that more than 50% of the participants have identified the corresponding input parameter as influential for the type of behaviour.

- For the maximum value of each output of interest

As regards the maximum value of every output, the most influential input parameters have been identified not only with respect to the type of behaviour considered, as gathered in Table 4.5, but also on each individual output, as gathered in Table 4.6. Table 4.6 is to be compared with Table 4.9 of the Phase II report (NEA, 2017).

Table 4.5. Influential input parameters with respect to the type of behaviour when focusing on the maximum value of each output

	Fuel thermal (DHR, TFC, TFM, TFO)	Clad thermal (TCI, TCO)	Fluid thermal (TNa1, TNa2)	Fuel mechanical (EFT, RFO)	Clad mechanical (ECT, ECTH, SCH)	GAP	HFC	FGR	CFP
Fuel-clad radial gap	37.5%	25.0%	14.3%	71.4%	87.5%	25.0%	50.0%	25.0%	100.0%
Cladding roughness	60.0%	60.0%	55.6%	30.0%	30.0%	10.0%	60.0%	10.0%	50.0%
Fuel roughness	50.0%	50.0%	50.0%	12.5%	12.5%	0.0%	50.0%	12.5%	25.0%
Zirconia thickness	55.6%	77.8%	75.0%	62.5%	88.9%	66.7%	11.1%	22.2%	50.0%
Injected energy in the rod	100.0%	100.0%	88.9%	100.0%	90.0%	100.0%	10.0%	80.0%	83.3%
Radial power profile	87.5%	75.0%	85.7%	71.4%	37.5%	25.0%	25.0%	37.5%	60.0%
Power pulse width	77.8%	44.4%	50.0%	33.3%	33.3%	11.1%	11.1%	44.4%	20.0%
Fuel thermal conductivity model	70.0%	70.0%	88.9%	10.0%	20.0%	0.0%	10.0%	30.0%	66.7%
Fuel thermal-expansion model	0.0%	0.0%	0.0%	100.0%	100.0%	100.0%	30.0%	30.0%	83.3%
Fuel enthalpy	100.0%	40.0%	50.0%	80.0%	80.0%	70.0%	0.0%	50.0%	83.3%
Clad thermal-expansion	0.0%	0.0%	0.0%	11.1%	30.0%	40.0%	10.0%	0.0%	50.0%
Clad yield stress	0.0%	0.0%	0.0%	33.3%	66.7%	44.4%	0.0%	0.0%	40.0%

Notes: DHR: variation of radial average enthalpy; TFC: temperature of fuel centreline; TFM: maximum fuel temperature; TFO: temperature of fuel outer surface; TCI: temperature of clad inner surface; TCO: temperature of clad outer surface; EFT: fuel column total axial elongation; RFO: fuel outer radius; ECT: clad total axial elongation; ECTH: clad total (thermal + elastic + plastic) hoop strain; SCH: clad hoop stress at outer part of the clad; GAP: fuel-clad gap width; HFC: fuel-to-clad heat exchange coefficient; FGR: fission gas release; CFP: clad failure prediction.
A dark blue cell in the tables means that more than 50% of the participants have identified the corresponding input parameter as influential for the type of behaviour.

An analysis of these two tables allows the following conclusions to be drawn:

- The injected energy is the most influential input parameter: it is considered influential by a large majority of participants for 16 out of the 17 outputs.
- Input data related to the end-of-life state (zirconia thickness, radial power profile, gap size, roughness) are also very influential.
- Fuel physical properties, thermal-expansion and thermal conductivity models have a significant impact on the rod mechanical and thermal behaviours.
- Regarding the fission gas release, except for injected energy, participants did not identify any common influential input parameter.
- The clad failure evaluation is the most sensitive output data (9 influential input parameters out of the 12 studied here).
- The clad physical properties (thermal-expansion and yield stress) have little impact on the outputs.
- It is worth noting that some outputs classified under the same behaviour type do not always have the same influential parameters (for instance, DHR and TFC).

Table 4.6. Percentage of participants that have identified a given input parameter as influential for the maximum value of each output of interest

	DHR	TFC	TFM	TFO	TCI	TCO	TNa1	TNa2	ECTH	ECT	EFT	SCH	RFO	GAP	HFC	FGR	CFP
Fuel-clad radial gap	13%	0%	13%	38%	13%	25%	13%	14%	88%	88%	71%	88%	50%	25%	50%	25%	100%
Cladding roughness	50%	10%	30%	60%	60%	60%	50%	56%	30%	10%	0%	30%	30%	10%	60%	10%	50%
Fuel roughness	38%	0%	25%	50%	50%	50%	50%	38%	13%	13%	13%	13%	13%	0%	50%	13%	25%
Zirconia thickness	56%	0%	33%	33%	78%	78%	67%	75%	33%	56%	63%	89%	22%	67%	11%	22%	50%
Injected energy in the rod	100%	100%	100%	90%	100%	80%	80%	89%	90%	90%	89%	50%	100%	100%	10%	80%	83%
Radial power profile	88%	75%	63%	75%	75%	75%	75%	86%	25%	38%	71%	38%	25%	25%	25%	38%	60%
Power pulse width	78%	33%	78%	56%	44%	44%	44%	50%	33%	33%	13%	22%	33%	11%	11%	44%	20%
Fuel thermal conductivity model	50%	10%	70%	30%	50%	70%	80%	89%	10%	20%	0%	10%	10%	0%	10%	30%	67%
Fuel thermal-expansion model	0%	0%	0%	0%	0%	0%	0%	0%	90%	100%	100%	100%	100%	100%	30%	30%	83%
Fuel enthalpy	40%	100%	80%	50%	40%	40%	50%	44%	80%	70%	78%	40%	80%	70%	0%	50%	83%
Clad thermal-expansion	0%	0%	0%	0%	0%	0%	0%	0%	20%	30%	11%	10%	0%	40%	10%	0%	50%
Clad yield stress	0%	0%	0%	0%	0%	0%	0%	0%	0%	33%	33%	67%	0%	44%	0%	0%	40%

The darker blue is associated with a percentage greater than 50%, lighter blue with a percentage between 0% and 50% and white with 0%.

References

Baccou, J. and E. Chojnacki (2014), "A practical methodology for information fusion in presence of uncertainty: Application to the analysis of a nuclear benchmark", *Environment Systems and Decisions*, Vol. 34/2, pp. 237-248, https://doi.org/10.1007/s10669-014-9496-3.

Destercke, S. and E. Chojnacki (2008), "Methods for the evaluation and synthesis of multiple sources of information applied to nuclear computer codes", *Nuclear Engineering and Design*, Vol. 238/9, pp. 2484-2493, https://doi.org/10.1016/j.nucengdes.2008.02.003.

Iooss, B. and P. Lemaitre (2015), "A review on global sensitivity analysis methods", in Meloni, C. and G. Dellino (eds.), *Uncertainty Management in Simulation-Optimisation of Complex Systems: Algorithms and Applications*, Springer.

NEA (2017a), "Reactivity-Initiated Accident (RIA) Fuel-Codes Benchmark Phase II: Uncertainty and Sensitivity Analyses", NEA/CSNI/R(2017)1, OECD Publishing, Paris, https://www.oecd-nea.org/jcms/pl_19762.

NEA (2017b), "Post-BEMUSE Reflood Model Input Uncertainty Methods (PREMIUM) Benchmark: Final Report", NEA/CNSI/R(2016)18, OECD Publishing, Paris, www.oecd-nea.org/jcms/pl_19752.

5. Conclusions and recommendations

The third phase of the WGFS RIA fuel codes benchmark focused on the uncertainty assessment of the calculation results for the irradiated case CIP0-1. The objective was to evaluate the impacts of the initial state and key models on the results during and after the transient in order to study the influence of the transient code, not the modelling of the base irradiation code. In addition, a sensitivity study was performed to identify or confirm the most influential input parameters.

Ten organisations representing nine countries participated in the RIA benchmark Phase III. For the uncertainty analysis, they provided the lower and upper bounds associated with specified output parameters; for the sensitivity analysis, they provided the partial rank correlation coefficients associated with each uncertain input for each specified output parameter at each specified time, including for their maximum values.

In terms of transient computer codes used, the spectrum was large as analyses were performed with ALCYONE, FALCON, FRAPTRAN, RANNS, SCANAIR, TESPA-ROD and TRANSURANUS.

The specifications of the RIA benchmark Phase III decoupled steady-state and transient simulations. Some codes have been developed to perform both base irradiation and transient calculations, which can ensure continuity between the two phases but makes it more difficult to perform the decoupling. Their users therefore had difficulty matching the pre-transient state defined in the specifications. More precisely, participants that usually do not use FRAPCON to evaluate the rod state after base irradiation had difficulty initialising their transient calculations according to FRAPCON outcomes, which somewhat biased the comparison among all the participants' results.

The statistical study included not only input parameters already identified for fresh fuel, but also extra "irradiation parameters" such as zirconia thickness, power profile, initial fuel-to-clad gap.

The uncertainty analysis has led to the following main conclusions:

- The experimental results (time/height trend and scalar values) were well caught by most of the participants, except for fission gas release.
- The strongest agreement with experimental measurements was associated to the evaluation of clad hoop strain and clad elongation, then sodium temperatures.
- The maximum (relative) uncertainty band width depends on the type of outputs. As in Phase II, the narrowest intervals are obtained for fuel thermal outputs. The uncertainty interval width increases slightly for clad thermal outputs, then more significantly for fuel and clad mechanical ones. Finally, a large uncertainty was observed for the new outputs (that were not considered in Phase II) fuel-clad gap width, fission gas release, fuel-to-clad heat exchange coefficient and clad failure prediction.
- The same magnitude was observed for the relative uncertainty width and for reference calculation dispersion for numerous outputs.
- When comparing participants' uncertainty results for outputs considered in Phase II, the coherence ranking is the same. These are, from the highest coherence

to the lowest: 1) fuel thermal outputs (except temperature of fuel outer surface); 2) fuel and clad mechanical outputs (except clad hoop stress at the outer part of the clad); 3) temperature of fuel outer surface, clad hoop stress at outer part of the clad, fuel-clad gap width, clad and fluid thermal outputs; and 4) fuel-to-clad heat exchange coefficient, fission gas release and clad failure prediction.

The sensitivity analysis led to the following conclusions:

- The injected energy is the most influential input parameter during the whole transient and on almost all output data.
- Input data related to rod state after base irradiation (initial fuel-to-clad gap, zirconia thickness, radial power profile, roughness) are also very influential. Initial fuel-to-clad gap is the most influential one in terms of clad failure prediction.
- Fuel physical properties (fuel thermal-expansion and thermal conductivity models) have a significant impact on the behaviour.
- With the exception of injected energy, participants did not identify any common influential input parameters for the fission gas release.
- The clad failure prediction is challenging because it is sensitive to many input data (9 influential input parameters out of the 12 studied here).
- The clad physical properties (thermal-expansion and yield stress) have an impact on few, but major, outputs (clad stress and clad failure prediction).

Phase III confirmed the conclusions of Phase II concerning the strong dependence of the uncertainty results on the type of behaviour (in terms of uncertainty band width and coherence between participants). Moreover, it allowed enlargement of the list of influential input parameters with some due to the irradiation period.

Based on the main outcomes of the analysis, the recommendations for further work are:

- Safety analysis studies can require uncertainty analysis on parameters associated with the state of the rod at the end of irradiation. However, for some RIA codes, the pulse-irradiation and base irradiation are not considered apart. It could be interesting to develop strategies to allow the propagation of uncertainties on input parameters associated with irradiation behaviour.
- Further developments are required with a view to validated fission gas release and clad failure prediction models. It first involves gathering more high-quality data.
- Mechanical models need to be improved, including cladding failure criteria and cladding stress behaviour.
- A first task before uncertainty and sensitivity analyses is the quantification of input uncertainties, which was partly performed in this benchmark by expert judgement. The recent SAPIUM guidance (Baccou et al., 2020; NEA, forthcoming) could be used to create a transparent and rigorous model for input uncertainty quantification in order to minimise the user effect.

References

Baccou, J. et al. (2020), "SAPIUM: A Generic Framework for a Practical and Transparent Quantification of Thermal-Hydraulic Code Model Input Uncertainty", *Nuclear Science and Engineering*, 194, pp. 721-736. https://doi.org/10.1080/00295639.2020.1759310.

NEA (forthcoming), "SAPIUM: Development of a Systematic Approach for Input Uncertainty quantification of the physical Models in thermal-hydraulic codes Good Practices Guidance Report", OECD Publishing, Paris.

Annex A. Description of the transient codes used

A.1 ALCYONE (CEA)

ALCYONE is a multidimensional pressurised water reactor (PWR) fuel performance code developed at the French Alternative Energies and Atomic Energy Commission (CEA) in Cadarache (France) within the PLEIADES software environment (Michel et al., 2013). ALCYONE release 1.4 contains four schemes (Sercombe et al., 2013): 1) a standard 1.5D description of the fuel rod; 2) a 3D scheme dealing with one-quarter of a pellet fragment and associated cladding; 3) a 2D(r,θ) scheme describing the behaviour of the mid-pellet plane of a 3D pellet fragment (Sercombe et al., 2012); and 4) a 3D multipellet fragment scheme where part or the complete fuel rod can be simulated.

The different schemes use the same finite-element code CAST3M to solve the thermo-mechanical pellet – gap – cladding problem and share the same physical material models at each node or integration point of the finite-element mesh. This makes comparison of simulated results from one scheme to another possible with no dependency on the constitutive models.

ALCYONE was originally developed for the modelling of fuel rod behaviour during normal (base irradiation) and off-normal (power ramp) loading sequences. The following (main) phenomena are included in the fuel performance code (Michel et al., 2012): power deposition; heat conduction in the fuel pellet and cladding; creep and fragmentation of the pellet; generation and diffusion of fission gases in the fuel microstructure; fission gas-induced swelling; fission gas release (FGR); pellet densification; high burn-up structure; heat convection at the clad – coolant and clad – pellet interface; irradiation creep; thermal creep and plasticity of the cladding; external clad corrosion; unilateral contact with friction at the clad-pellet interface (2D, 3D); clad – pellet axial locking after contact.

In ALCYONE, the pre-RIA transient state has been assessed by comparison to an extensive database of post-irradiation examinations of base-irradiated and ramp-tested UO_2-Zircaloy-4, UO_2-M5® and MO_X-Zircaloy-4 rods with burnups up to 80 GWd/tM (Struzik et al., 2012). The experimental measures include clad profilometry, zirconia thickness, rod elongation, radial concentration profiles of fission gas and fission gas bubble size, FGR, and internal pressure in the rod. The 3D scheme allows one to more precisely assess the local behaviour of the fuel rod by comparing the following experimental and calculated data: clad ridge heights at pellet – pellet interface and mid-pellet level, dish filling and number of radial-axial cracks in the pellets (Sercombe et al., 2013).

In the last ten years, ALCYONE's capabilities have been extended to accident conditions (RIA [Sercombe et al., 2010] and loss-of-coolant accident [Struzik et al., 2014]) with a very limited amount of new developments. In this way, the continuity between nominal and transient conditions has been ensured. Extension of the fuel code schemes to pulse-irradiation required the following improvements: solving of the transient thermal heat balance equation for the pellet – gap – cladding system, incorporation of material laws for irradiated Zircaloy-4 and M5® suitable for the large temperature and strain rate ranges encountered in reactivity-initiated accident (RIA) conditions (Le Saux et al., 2008; Hellouin de Menibus et al., 2014), incorporation of a material law describing the creep, plasticity and grain boundary cracking of irradiated fuel for the large temperature and strain rate ranges encountered in RIA conditions (Salvo et al., 2015), solving of the thermal and

mass balance equations for sodium or water coolant in transient conditions, implementation of the clad-water coolant heat exchange correlations proposed by Bessiron for PWR conditions (Bessiron, 2007) and stagnant liquid water (Bessiron et al., 2007). Simulations of RIA transients in ALCYONE have so far been focused on the CABRI REP-Na (Sercombe et al., 2010; Guénot-Delahaie et al., 2018), CIP tests and NSRR tests (Guénot-Delahaie et al., 2018) (UO_2-Zircaloy-4, UO_2-M5® and MO_X-Zircaloy-4). The assessment of the code predictions is based on the numerous measures available: online clad elongation, online sodium coolant temperatures at different axial positions, online clad temperatures, residual clad diameters and ridge heights, radial-axial cracking of the pellets, and dish filling. Rod failure assessment during RIA transients relies on 2D simulations, where the brittle cracking of hydride blisters in the cladding and the subsequent strain localisation in a shear band are explicitly taken into account (Sercombe et al., 2016).

A.2 FALCON (PSI)

FALCON is a light water reactor fuel rod analysis programme developed under the auspices of the Electric Power Research Institute (EPRI) in the United States (Rashid et al., 2004). Outside the EPRI, the programme is in use by a few research organisations worldwide, nuclear power utilities and the ANATECH Corporation, who developed the code for the EPRI. The programme originates from the ESCORE and FREY codes, which were earlier used by the EPRI to model fuel rod performance under steady-state operation and transients, respectively. These two codes have been merged into FALCON, which is applicable to a wide range of fuel operating regimes, from normal steady-state operation to fast transients. In 2012, the EPRI released the first version of a so-called redesigned version of the code, FALCON V1 (EPRI, 2014) with the source code being updated to FORTRAN 95 and providing a graphical user interface for input and post-processing based on the hierarchical data format. The current version is FALCON V1.4, which includes a mechanistic model, GRSW-A, for FGR and fuel swelling during base irradiation and thermal transients. The GRSW-A model was implemented and verified at the Paul Scherrer Institut (PSI) in Switzerland as part of a research, legacy version of the code, FALCON MOD01 (Khvostov et al., 2011).

FALCON comprises best-estimate models for the involved physical phenomena, and uses a 2D finite-element method to solve the coupled equations of heat conduction and mechanical equilibrium. The fuel rod can be modelled in either axisymmetric or cross-sectional geometry. Pellet-clad mechanical interaction can in both geometries be modelled with the Amontons-Coulomb law of friction for the tangential contact forces. The deformation mechanisms considered by FALCON for the cladding tube are thermoelasticity, plasticity, creep and irradiation growth. For the fuel pellets, FALCON considers thermal-expansion, solid- and gaseous-bubble swelling, elastoplasticity, cracking, and creep.

The GRSW-A model, as integrated into the FALCON code, predicts macroscopic variables of fuel state, such as FGR and pellet swelling, based on the analysis of meso- and microscopic processes in each integration point of the pellet mesh. A special option of analysis restart was developed for FALCON with the GRSW-A model in order to account for the fuel pre-irradiation and, eventually, refabrication before a simulated transient. Furthermore, the FALCON code has been recently extended by special models that are expected to have a considerable effect on fuel behaviour during the RIA, *viz.*: a model simulating the pellet-cladding bonding assisted trapping of the released fission gases during the base irradiation; a model that describes the so-called “burst” release during the thermal

transients, such as RIA, of the fission gases retained by the grain boundaries and trapped by bonding after the base irradiation; and a model for specific features of intragranular gas behaviour, such as inhibited bubble coalescence and enhanced intragranular gas release to the grain boundaries during fast thermal transients. Detailed description of the new models integrated into the FALCON code and dedicated to fuel behaviour during an RIA is presented in available open literature (Khvostov, 2018; Khvostov, 2022). In addition, a semi-empirical model for burst release of fission product gases, caused by grain boundary decohesion, is available in FALCON. This model is intended particularly for analyses of MO_X fuel under RIAs.

The cladding failure criterion for RIA in FALCON is based on the concept of a critical strain energy density, meaning that failure is assumed as soon as the strain energy density in the material reaches a critical value (Rashid et al., 2000). The critical strain energy density (CSED) is a measure of clad ductility. In FALCON, the CSED is correlated to cladding oxide thickness and pre-transient temperature, and the correlation is based on mechanical property tests performed on irradiated Zircaloy-4 cladding (Rashid et al., 2000). It should be noted that the CSED is not a true material property. As with total elongation, i.e. the plastic strain to failure, the CSED depends on the stress state and loading path up to failure. The CSED applied in clad tube failure criteria should therefore be determined from tests performed with a similar biaxial stress state as expected under a RIA. The correlation for the CSED used in FALCON has been determined from clad tube burst tests, ring tension tests and uniaxial tensile tests, using penalty factors to compensate for the non-prototypical stress states in the tests.

A.3 FRAPTRAN (TRACTEBEL)

FRAPTRAN is a computer code for analysing the thermal-mechanical behaviour of light water reactor fuel rods under transients and accidents, such as loss-of-coolant accidents and RIAs (Cunningham et al., 2001). The code originates from FRAP-T6, a fuel rod code for transient thermal-mechanical analysis from the 1970s. Compared to its ancestor, FRAPTRAN has extended capability for modelling high burn-up fuel rods. The code is based on best-estimate models, but comprises some conservative optional models, intended for licensing analyses.

FRAPTRAN is closely linked to FRAPCON-3, which is a fuel performance code for analysis of steady-state operating conditions (Berna et al., 1997). The necessary initial conditions for a transient analysis with FRAPTRAN can be generated with FRAPCON-3, whereby data for a selected burn-up step are streamlined from the output deck of FRAPCON-3 to the input deck of FRAPTRAN. Both codes were developed for the US Nuclear Regulatory Commission, and are maintained by the Pacific Northwest National Laboratory (PNNL) in the United States. The codes are used worldwide, and the user community contributes to the development and testing of new models.

FRAPTRAN uses an axisymmetric representation of the fuel rod geometry, but a model accounting for local non-axisymmetric cladding deformation (ballooning) can be used in analyses of loss-of-coolant accidents. The code is 1D in nature, and governing equations are solved with respect to the radial co-ordinate direction in a number of disjointed axial segments. Interaction between the axial segments of the rod is confined to calculations of coolant axial flow and rod internal gas pressure.

FRAPTRAN uses a thin shell model for the cladding. The temperature, material properties, stresses and strains are thus assumed to be uniform across the cladding thickness. This is a

definite drawback in analyses of RIAs, in which large radial gradients in temperature and stress arise in the cladding.

The pellets are assumed to deform only by thermal-expansion under the transient, whereas the cladding is assumed to deform by thermoelasticity, plasticity and creep. Pellet-clad mechanical interaction is treated in each axial segment separately. This local approach is somewhat simplistic, since axial contact forces induced in the cladding are not transferred to axial segments below the region of pellet-clad contact. Moreover, complete sticking is assumed, i.e. axial slip between the contacting pellet and cladding is precluded. FRAPTRAN-2.0 has a model for transient fission gas release in RIA conditions, and comprises a model for axial flow of gas in the pellet-clad gap. This model is of importance to clad ballooning.

Cladding failure under RIA is predicted by use of a strain-based failure criterion. The calculated plastic strain in the hoop direction is in each time step compared with a threshold value, which is correlated to the temperature and hydride content of the cladding material. The failure strain correlation is based on uniform elongation data from burst tests and uniaxial ring tensile tests on irradiated Zircaloy-2 and Zircaloy-4 cladding. This makes the failure criterion conservative, since observed failure strains under RIA fall somewhere between data for uniform elongation and total elongation. The advantage of using uniform elongation as a basis for the failure criterion is that uniform elongation is not much affected by stress state and loading path. It can therefore be viewed as a material property, in contrast to the total elongation.

A.4 RANNS (JAEA)

The RANNS code (Suzuki et al., 2006) was developed to analyse thermal and mechanical behaviours of a single fuel rod in RIA conditions. The code was originally based on the light water reactor fuel analysis code FEMAXI-7 (Suzuki et al., 2011), which was developed for normal operation conditions and anticipated transient conditions, and currently implemented on the latest version of FEMAXI: FEMAXI-8.

The same analytical geometry is applied to both codes: a single rod can be divided into a maximum of 40 axial segments in a cylindrical co-ordinate, and thermal analysis and FEM mechanical analysis are performed at each axial segment in which, in the default calculation mode, the pellet stack is divided into 36 iso-volumetric ring elements and cladding is divided into eight iso-thickness ring elements in the metal part, one oxide element at the inner surface and two oxide elements at the outer surface. The mesh configuration is more flexible in the latest version of the programme. In analyses of high burn-up fuels, rod conditions during their base irradiation in commercial reactors are analysed with the FEMAXI-8 code along power histories from BOL to EOL. The results of FEMAXI-8 calculations are then fed into the RANNS code calculation.

The code adopts, with some modifications, MATPRO models for material properties like pellet and cladding thermal-expansion coefficients (Hagrman and Reymann, 1979), Ohira's model and MATPRO-09 models for thermal conductivities, MATPRO-11 for specific heat, Ross and Stout's model for pellet-cladding gap conductance with consideration of bonding effect, MATPRO-11 for Young's moduli with consideration of pellet cracking effects, Tachibana's model for pellet plasticity (Tachibana et al., 1976), and the MATPRO model for cladding plasticity.

The RANNS code shares the basic framework and major part of its modules with the FEMAXI-8 code, but has its own specific models for transient fuel behaviour: a transient

FGR model, a cladding surface heat transfer model and a pellet-cladding mechanical interaction (PCMI) failure model.

A transient FGR model is implemented to simulate the grain separation and burst release of gas from grain boundary inventory in the rapidly heated pellet in RIA conditions. It is assumed that the grain separation occurs when the expanding force from gas bubbles exceeds the compressive force from its surroundings. This compressive force is a sum of grain boundary combining force, thermal stress and reactive force from cladding due to PCMI. RANNS calculates the compressive force from temperature, gas amount, bubble size, etc., and determines if the grain separation condition is fulfilled or not at each ring element, at each axial node and at each time step. In a ring element in which grain separation occurs, it is assumed that the whole grain boundary gas inventory is instantaneously released. On grain separation, the present model assumes that the swelling contribution of the original gas bubbles disappears, while rod internal pressure rise occurs due to released gas. The gas pressure inside a fuel element, in which grain separation occurs, is assumed to be in balance with the external force. Namely, the total gas volume increases as a result of grain separation, because gas bubble pressure decreases to be equal to the external pressure. The pellet internal stress state (deformation) and PCMI is recalculated within the time step by taking account of this gas pressure change.

The latest cladding surface heat transfer model for water coolant conditions in RANNS is based on the vapourisation model proposed by Bessiron et al. (2007) and a classical heat transfer coefficient approach. Four heat transfer phases are considered: 1) in Phase I, the cladding surface heat transfer coefficient h_{SURF} is calculated by Dittus-Boelter's correlation when T_{SURF} is below T_{SAT} and by Chen's correlation when T_{SURF} is above T_{SAT}. Here, T_{SURF} is the cladding surface temperature and T_{SAT} is the saturation temperature of water coolant. Once T_{SURF} reaches the critical temperature T_{CRIT}, heat transfer moves to Phase II.

In Phase II, T_{SURF} is imposed to remain at T_{CRIT}. Water vapourisation is assumed at the cladding surface and the thickness of generated vapour film, δ, is estimated considering heat unbalance between the conductive heat fluxes in the cladding wall and in the coolant water, which is induced by fixing T_{SURF}. During Phase II, effective h_{SURF} is proportional to the temperature gradient in the cladding wall in the vicinity of the cladding surface. A boiling crisis is assumed to be triggered and the heat transfer phase moves to Phase III when δ exceeds its critical value δC, which is one of the model parameters. The critical heat flux Φ_{CRIT} is defined as the cladding surface heat flux at the occurrence of boiling crisis.

In Phase III, h_{SURF} is determined so that the cladding surface heat flux at T_{SURF}, $\Phi(T_{SURF})$, satisfies the relation: $\Phi(T_{SURF}) = \Phi_{CRIT} f_1(T_{SURF}) + \Phi_{MIN} f_2(T_{SURF})$, where $f_1(T_{CRIT}) = f_2(T_{MIN}) = 1.0$, $f_1(T_{MIN}) = f_2(T_{CRIT}) = 0.0$, $f_1(T_{SURF}) = (T_{SURF} - T_{MIN})^2 / (T_{CRIT} - T_{MIN})^2$, $f_2(T_{SURF}) = 1.0 - f_1(T_{SURF})$, and Φ_{MIN} is the cladding surface heat flux at T_{MIN}, calculated by the modified Bromley's correlation described below. Once T_{SURF} reaches the temperature T_{MIN}, which is one of the model parameters, heat transfer phase moves to Phase IV.

In Phase IV, h_{SURF} is calculated by modified Bromley's film boiling correlation as $h_{BRM} = C_1 [k_G^3 \rho_G (\rho_L - \rho_G) h_{fg} g]^{0.25} / [\mu_G L \Delta T_{SUP}]^{0.25}$, and $h_{SURF} = h_{BRM} [1.0 + C_2 \Delta T_{SUB}]$, where k_G is vapour thermal conductivity, ρ_G is vapour density, ρ_L is saturated liquid density, h_{fg} is latent heat, g is acceleration of gravity, μ_G is vapour viscosity, L is fuel stack length, ΔT_{SUP} is cladding surface superheat, ΔT_{SUB} is liquid subcooling, and C_1 and C_2 are model parameters. T_{MIN} is used as quenching temperature, at which heat transfer moves to Phase I.

The aforementioned model parameters were fitted to the thermocouples (TCs) measurement data from RIA-simulation experiments with low flow conditions. Future development of the model will involve: solving a numerical instability problem which is seen in Phase III when T_{MIN} or δ_C is relatively large; further validation of the model, especially for the irradiated fuel test conditions after removing the limitations in tuning T_{MIN} and δ_C by solving the numerical instability; implementation and validation of film boiling models for high flow conditions.

The latest PCMI failure model in RANNS is based on the fracture mechanics approach proposed by Georgenthum et al. (2008). The J-integral, a fracture mechanics parameter that is applicable to crack tip stress and strain fields under both elastic and plastic deformation condition, is calculated at each axial node by a subroutine named "J_interpolation". The calculated J-integral is compared with critical J-integral values derived from high burn-up PWR fuel tests conducted in the NSRR reactor. If the calculated J-integral exceeds the critical J-integral, the code assumes that the cladding has failed at the axial node.

A.5 SCANAIR (IRSN, QT-SSM, VTT)

The French Institute for Radiological Protection and Nuclear Safety (IRSN) initiated the development of the SCANAIR computer code in parallel with the CABRI REP-Na test programme on RIA (Moal et al., 2014; Georgenthum et al., 2014). The code is used by the IRSN and by organisations participating in the CABRI REP-Na and the CABRI international programmes. SCANAIR is specifically designed for analyses of RIAs. It distinguishes itself by having models that link fission gas behaviour to fuel pellet deformation.

The fuel rod state before the transient is defined as input, and is usually generated by simulation of normal steady-state operation by a separate fuel performance code, such as FRAPCON. Developments are underway at the IRSN to extend the application domain of SCANAIR to normal operating conditions in order to improve the initialisation of the fuel rod state.

SCANAIR comprises three main modules dealing with thermal dynamics (including thermal hydraulics in the coolant channel), structural mechanics and gas behaviour. These modules communicate with each other through a database.

SCANAIR uses an axisymmetric representation of the fuel rod geometry, and the code is considered as 1.5D in makeup. All fundamental equations are solved with respect to the radial co-ordinate direction, treating each axial segment of the rod separately. However, the segments are collectively treated in calculations of coolant axial flow, rod internal gas pressure and transfer of axial forces from pellet-clad mechanical interaction. The axial contact forces are calculated by assuming perfect sticking of the two objects: when pellet and cladding come into contact anywhere along the rod, the code postulates zero relative axial motion between fuel and cladding, not only in the segment where contact occurs, but also in the segments below the contact point.

The fuel pellets are assumed to deform by thermoelasticity, plasticity, viscoplasticity, transient expansion of gaseous fission products and fuel cracking. Deformations due to fuel densification, irradiation creep and solid fission product swelling are not modelled in SCANAIR during RIA, since the code is intended for analysis of short-term transients. As fuel creep is significant at high temperature, according to experiments, transient fuel creep models are available in the code. The cladding tube is assumed to deform by thermoelasticity, plasticity and transient creep. The equations of mechanical equilibrium

are discretised in the radial direction and solved by using a finite-element method, both for the fuel pellet and the cladding tube. Hence, the cladding tube can be divided into several annuli, and the variation of temperature, hydrogen concentration and material properties across the cladding thickness can be considered in analyses. Different kinds of fuels (UO_2 or $(U,Pu)O_2$) and cladding materials (Zircaloy-2, Zircaloy-4, ZIRLO™, M5®, E110) can be modelled, thanks to a large set of correlations for thermo-physical and thermo-mechanical properties (Moal et al., 2014; Cazalis et al., 2007).

Three populations of pressurised cavities are modelled inside the fuel: intragranular bubbles, intergranular bubbles and pores. The transient FGR model does not account for the migration of individual gas atoms in the fuel, since all fission product gases are assumed to be collected in pores and bubbles. Hence, the slow diffusion of gas atoms in the fuel is not modelled, but the transport of intragranular gas bubbles into the grain boundaries and the formation of intergranular bubbles are modelled. Also, the release of intergranular bubble gas into large pores, through which it can be conveyed to the rod free volume, is considered. Release of fission gas takes place by rupture (overpressurisation or saturation) of grain boundaries and/or pores. Two models can be used to simulate the gas flow in the free volumes. The first one only considers the radial flow of fission gases through the open pores and assumes instantaneous equilibrium of pressure in the free volumes. The second one takes into account the mixture of gaseous species (fission gases, helium, argon, air) and simulates radial and axial flow with possible local overpressure in the pellet-clad gap.

The coolant is modelled as a single-phase fluid with heat transfer coefficients on the walls (Bessiron, 2007). The solution of the mass and energy conservation equations provides the coolant temperature and flowrate. The pressure is imposed in the channel. Heat exchanges between the coolant and the clad are modelled by use of heat transfer coefficients, following the successive boiling regimes (convection/conduction, nucleate boiling, transition boiling and film boiling). The specific boiling curve takes into account that the critical heat flux and film boiling phenomena involved in fast transient conditions are significantly different from steady-state conditions.

A cladding failure criterion to be used for the PCMI phase in analyses of RIA with SCANAIR is proposed by the IRSN (Georgenthum et al., 2008). Elastoplastic fracture mechanics is applied to calculate a critical initial crack length for cladding failure under the considered RIA. Cladding failure is assumed to occur if there are pre-transient defects or flaws at the cladding outer surface which are deeper than the calculated critical crack length. Moreover, for corroded cladding tubes, it is assumed that the depth of the surface defects is equal to the thickness of the densely hydrided rim at the cladding outer surface.

A.6 TESPA-ROD (GRS)

TESPA-ROD – TEmperature, Stress and Pressure Analysis of a Fuel ROD – is a transient computer code for fuel rod simulation in design basis accidents, operational transients and long-term spent fuel storage conditions.[1] TESPA-ROD models the fuel rod behaviour in 1.5D spatial resolution. It provides the transient radial temperature distribution in a cross-sectional area of a fuel rod, while the axial temperature distribution is approximated from an axial power factor which is user input. The rod can be divided into axial zones for the simulation axial distribution of hoop strain and fuel rod elongation in case of PCMI. Characteristic fuel rod volumes like fuel rod plena or gap volume are described with

1. https://www.grs.de/en/simulation-codes/tespa-rod.

designated volumes. Perfect fission gas communication among these volumes is assumed. The code provides models for UO_2, MO_X and gadolinium fuel.

The visco-plastic hoop stress/strain model in TESPA-ROD provides no radial stress resolution within the cladding. The effect of radially localised yielding in the cladding is considered in TESPA-ROD with the ratio of yield stress to burst stress. This ratio is deduced from the analytical solution of the 3D visco-plastic stress/strain relation for thick-walled cylinders. According to this analysis, the location of the elastic-plastic transition occurs at the inner cladding surface first, which is associated with yield stress. Finally, the location of the elastic-plastic transition reaches the outer surface, which is associated with both the plastic collapse of the cladding and the burst stress. For ductile cladding behaviour, the stress ratio depends on the cladding inner diameter and outer diameter. For brittle cladding behaviour, the stress ratio is close to unity with 0.985. In the TESPA-ROD code, the cladding is considered either brittle or ductile, depending on the average hydrogen pick-up in the cladding.

A pressure difference across the cladding, as well as the expansion of a pellet, may induce tensile hoop stresses in the cladding. These stresses may lead to cladding creep and/or cladding plastic deformation. Both effects on the cladding deformation are modelled in TESPA-ROD. While plastic deformation affects evenly the circumferential hoop strain, the creep strain can be circumferentially localised, depending on the eccentricity parameter provided by user input. All hoop strains result in cladding thinning, according to plastic flow rule. The irreversible deformation contributes to an additional heat-up of the cladding. If the hoop stress exceeds the hoop burst stress, burst of cladding is assumed. The burst stress in TESPA-ROD is determined based on the correlation developed at KfK Karlsruhe for Zircaloy-4 in the early 1980s. The EDGAR tests showed that this approach is still valid with some modification. Cladding creep models of the Norton type are available for Zry-4, Zry-2, Duplex, ZIRLO™, E110 and M5®. These high temperature creep models also take into account both the hydrogen and oxygen content. While increased hydrogen content increases the creep strain rate, the oxygen content reduces the creep strain rate. Furthermore, the creep rate strongly depends on the α-β phase transformation.

The gap between the pellet outer surface and the cladding inner surface contains helium and to some extent fission gas. The gap heat transfer model in TESPA-ROD is similar to that used in the fuel rod code SCANAIR.

TESPA-ROD provides an empirical FGR model for the operational fission gas release depending on the fuel rod average burn-up level only. If complex power histories need to be considered, a coupled code version TESPA-ROD/FRAPCON can be applied optionally. The transitional FGR in TESPA-ROD is modelled based on both a gas diffusion model for mid-term transients (in the time range of minutes) and a power density model for short-term transients (in the time range of milliseconds). The short-term transient model considers the transitional FGR from intergranular pellet location. This FGR rate is proportional to the fission gas content at grain boundaries. The fission gas release rate is validated with rod internal pressure data of NSRR test LS1.

In high power transients like RIA transients, the pellet expansion is controlled by both the thermal-expansion of the pellet and the power density related expansion. The second contribution is a result of a partial amorphous state of the fuel, due to the large atomic displacement rate at high power densities. Although the UO_2 crystal cannot reach a permanent amorphous state, a transitional amorphous state can be achieved. Under normal operation, the damage accumulation in UO_2 crystals becomes saturated at ten dpa without reaching a permanent amorphous state, but a transitional amorphous state is achievable

beyond that of ten dpa with a displacement rate of about ten dpa/s, e.g. during peak power of RIA transients. The additional fuel expansion associated with the transitional amorphous state is predicted in TESPA-ROD. Fresh fuel (fuel with less than ten dpa) has no damage accumulation in the crystal lattice and therefore the power density related expansion vanishes. Fission gas bubble expansion in the fuel is not considered in the TESPA-ROD code because of an almost complete loss of fission gas at intergranular locations during the early period of RIA transients predicted by TESPA-ROD.

Heat transfer between cladding and coolant can be provided as user input to the code. For RIA transients in water coolant, an extra heat transfer model is optionally available. This heat transfer model predicts departure from nucleate boiling (DNB) if the cladding surface temperature exceeds the DNB temperature deduced from the thermal-mechanical non-equilibrium (Schroeder-Richter, 1996). The film boiling heat transfer is modelled as a multiple of radiation heat transfer. The multiplier (~9.0) reflects the enhanced heat transfer due to the wavy steam/water interface. The cladding surface temperature must fall below the Leidenfrost temperature in order to re-establish both nucleate boiling heat transfer and a cladding surface that is wetted by liquid coolant. Before wetting occurs, a pre-cooling effect takes place, which is modelled by quadratic interpolation between film boiling heat transfer and nucleate boiling heat transfer. This interpolation starts if the cladding surface temperature approaches 25% of the Leidenfrost temperature after passing the peak cladding surface temperature.

A.7 TRANSURANUS (ENEA, ÚJV)

TRANSURANUS is a computer programme for the thermal and mechanical analysis of fuel rods in nuclear reactors. The code is owned by the European Commission and used by research centres, nuclear safety authorities, universities and industrial partners (Lassmann, 1992). The development of TRANSURANUS is carried out by a team of scientists working at the JRC/ITU Karlsruhe (Germany). In TRANSURANUS, the equations of the radial heat transfer are solved and the radial strain and stress distribution determined in both the fuel and the cladding. The analysis is based on the assumptions that the geometric modelling of fuel pin is 1D, plane and axisymmetric. A second assumption considers that Young's modulus of elasticity and Poisson's ratio are constant and isotropic within a cylindrical ring; finally, the constitutive equations take into account elastic and non-elastic strains.

The most important phenomena occurring under irradiation are modelled. Calculations account for: thermal and irradiation induced densification of fuel, swelling due to solid and gaseous fission products, creep, plasticity, pellet cracking and relocation, oxygen and plutonium redistribution, volume changes during phase transitions, formation and closure of a central void. The axial friction forces are evaluated when the gap between fuel and cladding is closed. Fuel restructuring, actinide redistribution, grain growth and, formation of high burn-up structure are tracked during a TRANSURANUS run.

The code accounts for the creation of fission gas in the fuel matrix, the diffusion of fission gas atoms to grain boundaries and its release to the rod free volume. This event occurs when the saturation concentration at the grain boundaries has been reached. Beside the conventional FGR model, a physics-based model has been recently developed and implemented in the code. This approach extends the description of fission gas diffusion taking into account the gas atoms trapped in bubbles. Bubble coalescence and micro-cracking are also modelled. Fuel swelling is estimated from bubble volumes.

The axial and radial geometrical mesh of both fuel column and cladding are flexible. Once the behaviour of fuel is solved in each slice, solutions are coupled by means of friction forces, axial deformation and pin inner pressure. Therefore, TRANSURANUS is a 1.5D fuel performance code, while 2D (3D) codes solve the equations simultaneously in two (three) dimensions. The TRANSURANUS code consists of a clearly defined mechanical–mathematical framework into which physical models can easily be introduced. The code has a comprehensive set of materials including: oxide, mixed oxide, carbide and nitride fuels; zircaloy and steel claddings; and several different types of coolant. It can be employed in two different versions: as a deterministic and as a statistical code. Besides its flexibility for fuel rod design, the TRANSURANUS code can deal with a wide range of different situations, as given in experiments under normal, off-normal and accident conditions. Furthermore, the code is used for boiling water reactors, pressurised water reactors and water-water energetic reactors. The code is capable of analysing problems with time scales spanning from milliseconds to years. Hence, complex irradiation experiments can be simulated where instrumented refabricated fuel rods are irradiated under different operating conditions.

References

Berna, G.A. et al. (1997), "FRAPCON-3: A computer code for the calculation of steady-state, thermal-mechanical behavior of oxide fuel rods for high-burn-up", NUREG/CR-6534, Vol. 2, US Nuclear Regulatory Commission, Washington, DC.

Bessiron, V. (2007), "Modelling of clad-to-coolant heat transfer for RIA applications", *Journal of Nuclear Science and Technology*, Vol. 44/2, pp. 211-221. https://doi.org/10.1080/18811248.2007.9711275

Bessiron, V. et al. (2007), "Clad-to-coolant heat transfer in NSRR experiments", *Journal of Nuclear Science and Technology*, Vol. 44/5, pp. 723-732. https://doi.org/10.1080/18811248.2007.9711861

Cazalis, B. et al. (2007), "The PROMETRA program: Fuel cladding mechanical behaviour under high strain rate", *Nuclear Technology*, Vol. 157/3, pp. 215-229, http://dx.doi.org/10.13182/NT07-A3814.

Cunningham, M.E. et al. (2001), "FRAPTRAN: A computer code for the transient analysis of oxide fuel rods", NUREG/CR-6739, Vol. 1, US Nuclear Regulatory Commission, Washington, DC, https://www.nrc.gov/docs/ML0125/ML012530260.pdf.

EPRI (2014*), Nuclear Industry Achieves Greater Fuel Reliability and Safety with FALCON Software*, Electric Power Research Institute, Palo Alto, CA.

Georgenthum, V. et al. (2014), "SCANAIR: A transient fuel performance code – Part two: Assessment of modelling capabilities", *Nuclear Engineering and Design*, Vol. 280, pp. 172-180, https://doi.org/10.1016/j.nucengdes.2014.04.030.

Georgenthum, V. et al. (2008), "Fracture mechanics approach for failure mode analysis in CABRI and NSRR RIA tests", in: *Proceedings of the 2008 Water Reactor Fuel Performance Meeting*, 19-23 October 2008, Seoul.

Guénot-Delahaie, I. et al. (2018), "Simulation of reactivity-initiated accident transients on UO2-M5 fuel rods with ALCYONE V1.4 fuel performance code", *Nuclear Engineering and Technology*, Vol. 50/2, pp. 268-279, https://doi.org/10.1016/j.net.2017.12.006.

Hagrman, D.L. and G.A. Reymann (1979), "MATPRO-Version 11: A handbook of materials properties for use in the analysis of light water reactor fuel rod behaviour", NUREG/CR-0497, US Nuclear Regulatory Commission, Washington, DC.

Hellouin de Menibus, A. et al. (2014), "Thermo-mechanical loading applied on the cladding tube during the pellet-cladding mechanical interaction phase of a rapid reactivity-initiated accident", *Journal of Nuclear Materials*, Vol. 453/1-3, pp. 210-213, https://doi.org/10.1016/j.jnucmat.2014.06.046.

Khvostov, G. (2022), "Modelling effects of transient FGR in LWR fuel rods during a LOCA", Journal of Nuclear Materials, 559, 153446 (26 pp.). https://doi.org/10.1016/j.jnucmat.2021.153446.

Khvostov, G. (2018), "Models for numerical simulation of burst FGR in fuel rods under the conditions of RIA", *Nuclear Engineering and Design*, Vol. 328, pp. 36-57, https://doi.org/10.1016/j.nucengdes.2017.12.028.

Khvostov, G. et al. (2011), "A model for fission gas release and gaseous swelling of the uranium dioxide fuel coupled with the FALCON code", *Nuclear Engineering and Design*, Vol. 241/8, pp. 2983-3007, https://doi.org/10.1016/j.nucengdes.2011.06.020.

Lassmann, K. (1992), "TRANSURANUS: A fuel rod analysis code ready for use", *Journal of Nuclear Materials*, Vol. 188, pp. 295-302, https://doi.org/10.1016/0022-3115(92)90487-6.

Le Saux, M. et al. (2008), "A model to describe the anisotropic behaviour of fresh and irradiated Zircaloy-4 fuel claddings under RIA loading conditions", *Journal of Nuclear Materials*, Vol. 378/1, pp. 60-69, https://doi.org/10.1016/j.jnucmat.2008.04.017.

Michel, B. et al. (2017), "Simulation of pellet-cladding interaction within the PLEIADES fuel performance software environment", *Nuclear Technology*, Vol. 182/2, pp. 124-137, https://doi.org/10.13182/NT13-A16424.

Michel, B., et al. (2012), "3.22 – Modelling of pellet-cladding interaction", in *Comprehensive Nuclear Materials*, pp. 677-712, http://dx.doi.org/10.1016/B978-0-08-056033-5.00074-4.

Moal, A. et al. (2014), "SCANAIR: A transient fuel performance code – Part one: General modelling description", *Nuclear Engineering and Design*, Vol. 280, pp. 150-171, https://doi.org/10.1016/j.nucengdes.2014.03.055.

Rashid, Y.R. et al. (2004), "Fuel analysis and licensing code: FALCON MOD01: Volume 1: Theoretical and numerical bases", TR-1011307, EPRI, Palo Alto, CA, https://www.epri.com/research/products/000000000001011307.

Rashid, Y.R. et al. (2000), "A cladding failure model for fuel rods subjected to operational and accident transients", in: *Nuclear Fuel Behaviour Modelling at High-Burn-up and Its Experimental Support*, IAEA-TECDOC-1233, International Atomic Energy Agency, Vienna, https://www-pub.iaea.org/MTCD/Publications/PDF/te_1233_prn.pdf.

Salvo, M. et al. (2015), "Experimental characterization and modelling of UO2 grain boundary cracking at high temperatures and high strain rates", *Journal of Nuclear Materials*, Vol. 460, pp. 184-199, https://doi.org/10.1016/j.jnucmat.2015.02.018.

Schroeder-Richter, D. (1996), "Analytical modelling of complete Nukiyama curves corresponding to expected low void fraction at high subcooling and flow rate", *Fusion Technology*, Vol. 29/4, pp. 468-486, https://doi.org/10.13182/FST96-A30691.

Sercombe, J. et al. (2016), "2D simulation of hydride blister cracking during a RIA transient with the fuel code ALCYONE", *EPJ Nuclear Science and Technology*, Vol. 2/22, https://doi.org/10.1051/epjn/2016016.

Sercombe, J. et al. (2013), "3D modelling of strain concentration due to PCI within the fuel code ALCYONE", in: *LWR Fuel Performance Meeting TopFuel 2013*.

Sercombe, J. et al. (2012), "Power ramped cladding stresses and strains in 3D simulations with burn-up-dependent pellet – clad friction", *Nuclear Engineering and Design*, Vol. 242, pp. 164-181, https://doi.org/10.1016/j.nucengdes.2011.08.069.

Sercombe, J. et al. (2010), "1D and 3D modelling of PCMI during a RIA with ALCYONE V1.1", in *Proceedings of the 2010 LWR Fuel Performance Meeting/Top Fuel/WRFPM*, American Nuclear Society.

Struzik, C. et al. (2014), "LOCA tests IFA 650 analysis through the fuel state at the end-of-base irradiation and its thermo-mechanical behaviour during the experiment", EHPG, Norway.

Struzik, C. et al. (2012), "Validation of fuel performance CEA code ALCYONE, scheme 1D, on extensive database", in *Proceedings of Top Fuel Conference*, Manchester, United Kingdom.

Suzuki, M. et al. (2011), "Light water reactor fuel analysis code FEMAXI-7: Model and structure", JAEA-Data/Code 2010-035, Japan Atomic Energy Agency, Tokai-mura, Japan.

Suzuki, M. et al. (2006), "Analysis on pellet-clad mechanical interaction process of high-burn-up PWR fuel rods by RANNS code in reactivity-initiated accident conditions", *Nuclear Technology*, Vol. 155/3, pp. 282-292, https://doi.org/10.13182/NT06-A3762.

Tachibana, T. et al. (1976), "Dependence on strain rate and temperature shown by yield stress of uranium dioxide", *Journal of Nuclear Science and Technology*, Vol. 13/9, pp. 497-502. https://doi.org/10.1080/18811248.1976.9734063

Annex B. Description of the codes used by the participants during the benchmark

B.1 French Alternative Energies and Atomic Energy Commission (CEA)

The same fuel performance code, namely ALCYONE, was used by the CEA for base-irradiation and transient calculations, complemented by the URANIE platform (Gaudier, 2010) tools as regards the uncertainty quantification and sensitivity analysis.

ALCYONE pulse-irradiation simulations clearly take advantage of starting from the base irradiation conditions that the code itself computes. Among the important phenomena for UO_2 and MO_X fuels, the fission gas model deals with fission gas creation and evolution at the grain scale. With no need for any user-dependent specific initialisation of the variables prior to pulse-irradiation simulations, the precise and relevant description of the initial fuel rod state and spatial distribution of fission gases in each phase – inter- or intragranular, in bubbles or dissolved, with partial to total restructuration (high burn-up structure) – is automatically ensured.

The URANIE platform developed by the CEA is based on the ROOT data analysis framework (http://root.cern.ch). This open source project (available at: http://sourceforge.net/projects/uranie) offers various possibilities and methods in terms of definition of the uncertain variables and sampling from their characteristics, to-be-interfaced code launching, uncertainty propagation and sensitivity analysis between the inputs and the outputs of the code, as well as optimisation for automatic calibration of codes, and reliability considerations.

Within the scope of the RIA benchmark Phase III, only the 1.5D scheme of ALCYONE release 1.4 was used. The fuel porosity radial profile at the end-of-base irradiation given by ALCYONE fission gas model was found to differ significantly from the specified FRAPCON profile. As any modification in the fission gas model parameters could have led to non-negligible and non-physical impacts on gas inventory, clad strain, fission gas release (FGR), etc., CEA calculations were thus based on the fuel porosity radial profile given by the ALCYONE fission gas model.

All uncertain parameters were treated with URANIE release 4.1 as requested through a 200-run design of experiment generated by Latin hypercube sampling.

B.2 National Agency for New Technologies, Energy and Sustainable Economic Development (ENEA)

Results provided by the ENEA were obtained by means of the TRANSURANUS fuel performance code (version v1m1j18) (Lassmann, 1992). TRANSURANUS has the modelling capabilities and a built-in Monte-Carlo technique (random number generator, probability density functions, up to 70 random input variables) required to accomplish the objectives of the benchmark. The type of TRANSURANUS run employed for the benchmark is a combination of deterministic (base irradiation) and statistical restart run (transient test). A TRANSURANUS tool (RSTRTM) was used to take into account the refabrication of CIP0-1. The output variables indicated in the specifications were written to the statistic file during each statistical run. Results were then extracted to the Excel templates distributed to the participants. This step was performed by means of a purpose-

developed code in FORTRAN95. In addition, this tool calculates the Spearman's rank correlation coefficients for the analysis of sensitivity.

The ENEA's results are based on the analysis of nine uncertain inputs instead of 12, as indicated in the specifications. This choice was mainly due to lack of time. The random input variables not accounted for are: the radial power profile, pulse width and gap size. Most of the uncertain inputs considered in the analysis of uncertainties and sensitivity are available in the code version distributed to the users. Three uncertain inputs were introduced in the code for the purpose: fuel and cladding roughness and zirconia thickness. All the output variables considered in the benchmark were calculated during a TRANSURANUS run. The clad failure prediction parameter was defined according to the overstress criterion adopted in the calculations.

With regard to the cladding material, a complete set of ZIRLO™ correlations is not available in TRANSURANUS. For this reason, the generic Zircaloy correlations were applied. The yield stress used in calculations is based on the Zr1%Nb correlation multiplied by an empirical factor. The development of ZIRLO™ correlations is underway.

B.3 Gesellschaft Für Anlagen- Und ReaktorSicherheit (GRS)

1. Base irradiation:

The base irradiation results of FRAPCON 4 provided by the IRSN were used to match specifications adequately.

2. RIA transient:

The GRS fuel rod code TESPA-ROD version 20.3 was used for the transient calculations. Some parameters were adapted from the FRAPCON 4 code provided by the IRSN.

2.1 The code used nine axial zones

The following parameters were separated into nine values:

- rod relative power during transient: 0.801, 0.927, 1.022, 1.095, 1.143, 1.135, 1.090, 0.991, 0.808;
- averaged outer oxide layer (three taken from FRAPCON, the other six were interpolated and extrapolated close to measurements: 62, 63, 67, 75, 80, 83, 85, 87, 88 [µm]).

The following parameters were distributed on three axial nodes (three each):

- pellet outer radius (FRAPCON);
- clad outer diameter: based on pellet diameter, gap size cladding thickness: 9.553, 9.560, 9.540 mm;
- density of fuel (FRAPCON).

The following parameters were equal to all zones:

- design cladding thickness;
- burn-up of 76.6 MWd/kg (radial pellet averaged);

- radial power profile: pellet divided in ten equidistant rings - ring 10 power shift of +37.9 %, rings 1-9 power shift of -8.9%. Values derived from the FRAPCON 4 power profile.

3. Uncertainty and sensitivity analysis:

The GRS code SUSA 4.1 was used.

All uncertain parameters have been considered except for:

- Yield strength uncertainty and reduction in reference case are not considered (the high hydrogen content effects the fracture limits).
- One value for fuel roughness as cladding roughness (sum of both).
- Fuel gap and roughness may lead to geometrical overlap of cladding and fuel (roughness > gap). Adjustment of gap to prevent overlap.
- All samples start with full zirconia thickness at the beginning of the transient. Spallation model leads to X% of spallation as specified in uncertainty of zirconia thickness. Spallation occurs at transient hoops strains of 0.5%.
- All cases with burst of cladding (CFP = 1) are included in the uncertainty and sensitivity analysis.

B.4 IRSN

Base irradiation

The rod state at the end of the base irradiation was evaluated through the code FRAPCON V4.0 Patch1 using the FRAPCON input file given in the specifications.

SCANAIR input data deck

An interface tool named FRAPSCAN was used to read the results coming from FRAPCON to create most of the SCANAIR input data deck. In order to complete the data deck, hypotheses were made for the end of state data not given by the FRAPCON code and for SCANAIR calculations:

- rod initial state hypotheses:
  - gas repartition between intra and inter pore, intra and inter bubble size (radial distribution), grain size in the high burn-up structure: deduced from examinations on other fuels;
  - fuel-clad roughness: only one roughness can be taken into account in SCANAIR calculations; the value of the global roughness ranged from 0.1 µm to 4.0 µm.
- SCANAIR calculation hypotheses:
  - Failure evaluation: CLARIS approach was used. This approach is based on the hypothesis that the pellet-cladding mechanical interaction failure may result from the propagation in the outer part of the cladding of an existing incipient crack (due to the presence of brittle area with dense hydride). An initial incipient crack of 50 µm was evaluated on metallographic examinations performed before the tests.

- Fuel and clad mechanical modelling: perfectly elastoplastic behaviour with the Canon's yield stress law for UO_2 fuel and the so-called Crocodile visco-plastic model based on the Lemaitre formulation for ZIRLO™ cladding.
- Fuel failure limit (for grain boundary FGR): the limit was set at 120 MPa.

Statistical analysis

SUNSET (Sensitivity and Uncertainty Statistical Evaluation Tool) software was used to perform this analysis. It is a statistical tool providing a collection of methods for information treatment in risk analysis studies. It includes statistical tools to perform a probabilistic assessment of uncertainties, where the uncertainty sources are modelled using random variables. To be able to handle both aleatory and epistemic uncertainties, techniques based on the Dempster-Shafer evidence framework are also available, but were not exploited during this benchmark. SUNSET can be used for sensitivity analyses to identify the variables which have the largest contributions to the overall model response uncertainty. The methods are based on algebraic and statistical tools combining design of experiment theory and regression techniques.

A more exhaustive description of the software can be found at: www.irsn.fr/en/research/scientific-tools/computer-codes/pages/sunset.aspx. This software can be downloaded for free at: https://gforge.irsn.fr/gf/project/sunset.

B.5 JAEA

Base irradiation

The EOL fuel-rod state was computed by the code FEMAXI-8 (version 8.1.102f). The model set adopted for the present benchmark is identified as 00018lq6dIC8R. Differences from the "reference" model, whose detailed description can be found in a recent publication (model-ID:00015ix3c [569]), are enumerated below; they were introduced mainly to follow the benchmark specification.

- FGR model further tuned to match the FRAPCON calculation;
- mesh configuration changed so that the number of cladding radial meshes for mechanical calculation is eight;
- fuel cracking model inactivated;
- HBS swelling model activated;
- more rigid behaviour of fuel pellet: higher yield stress of fuel pellet so that the calculated cladding elongation agrees better with the measurement in CIP0-1.

RIA transient

The transient fuel behaviour during CIP0-1 was computed by the RANNS code. The code version and model set are common with the FEMAXI-8 calculation for its base irradiation. Additional or RIA-specific models adopted in the present benchmark are described in Annex A. RANNS read the result coming from the base irradiation calculation by FEMAXI-8 to initialise fuel states for the transient simulation. The following special options were introduced to satisfy requirements in the benchmark:

- a restart option which forces the clad inner radius to some different values from EOL(FEMAXI) state was added to treat fuel-clad gap as an input uncertainty parameter;

- a restart option which forces force clad oxide thickness to some different values/distribution from EOL(FEMAXI) state was added to treat zirconia thickness as an input uncertainty parameter;
- a restart option which scales history input in the time-axis direction and keeping time-integrated power constant was added to treat pulse width as an input uncertainty parameter.

Statistical analysis

The uncertainty and sensitivity analyses were performed with Dakota 6.5 developed and provided by the Sandia National Laboratories (SNL). Dakota read the regressor (uncertain input parameters) information through its input file, generated sampled input parameters within given uncertain range and associated RANNS input files, launched RANNS calculations, read the outputs, and computed statistical measures required in the benchmark.

B.6 Paul Scherrer Institute (PSI)

The current analyses of base irradiation and RIA transients were carried out using FALCON v1.4.1 and the GRSW-A 3.02 model for FGR and swelling. FALCON utilised a fully 2D thermo-mechanical calculation of an axisymmetric fuel rod. The rod geometry is presented in the R-Z co-ordinate system.

For the full-length mother rods, the radial mesh is formed using three element-columns in the pellets and three columns in the cladding. Nine element-rows were used to form the axial mesh in the active part of the full-length mother rod for the tests.

The standard FALCON-based methodology was used for calculation of the thermal transients in refabricated rodlets, including the advanced restart procedure. It writes the whole array of the integrated microscopic and macroscopic variables for each calculation node and time step of the base irradiation analysis into a binary file. When the following calculation of the thermal transient starts, the variable arrays are "plugged out" from the binary file for the predetermined lifetime – when the transient starts – and an interpolation technique is applied to determine the array variables in the nodes of the new finite-element mesh, which now corresponds to the new rod refabricated from the "mother" rod after the base irradiation (Ribeiro and Khvostov, 2015).

As regards the uncertainty quantification and sensitivity analysis, all studies were performed using an in-house Pythontool, for which an interface with FALCON was developed to manage data I/O, job executions on clusters and data extraction in the scope of benchmark specifications. The Latin hypercube sampling was used to generate the matrix of uncertain parameters. Sensitivity analysis was based on the computation of Spearman rank correlation coefficients.

The PSI's results are based on an analysis of 11 of the 12 uncertain variables, as the radial power profile was not included, since this property is not available in FALCON as an input parameter. For the fuel-clad radial gap, in order not to change the fuel and clad geometries (as requested in the specifications), FALCON uses a relocation model with a parameter that sets the gap as the ratio of the cold gap to the as-manufactured gap. This was used as input, the reference value of 10 μm corresponding to a ratio of approximately 0.12 of the cold gap (0.0825 mm). A uniform thickness of 43.5 μm (C=1/2) was considered as a reference for the zirconia thickness because an axial distribution cannot be given as input in FALCON (as requested in the specifications).

B.7 QT-SSM

Base irradiation

The calculated results from the FRAPCON-4.0P1 computer programme, which were provided together with the benchmark specifications, were used to define the state of the fuel rod at the end-of-base irradiation. All FRAPCON results provided with the specifications were used, except for the calculated partitioning of retained fission gas. The reason for this exception is that FRAPCON-4.0P1 calculates an intragranular gas concentration in the outermost part of the HBS (rim zone) that is several times higher than what is typically observed in measurements on fully restructured HBS material. For this reason, the gas partitioning was calculated as a function of axial and radial position, based on the assumed spatial variation of fuel microstructure (see below).

SCANAIR input data deck

The input data deck to SCANAIR V_7_8 was prepared by combining the aforementioned FRAPCON results for the rodlet pre-test conditions with the CABRI test parameters defined in the specifications. The following hypotheses and assumptions were made for parameters not defined in the specifications:

- Rod pre-test state:
  - Axial-radial distributions of fuel microstructural properties, *viz.* grain size and size of intra- and intergranular fission gas bubbles, were deduced from results reported from examinations of similar fuel. These results were adapted to the assumed extension of the restructured rim zone, as defined by the porosity distribution calculated with FRAPCON-4.0P1.
  - The partitioning of retained fission gas between intragranular bubbles, intergranular bubbles and larger scales pores was calculated as a function of axial and radial position by models in SCANAIR V_7_8, based on the assumed distributions for totally retained gas, porosity and the microstructural properties mentioned above.
  - The effective fuel-clad roughness was taken as the sum of the fuel and cladding roughnesses, which were assumed to be independent, uniformly distributed parameters. The effective fuel-clad roughness used in the calculations with SCANAIR V_7_8 therefore followed an Irwin-Hall distribution. This is a major difference from the calculations done by the IRSN and the VTT, with a large impact on the calculated results.
- SCANAIR calculations:
  - SCANAIR V_7_8 was used with recommended models and settings, except for the cladding failure criterion. More precisely, the "strain" option was used, which invokes a strain-based failure criterion that had earlier been used for RIA analyses in Sweden (Jernkvist, 2006). The ZIRLO™ cladding was modelled as a perfectly elasto-plastic material, with the yield strength given by the correlation defined in the benchmark specifications.

Statistical analysis

The SUNSET software was used for statistical analyses; see Section B.4.

B.8 TRACTEBEL

The simulation of the base irradiation was performed with the input file provided by the task leaders, with the last production version of the FRAPCON code (FRAPCON 4.0 P1). The rod state at the end of the base irradiation was communicated to FRAPTRAN through the use of a restart file.

The transient modelling was performed with a beta version of FRAPTRAN 2.1 containing the sodium correlations and provided by the US NRC specifically for this task. Except for the use of the sodium correlations, the default models selected by the code were used.

The uncertainty and sensitivity analyses were performed with Dakota 6.2. The sampled parameters were automatically implemented in the FRAPTRAN input file and the FRAPCON restart file before running the calculations.

B.9 ÚJV Řež (ÚJV)

TRANSURANUS code version V1M3J12modCEZ was used for the simulation. Only a few modifications regarding the time step control were made in the code to improve the applicability in RIA conditions. Scripts written in ROOT were used to generate and process the statistical results. This set of computational tools is used for the core reload and safety analysis of the Czech nuclear power plants at ÚJV.

The CIP0-1 experiment modelling was done in three steps:

- whole rod calculation of base irradiation with nominal parameters;
- modelling of the CIP0-1 segment base irradiation, where the coolant properties and free volume were tuned to obtain the same results as in the whole rod calculation;
- statistical calculations of CIP0-1 – only the segment with the tuned base irradiation input was modelled.

Free volume and rod internal pressure were adjusted during the restart according to required input data.

The porosity profile and gap size prior to CIP0-1 test would be difficult to adjust since they are integrally calculated by TRANSURANUS during the base irradiation. These were not varied independently of the other models.

Uncertainties in code models were applied already for the base irradiation and the pellet-cladding gap variation was achieved by this approach. Therefore, the initial pellet-cladding gap is strongly correlated with code models multipliers and the pellet-cladding gap was therefore not taken into account in sensitivity analyses.

The radial power profile during the base irradiation was modelled according to the TRANSURANUS “TuBrnp” model. For the CIP0-1 test, benchmark specifications were followed.

The porosity profile is linked to the base irradiation modelling and was not varied independently.

Pulse width was varied according to the specifications (not in TRANSURANUS itself but by the pre-processing script).

A cladding corrosion layer was assumed to be present for thermal analysis, but spalled for a mechanical one (modelling of spallation during the test is not possible in the TRANSURANUS code without further modifications).

Fission gas release during CIP0-1 was modelled by simple correlation based on the FRAPTRAN model – temperature threshold for grain boundary (1 100°C) and HBS (800°C) release (activated by user for transient only).

B.10 VTT Technical Research Centre of Finland Ltd (VTT)

Base irradiation

Steady-state irradiation parameters generated by the IRSN with FRAPCON V4.0 Patch1 were used.

SCANAIR input data deck

An in-house Python script was used to generate the SCANAIR inputs for the uncertainty analysis. Not all of the necessary input parameters are provided by FRAPCON, and therefore some hypotheses had to be made:

- Rod initial state hypotheses:
  - In SCANAIR input, the total amount of gas taken from FRAPCON initialisation is given radially for each axial segment. SCANAIR then divides the gas into intergranular and intragranular and porosity gas. For this partition, SCANAIR needs the fuel end-of-life temperature distribution and porosity pressure. Grain size distribution and intragranular and intergranular bubble size distributions also affect the partition. An arbitrary constant value of 15.7 MPa is here used for the porosity pressure, and VTT-ENIGMA fuel performance code results from RIA benchmark Phase 1 were applied as end-of-life radial temperature profiles in fuel. A grain size of 0.1 μm was used for the outmost radial nodes. Arbitrary values were given for intergranular and intragranular bubbles sizes, ranging between 10 and 500 Å, depending on the radial location.
  - Fuel-clad roughness: Only one roughness can be taken into account in SCANAIR calculations. In the specifications, fuel and cladding roughnesses are given separately, and therefore the single roughness value given in the input is taken as the sum of these two (sampled) roughnesses.
- SCANAIR calculation hypotheses:
  - ZIRLO™ cladding material property models are not included in the SCANAIR version delivered to the VTT, therefore Zircaloy-4 properties were used for cladding thermal conductivity, Young modulus, thermal-expansion, enthalpy and visco-plastic behaviour.
  - No visco-plastic model was applied for the fuel. A high temperature visco-plastic model developed for Zircaloy-4 in slow transient conditions was used for the cladding.
  - Chamfers or dishings were not taken into account (high burn-up fuel).

- Inner oxide layer is defined in the specifications to be about 10 μm, but it cannot be taken into account in SCANAIR.
- Channel wall calculation and by-pass modelling were enabled. The material properties of the channel wall and by-pass are taken from CABRI sodium loop example inputs delivered with the SCANAIR code.
- Rupture stress limit for grain boundary fission gas release: 50 MPa.
- Cladding failure prediction was done with SCANAIR's fracture mechanics approach called CLARIS. As the cladding hydride rim thickness given in the specifications was 50 μm, this value was used as the outer brittle zone depth needed in the fracture mechanical approach.

References

Gaudier, F. (2010), "URANIE: The CEA/DEN uncertainty and sensitivity platform", *Procedia: Social and Behavioral Sciences*, Vol. 2/6, pp. 7660-7661, https://doi.org/10.1016/j.sbspro.2010.05.166.

Jernkvist, L.O. (2006), "Computational assessment of burnup-dependent fuel failure thresholds for reactivity initiated accidents", *Journal of Nuclear Science and Technology*, Vol. 43/5, pp. 546-561. https://doi.org/10.1080/18811248.2006.9711133

Lassmann, K. (1992), "TRANSURANUS: A fuel rod analysis code ready for use", *Journal of Nuclear Materials*, Vol. 188, pp. 295-302, https://doi.org/10.1016/0022-3115(92)90487-6.

Ribeiro, F. and Khvostov, G. (2015), "Multi-scale approach to advanced fuel modelling for enhanced safety', *Progress in Nuclear Energy*, 84, 24-35. https://doi.org/10.1016/j.pnucene.2015.03.022.